

Aus dem Bereich Physiologie  
Theoretische Medizin und Biowissenschaften  
der Medizinischen Fakultät  
der Universität des Saarlandes, Homburg (Saar)

# **Trpm4 and Trpm5 in the murine olfactory system**

**Dissertation zur Erlangung des Grades eines Doktors der  
Naturwissenschaften**

**der Medizinischen Fakultät**

der UNIVERSITÄT DES SAARLANDES

2019

Vorgelegt von

**Eugenia Eckstein (M.Sc.)**

geb. am: 08.05.1987 in Langeepas

Tag des Kolloquiums:	07.01.2020
Dekan:	Prof. Dr. M. D. Menger
Berichterstatter:	Prof. Dr. Dr. F. Zufall Prof. Dr. B. Niemeyer-Hoth PD Dr. S. Philipp
Vorsitz:	Prof. Dr. U. Boehm

“Without ambition, one starts nothing. Without work, one finishes nothing.  
The prize will not be sent to you. You have to win it.”

Ralph Waldo Emerson

<b>CONTENT</b>	<b>I</b>
<b>SUMMARY</b>	<b>IV</b>
<b>ZUSAMMENFASSUNG</b>	<b>V</b>
<b>LIST OF FIGURES</b>	<b>VII</b>
<b>LIST OF TABLES</b>	<b>VIII</b>
<b>ABBREVIATIONS</b>	<b>IX</b>
<b>1 INTRODUCTION</b>	<b>1</b>
1.1 The murine olfactory system.....	1
1.1.1 Structure and function of the main olfactory epithelium (MOE).....	2
1.1.2 Structure and function of the vomeronasal organ (VNO) .....	4
1.2 The superfamily of Transient receptor potential channels (Trp).....	6
1.2.1 Trpm4 and Trpm5 .....	8
1.3 Trp channel expression and function in the olfactory system .....	10
1.4 The interaction between olfaction and female cyclicity .....	12
1.5 Aims.....	15
<b>2 MATERIALS</b>	<b>16</b>
2.1 Mouse strains .....	16
2.2 Chemicals and enzymes.....	17
2.3 Antibodies and sera .....	18
2.4 Solutions.....	18
2.5 Critical commercial kits and compounds.....	20
2.6 Oligonucleotides .....	20
2.7 Consumables and equipment.....	21
2.8 Software .....	22
<b>3 METHODS</b>	<b>23</b>
3.1 Nucleic acid techniques .....	23
3.1.1 RNA extraction from olfactory tissue.....	23
3.1.2 RNA extraction from isolated cells .....	23
3.1.3 cDNA synthesis.....	24
3.1.4 RT-PCR .....	24
3.1.5 Rapid amplification of cDNA ends (RACE) .....	26

3.1.6	Quantitative real-time RT-PCR .....	26
3.1.7	Gel electrophoresis .....	27
3.2	Immunohistochemical methods .....	28
3.2.1	Transcardial perfusion and olfactory tissue preparation .....	28
3.2.2	Cryostat sections.....	28
3.2.3	Immunohistochemistry .....	29
3.2.4	Dissociation of VSNs and immunocytochemistry .....	29
3.2.5	Cell counts .....	30
3.2.6	Fluorescence and confocal imaging microscopy.....	31
3.3	Estrous cycle assessment .....	31
3.4	Surgical procedures and hormone replacement.....	32
3.4.1	Ovariectomy.....	32
3.4.2	Scrotal orchiectomy.....	32
3.4.3	Hormone replacement.....	33
3.4.4	Systemic block of aromatase activity .....	35
3.5	Statistics .....	35

## **4 RESULTS 36**

4.1	Trpm4 .....	36
4.1.1	Trpm4 expression and distribution in the murine olfactory system.....	36
4.1.2	The Trpm4-IC/ $\tau$ GFP reporter mouse line .....	36
4.1.3	$\tau$ GFP expression in the MOE of Trpm4-IC/ $\tau$ GFP mice .....	37
4.1.4	Expression of Trpm4 during postnatal development of the VNO .....	41
4.1.5	Sexually dimorphic Trpm4 expression in VSNs of adult mice .....	42
4.1.6	Trpm4 expression in VSNs is estrous cycle dependent .....	46
4.1.7	Regulation of Trpm4 expression in pregnant and aged females .....	49
4.1.8	Cyclic regulation of Trpm4 expression depends on ovarian hormones .....	50
4.1.8.1	Ovariectomy causes loss of Trpm4 expression in the female VNO .....	50
4.1.8.2	Effect of 17 $\beta$ -estradiol is dampened by progesterone.....	52
4.1.8.3	17 $\beta$ -estradiol restores Trpm4 expression in the ORX male VNO.....	53
4.1.8.4	Pharmacological block of endogenous 17 $\beta$ -estradiol synthesis diminishes Trpm4 expression in VSNs of both males and females .....	54
4.1.9	Trpm4 expression in the SOM and in the GG .....	56
4.1.10	Trpm4 and $\tau$ GFP expression in the olfactory bulb.....	58
4.2	Trpm5 .....	61
4.2.1	Trpm5 expression and distribution in the murine olfactory system.....	61
4.2.2	$\tau$ GFP expression in the MOE of Trpm5-IC/eR26- $\tau$ GFP mice.....	61
4.2.3	Axonal projections of $\tau$ GFP OSNs to the MOB .....	64
4.2.4	$\tau$ GFP expression in the accessory olfactory system and in the septal organ of Masera .....	65
4.2.5	Trpm5 protein expression in the adult MOE.....	66

---

4.2.6	Trpm5 protein in the postnatal MOE is not expressed in OSNs .....	69
4.2.7	Trpm5 protein is transiently expressed in a subpopulation of embryonic OSNs .....	70
4.2.8	Trpm5-9, a novel splice variant in genetically-labeled adult OSNs .....	73
<b>5</b>	<b><u>DISCUSSION</u></b>	<b>78</b>
5.1	Trpm4 protein is transiently expressed during postnatal MOE development.....	78
5.2	Trpm4 protein is expressed in sensory neurons of the vomeronasal organ.....	79
5.3	Trpm4 expression in VSNs is sexually dimorphic and estrous cycle dependent .....	80
5.4	Trpm4 protein expression in VSNs is down-regulated during pregnancy .....	82
5.5	Trpm4 protein expression in VSNs depends on gonadal hormones.....	83
5.6	Trpm4 protein expression in VSNs depends on endogenous E2 production.....	84
5.7	Trpm5 protein is exclusively expressed in MV cells of the adult MOE.....	85
5.8	Trpm5 protein is transiently expressed in a subset of embryonic OSNs.....	86
5.9	A novel Trpm5 splice variant exists in OSNs of the adult MOE .....	88
5.10	Outlook .....	90
<b>6</b>	<b><u>REFERENCES</u></b>	<b>94</b>
<b>7</b>	<b><u>APPENDIX</u></b>	<b>114</b>
7.1	Publications .....	114
7.2	Acknowledgements.....	115
7.3	Curriculum Vitae .....	117

## Summary

The olfactory system allows the evaluation of critical environmental situations and the adaptation to different environmental conditions through a variety of behavioral responses. Several members of the Trp- (transient receptor potential) family were reported to play a crucial role in the function of the main and accessory olfactory system. This study concentrates on the expression and possible function of the Ca<sup>2+</sup>-activated monovalent cation channels Trpm4 and Trpm5 in the olfactory system. Both channels play a major role in taste chemo-transduction, but their precise role in the olfactory system is not yet clear or even unknown. Here, I used a novel generation of  $\tau$ GFP reporter mouse lines, Trpm5-IC/eR26- $\tau$ GFP and Trpm4-IC/ $\tau$ GFP, in combination with Trpm4 and Trpm5 antibodies to map channel expression in different olfactory tissues. Furthermore, I employed molecular techniques such as RT-PCR and quantitative real-time PCR to identify Trpm5 splice variants and to assess Trpm4 and Trpm5 expression levels during development of the olfactory system. Additionally, I addressed gender-specific differences in Trpm4 expression in male and female mice and the sex-hormone regulated expression of Trpm4 following surgical gonadectomy in combination with hormone treatments. I discovered that besides the previously described Trpc2, Trpm4 is also expressed in vomeronasal sensory neurons (VSNs). Contrasting the expression of Trpc2, Trpm4 is sexually dimorphic and is estrous cycle dependent. In detail, Trpm4 expression in VSNs is high during receptive periods (proestrus, estrus), and low during non-ovulatory/-receptive phases (metestrus, diestrus/ pregnancy). Trpm4 expression is regulated by gonadal hormones, as surgical gonadectomy performed on male and female mice leads to a loss of Trpm4 signal in VSNs. However, Trpm4 expression can be restored by systemic treatment with 17 $\beta$ -estradiol and is maintained by endogenous aromatase activity in gonadal-intact mice. This study furthermore shows that the classical Trpm5 channel, known from taste receptor cells, is exclusively expressed in microvillar cells of the main olfactory epithelium (MOE) but not in adult olfactory sensory neurons (OSNs) which contain a novel short and likely non-functional splice variant. However, the classical Trpm5 is transiently expressed in a subpopulation of early-mature OSNs in the embryonic MOE. Summarizing, the spatial segregation of Trpm4 and Trpm5 in the olfactory system reveals that these channels play different roles and are not functionally interchangeable. This study suggests a differential role for Trpm4 in VSN signal processing during sexually receptive and non-receptive phases and a functional role of Trpm5 in OSNs during embryonic development. Concluding, this work provides a critical platform for understanding the role of Trp channels in the olfactory system.

## Zusammenfassung

Das olfaktorische System ermöglicht die Erfassung kritischer Umweltsituationen und die Anpassung an unterschiedliche Umgebungsbedingungen durch eine Vielzahl von Verhaltensreaktionen. Mehrere Mitglieder der Trp- (Transient-Rezeptor-Potential) Familie spielen eine entscheidende Rolle in der Funktion des Haupt- und akzessorischen olfaktorischen Systems. Die vorliegende Arbeit befasst sich mit der Expression und der möglichen Funktion der  $\text{Ca}^{2+}$  aktivierten monovalenten Kationenkanäle Trpm4 und Trpm5 im olfaktorischen System. Beide Kanäle spielen eine wichtige Rolle bei der Geschmacks-Chemotransduktion, jedoch ist ihre genaue Rolle im olfaktorischen System noch nicht klar oder gar unbekannt. Im Rahmen dieser Arbeit habe ich eine neue Generation von GFP-Reporter-Mauslinien, Trpm5-IC/eR26- $\tau$ GFP und Trpm4-IC/ $\tau$ GFP, in Kombination mit Trpm4- und Trpm5-Antikörpern verwendet, um die Kanalexpression in verschiedenen olfaktorischen Geweben zu untersuchen. Darüber hinaus habe ich molekularbiologische Techniken wie die RT-PCR und die quantitative Echtzeit-PCR eingesetzt, um Trpm5-Spleißvarianten zu identifizieren und um die Expressionsniveaus von Trpm4 und Trpm5 während der Entwicklung des olfaktorischen Systems zu ermitteln. Zusätzlich untersuchte ich geschlechtsspezifische Unterschiede in der Expression von Trpm4 in männlichen und weiblichen Mäusen und die Regulation der Trpm4-Expression über Geschlechtshormone durch chirurgische Gonadektomie in Kombination mit Hormonbehandlungen. Ich habe festgestellt, dass Trpm4, neben dem zuvor beschriebenen Trpc2, auch in vomeronasalen sensorischen Neuronen (VSNs) exprimiert ist. Im Gegensatz zur Expression von Trpc2 ist die Expression von Trpm4 sexuell dimorph und ist abhängig vom Östruszyklus. Im Detail ist die Expression von Trpm4 in VSNs während der rezeptiven Perioden (Proöstrus, Östrus) erhöht und während der nicht-ovulatorischen/ -rezeptiven Phasen (Metöstrus, Diöstrus/ Schwangerschaft) erniedrigt. Die Trpm4-Expression wird durch Gonadenhormone reguliert und eine chirurgische Gonadektomie bei männlichen und weiblichen Mäusen resultiert in dem Verlust des Trpm4-Signals in VSNs. Allerdings kann die Trpm4-Expression durch eine systemische Behandlung mit  $17\beta$ -Estradiol wiederhergestellt werden und wird durch die endogene Aromatase-Aktivität bei gonadal-intakten Mäusen aufrechterhalten. Die vorliegende Arbeit zeigt zudem, dass der klassische Trpm5-Kanal, bekannt aus den Geschmacksrezeptorzellen, ausschließlich in Mikrovillarzellen des olfaktorischen Hauptepithels (MOE) exprimiert wird, aber nicht in adulten olfaktorischen sensorischen Neuronen (OSNs), die eine neuartige kurze und wahrscheinlich nicht-funktionale Spleißvariante enthalten. Der klassische Trpm5 Kanal wird jedoch transient in einer Subpopulation von frühreifen OSNs im embryonalen MOE exprimiert.

Zusammenfassend zeigt die räumliche Trennung der Expression von Trpm4 und Trpm5 im olfaktorischen System, dass diese Kanäle unterschiedliche Rollen übernehmen und funktionell nicht miteinander austauschbar sind. Die vorliegende Arbeit weist auf eine differenzierte Rolle von Trpm4 in der VSN-Signalverarbeitung während sexuell rezeptiver und nicht-rezeptiver Phasen und eine funktionelle Rolle von Trpm5 in OSNs während der embryonalen Entwicklung hin. Abschließend stellt diese Arbeit eine wertvolle Plattform zum Verständnis der Rolle der Trp-Kanäle im olfaktorischen System dar.

## List of figures

Figure 1: Schematic representation of the murine olfactory system.....	1
Figure 2: Anatomy of the MOE and signal transduction of odorant cues .....	3
Figure 3: Anatomy of the VNO and signal transduction of pheromonal stimuli.....	5
Figure 4: Phylogenetic tree of the Trp channel superfamily .....	7
Figure 5: Molecular structure of Trpm4 and Trpm5 .....	8
Figure 6: Hormone levels during the female rodent estrous cycle.....	13
Figure 7: Cellular composition of the vaginal fluid during the estrous cycle .....	31
Figure 8: Ovariectomy of female mice.....	32
Figure 9: Scrotal orchiectomy of male mice .....	33
Figure 10: Schematic representation of hormonal treatment groups.....	34
Figure 11: Hormone reservoir implantation .....	34
Figure 12: Schematic representation of exemestane treatment groups .....	35
Figure 13: Generation of the Trpm4-IC/ $\tau$ GFP mouse.....	37
Figure 14: Transient expression of Trpm4 during MOE development.....	38
Figure 15: RT-PCR analysis of Trpm4 mRNA derived from whole MOE and isolated OSNs.....	40
Figure 16: Trpm4 expression in the developing VNO.....	41
Figure 17: Trpm4 expression in the vomeronasal organ .....	43
Figure 18: RT-PCR analysis of Trpm4 mRNA derived from whole VNO and isolated VSNs.....	44
Figure 19: Colocalization of Trpm4 and Trpc2 in VSNs.....	45
Figure 20: Trpm4 expression in female mice depends on the reproductive stage .....	47
Figure 21: Quantitative RT-PCR shows upregulation of Trpm4 mRNA in females at estrus .....	48
Figure 22: Trpm4 expression in pregnant and senescent female mice .....	49
Figure 23: 17 $\beta$ -estradiol restores OVX induced loss of Trpm4 expression in VSNs.....	51
Figure 24: Progesterone diminishes 17 $\beta$ -estradiol induced Trpm4 expression.....	52
Figure 25: 17 $\beta$ -estradiol restores Trpm4 expression in the ORX male VNO.....	53
Figure 26: Regulation of Trpm4 expression by aromatase function in the female VNO .....	55
Figure 27: Regulation of Trpm4 expression by aromatase function in the male VNO .....	56
Figure 28: Trpm4 and $\tau$ GFP expression in the septal organ of Masera of Trpm4-IC/ $\tau$ GFP mice .....	57
Figure 29: Trpm4 and $\tau$ GFP expression in the Grueneberg ganglion .....	58
Figure 30: Trpm4 and $\tau$ GFP expression in the olfactory bulb.....	59
Figure 31: Reporter gene expression in the MOE of Trpm5-IC/eR26- $\tau$ GFP mice.....	62
Figure 32: Distribution of $\tau$ GFP positive cells in the MOE of Trpm5-IC/eR26- $\tau$ GFP mice .....	63
Figure 33: Reporter gene expression in the MOB of Trpm5-IC/eR26- $\tau$ GFP mice.....	64
Figure 34: Expression of $\tau$ GFP in the accessory olfactory system and in the SOM.....	66
Figure 35: Trpm5 protein expression in the adult MOE.....	67
Figure 36: Specificity and binding sites of Trpm5 antisera .....	68
Figure 37: Trpm5 protein expression during postnatal MOE development.....	69

---

Figure 38: Trpm5 protein is transiently expressed in embryonic OSNs.....	71
Figure 39: Trpm5 and $\tau$ GFP expression in Trpm5-IC/eR26- $\tau$ GFP embryos .....	72
Figure 40: A novel splice variant in a genetically-labeled subpopulation of OSNs .....	74
Figure 41: 5'-RACE-PCR and sequence analysis of Trpm5-9 suggests one putative transmembrane domain.....	76
Figure 42: 3'RACE-PCR in search for additional Trpm5 splice variants.....	77
Figure 43: Role of Trpm4 in female VSNs during periods of high receptivity .....	92

## List of tables

Table 1: Chemicals and enzymes .....	17
Table 2 : Antibodies and sera.....	18
Table 3: Critical commercial kits and compounds .....	20
Table 4: Oligonucleotides.....	20
Table 5: Consumables and equipment.....	21
Table 6: Software .....	22
Table 7: cDNA synthesis .....	24
Table 8: RT-PCR reaction solution content.....	24
Table 9: RT-PCR.....	25
Table 10: RACE-PCR.....	26
Table 11: qRT-PCR.....	27

## Abbreviations

<b>ACIII</b>	Adenylyl cyclase 3
<b>AOB</b>	Accessory olfactory bulb
<b>B6</b>	C57B6/N
<b>bp</b>	Base pair
<b>°C</b>	Degree Celsius
<b>CAGS</b>	Chicken $\beta$ -actin promoter and CMV enhancer
<b>CMV</b>	Cytomegalovirus
<b>CNG</b>	Cyclic nucleotide gated
<b>Cre</b>	Cyclization recombinase
<b>CTX</b>	Cortex
<b>D</b>	Diestrus
<b>DAG</b>	Diacylglycerol
<b>DMEM</b>	Dulbecco 's modified eagle medium
<b>DNA</b>	Deoxyribonucleic acid
<b>dNTP</b>	Desoxyribonucleotide-5'-trisphosphate
<b>DPBS</b>	Dulbecco's Phosphate-buffered saline
<b>dr</b>	Dorsal roof
<b>E</b>	Estrus
<b>E2</b>	17 $\beta$ -estradiol
<b>E(1)</b>	Embryonic day 1
<b>EDTA</b>	Disodium-ethylene diamine-tetra acidic acid
<b>EGFP</b>	Enhanced green fluorescent protein
<b>EXE</b>	Exemestane
<b>FPR</b>	Formyl peptide receptor
<b>FSH</b>	Follicle stimulating hormone
<b>g</b>	Gram or g-force
<b>Gap43</b>	Growth associated protein 43
<b>GAPDH</b>	Glyceraldehyde-3-Phosphate Dehydrogenase

<b><math>\tau</math>-GFP</b>	tau-GFP fusion protein
<b>GD (1)</b>	Gestational day 1
<b>GG</b>	Grueneberg ganglion
<b>GGN</b>	Grueneberg ganglion neuron
<b>GFP</b>	Green fluorescent protein
<b>GL</b>	Glomerular layer
<b>h</b>	Hour
<b>HPG</b>	Hypothalamic-pituitary-gonadal axis
<b>IC</b>	IRES-Cre
<b>ICC</b>	Immunocytochemistry
<b>IF</b>	Interference
<b>IHC</b>	Immunohistochemistry
<b>i.p.</b>	Intraperitoneal
<b>IP<sub>3</sub></b>	Inositol 1,4,5-triphosphate
<b>ir</b>	Immunoreactivity/Immunoreactive
<b>IRES</b>	Internal ribosome entry site
<b>LH</b>	Luteinizing hormone
<b>L</b>	Litre
<b>LP</b>	Long pass
<b>M</b>	Metestrus or Molar
<b>m</b>	Meter
<b><math>\mu</math>~</b>	Micro
<b>MCL</b>	Mitral cell layer
<b>min</b>	Minutes
<b>MOB</b>	Main olfactory bulb
<b>MOE</b>	Main olfactory epithelium
<b>mRNA</b>	Messenger RNA
<b>MV</b>	Microvillar/ microvilli
<b>n</b>	Number of performed experiments/of animals
<b>n~</b>	Nano (meter)
<b>NL</b>	Nerve layer

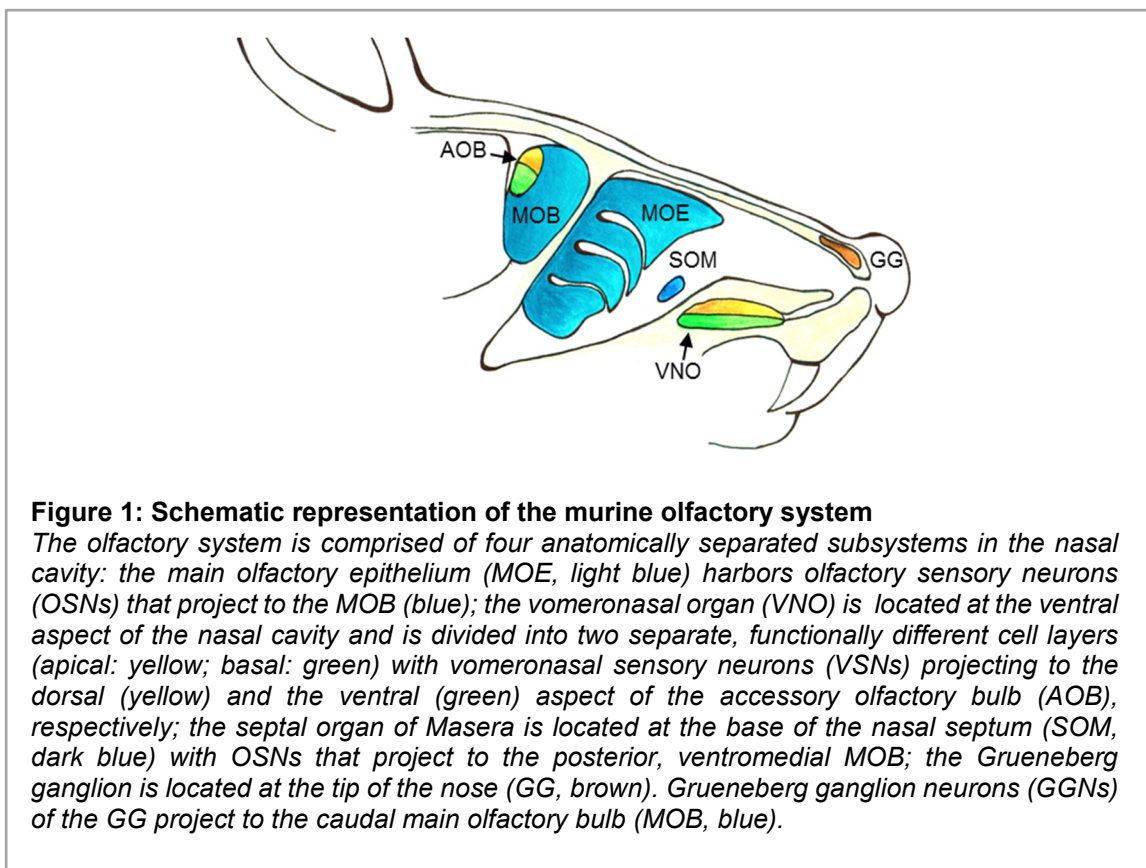
<b>ns</b>	Non-significant
<b>OB</b>	Olfactory bulb
<b>OD</b>	Optical density
<b>OSN</b>	Olfactory sensory neuron
<b>OMP</b>	Olfactory marker protein
<b>OR</b>	Olfactory receptor
<b>ORX</b>	Orchiectomy/Orchiectomized
<b>OVX</b>	Ovariectomy/Ovariectomized
<b>P</b>	Proestrus
<b>P4</b>	Progesterone
<b>PBS</b>	Phosphate buffered saline
<b>PFA</b>	Paraformaldehyde
<b>PIP<sub>2</sub></b>	Phosphoinositol-4,5-bisphosphate
<b>qRT-PCR</b>	Quantitative real-time RT-PCR
<b>rpm</b>	Rounds per minute
<b>RACE</b>	Rapid amplification of cDNA ends
<b>RNA</b>	Ribonucleic acid
<b>RNase</b>	Ribonuclease
<b>RT</b>	Room temperature
<b>RT-PCR</b>	Reverse-transcriptase polymerase chain reaction
<b>s</b>	Second
<b>SD</b>	Standard deviation
<b>SDS</b>	Sodium dodecyl sulphate
<b>SEM</b>	Standard error of the mean
<b><math>\tau</math>-protein</b>	small microtubule-associated protein
<b>TAAR</b>	trace-amine associated receptor
<b>TM</b>	Transmembrane domain
<b>tRNA</b>	Transfer RNA
<b>Trp</b>	Transient receptor potential
<b>Trpa</b>	Transient receptor potential, ankyrin
<b>Trpc</b>	Transient receptor potential, canonical/classical

<b>Trpm</b>	Transient receptor potential, melastatin
<b>Trpm1</b>	Transient receptor potential, mucolipin
<b>Trpn</b>	Transient receptor potential, no mechanopotential
<b>Trpp</b>	Transient receptor potential, polycystin
<b>Trpv</b>	Transient receptor potential, vanilloid
<b>SOM</b>	Septal organ of Masera
<b>UV</b>	Ultraviolet
<b>V</b>	Volt
<b>V1R</b>	Vomeronasal receptor type 1
<b>V2R</b>	Vomeronasal receptor type 2
<b>VNO</b>	Vomeronasal organ
<b>VSE</b>	Vomeronasal sensory epithelium
<b>VSN</b>	Vomeronasal sensory neuron
<b>v/v</b>	Volume per volume
<b>W</b>	Week
<b>w/v</b>	Weight per volume
<b>Wt</b>	Wild type

# 1 Introduction

## 1.1 The murine olfactory system

The sense of smell, olfaction, is crucial for the survival of an organism. Olfaction enables to assess the environment through volatile and non-volatile compounds and guides a large variety of behavioral responses, like foraging, mating, nesting, inter-, and intraspecific communication. Furthermore, the sense of smell can alert to dangers, like rotten food, toxic environments, or predator species (Restrepo *et al.*, 2004; Tirindelli *et al.*, 2009; Bleyemehl *et al.*, 2016). These tasks are performed by the olfactory system through recognition and conversion of molecular cues into electrical information, which in turn is processed by the brain. In rodents, the olfactory system is comprised of four anatomically segregated subsystems in the nasal cavity (Figure 1). (1) The main olfactory epithelium (MOE), which occupies the largest area of the nasal cavity is responsible for the common sense of smell (Firestein 2001; Munger *et al.*, 2009). (2) The vomeronasal organ (VNO), located on the base of the nasal cavity, conveys information about pheromonal cues, and thereby induces social and sexual behaviors (Zufall *et al.*, 2005, Brennan and Zufall, 2006; Chamero *et al.*, 2012; Wyatt 2014; Trouillet *et al.*, 2019).



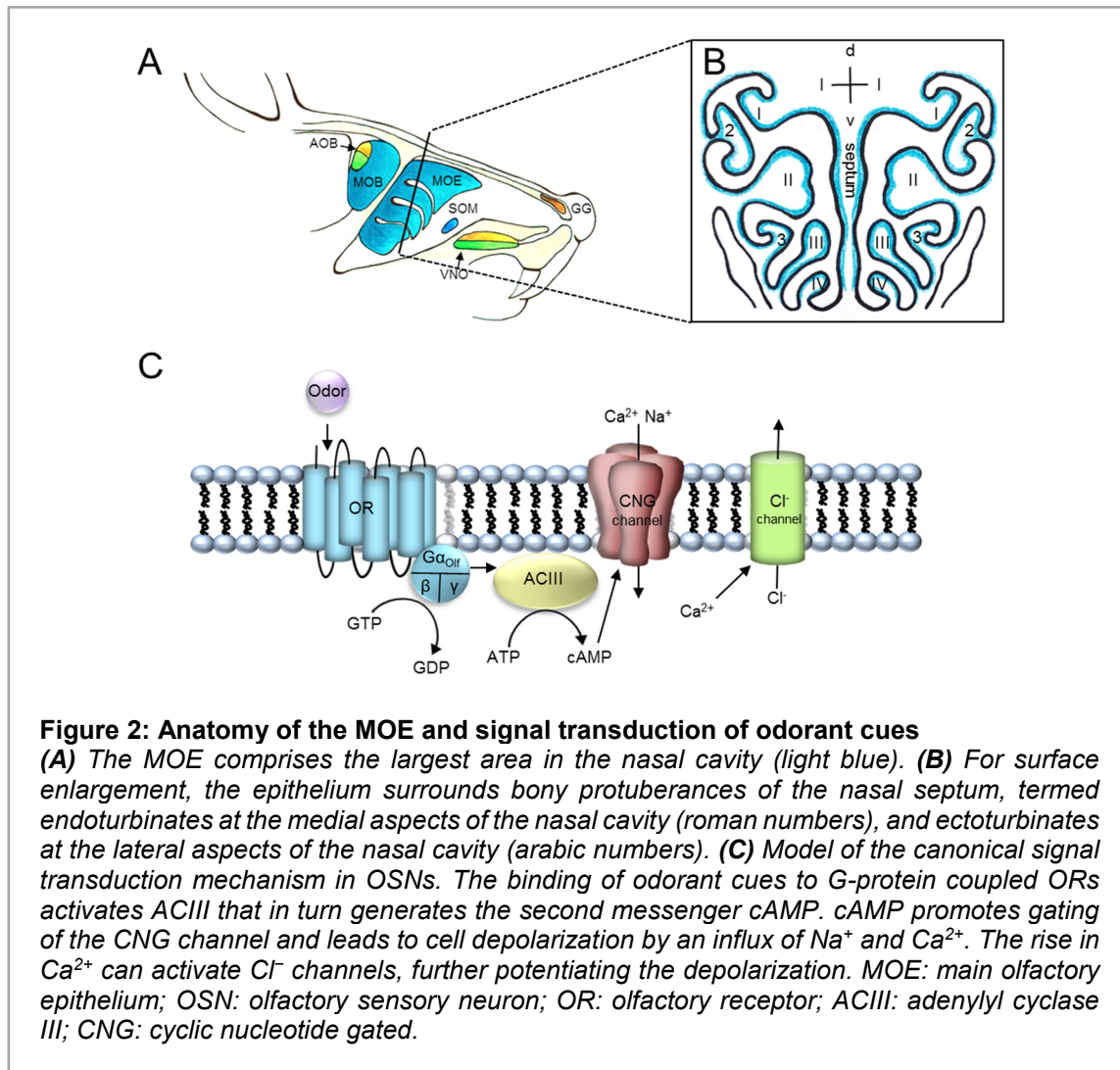
(3) the Grueneberg ganglion (GG), located at the tip of the nose, is responsible for fear- and stress-evoked behaviors through detection of predator odors, volatile alarm pheromones, and cold temperatures (Brechbuhl *et al.*, 2008; Schmid *et al.*, 2010; Pérez-Gómez *et al.*, 2015). (4) The septal organ of Masera (SOM), located at the ventral base of the nasal septum, is a separated island of the MOE and similar to the MOE detects volatile odorants. A specific function of the SOM has yet to be determined (Ma *et al.*, 2003; Tian and Ma 2004).

### 1.1.1 Structure and function of the main olfactory epithelium (MOE)

The MOE is a pseudostratified epithelium lining the dorsal aspect of the nasal cavity, including the dorsal roof, the endo- and ectoturbinates, and the dorsal nasal septum (Figure 2A,B). It is covered by a thin layer of mucus and contains different cell types of neuronal and non-neuronal origin, differing in morphology and function. The major cell type of the MOE is olfactory sensory neurons (OSNs) that are the main detectors of general odorants (Munger *et al.*, 2009; Touhara *et al.*, 2009; Rodriguez, 2013; Low and Mombaerts, 2017). All cells, including OSNs, regenerate from a pool of mitotically active stem cells. Non-neuronal cells are basal stem cells, Bowman gland cells, sustentacular cells, and microvillar (MV) cells (Hansen and Finger 2008; Lin *et al.*, 2008; Elsaesser and Paysan 2008; Hegg *et al.*, 2010; Ogura *et al.*, 2011). Compounds like semiochemicals can also be detected by the MOE, resulting in hormonal changes and specific behaviors in mice (Pérez-Gómez *et al.*, 2015; Zufall and Leinders-Zufall 2007; Liberles 2014).

OSNs are bipolar neurons, exhibiting a single dendrite and a single axon at the apical and the basal soma, respectively. The dendritic process protrudes towards the luminal surface, terminating in a dendritic knob, that is populated with approximately 10 cilia (Menco 1983). OSN axons in contrast, protrude beyond the basal lamina of the MOE, group into axon bundles that further project towards the main olfactory bulb (MOB). Here, OSN axon terminals form the first olfactory synapse, organized in ball-like structures of neuropil (glomeruli), located in the glomerular layer of the MOB (Mombaerts 2006; Soucy *et al.*, 2009). The vast majority of OSNs are classical or canonical OSNs that transduce olfactory cues in a G protein-coupled, cAMP-mediated cascade. They are characterized by ciliary membrane expression of one member of the large family of more than 1000 odor receptor (OR) genes (Buck and Axel 1991; Mombaerts 2004; Rodriguez, 2013; Saraiva *et al.*, 2015). ORs belong to the superfamily of G protein-coupled receptors and

mediate olfactory signal transduction (Fleischer, Bree and Strotmann, 2009; Low and Mombaerts, 2017).



In detail, odor perception is characterized by binding of odorants to specific odorant receptor (OR) proteins (Figure 2C). This process triggers an intra-ciliary signal transduction cascade, which includes binding of guanosine triphosphate (GTP) by the G-protein  $G_{\text{Olf}}$ , leading to activation of the G-protein's  $\alpha$ -subunit. The activated  $G_{\alpha\text{Olf}}$  stimulates the membrane bound adenylyl cyclase III (ACIII) to convert adenosine triphosphate (ATP) to cyclic adenosine monophosphate (cAMP). The rise in cAMP in turn results in opening of a cyclic nucleotide gated cation channel (CNG). The CNG channel contributing to olfactory signal transduction is composed of the subunits Cnga2, Cnga4, and Cngb1b (Zheng and Zagotta, 2004; Nache *et al.*, 2016), and by its activation causes an influx of  $\text{Na}^+$  and  $\text{Ca}^{2+}$  ions, which results in an initial depolarization of the ciliary membrane (Pifferi *et al.*, 2006; Munger *et al.*, 2009). Moreover, the elevation in

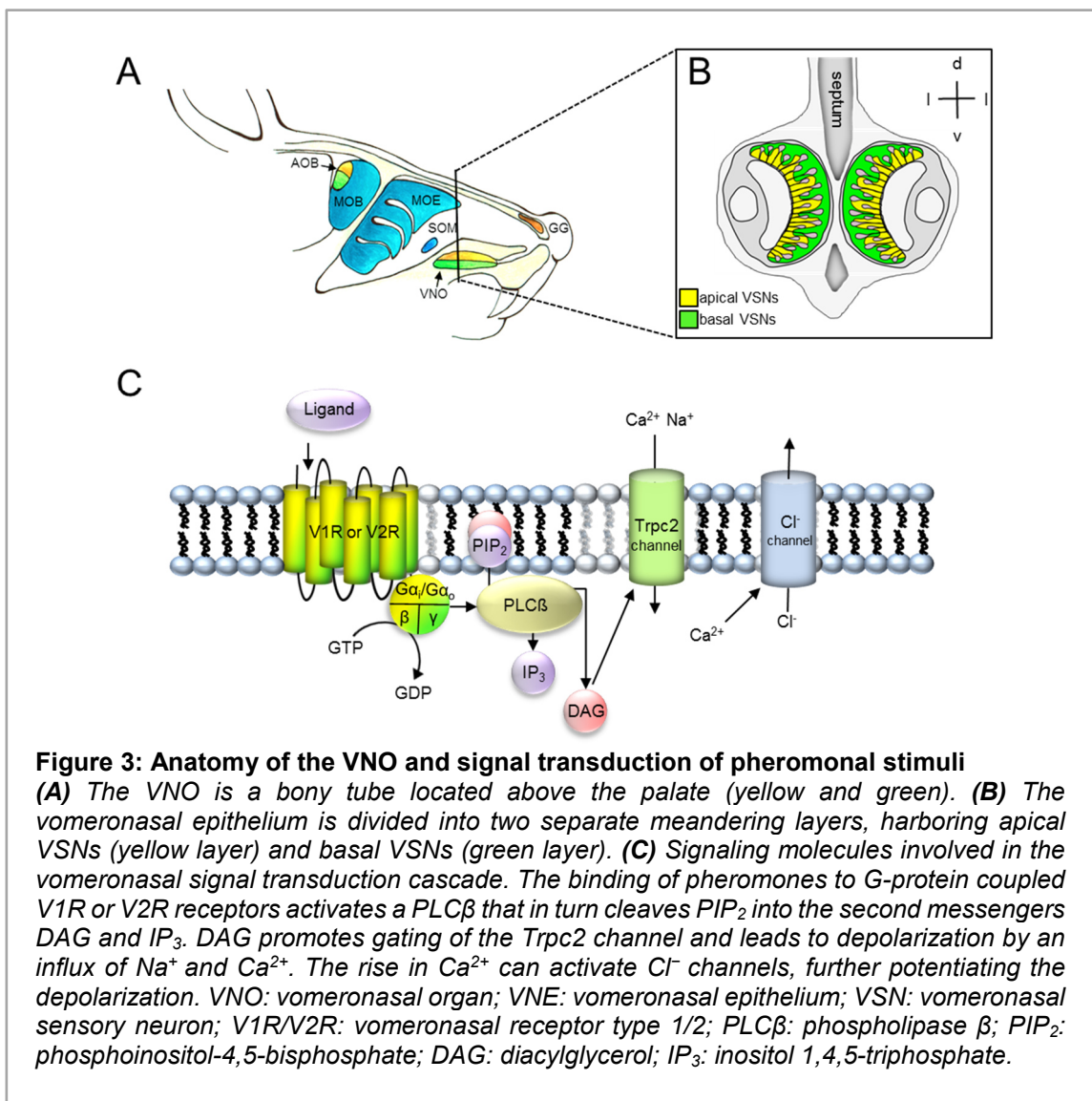
$\text{Ca}^{2+}$  leads to opening of  $\text{Ca}^{2+}$ -activated chloride channels and an efflux of  $\text{Cl}^-$  resulting in enhanced depolarization of the cell and subsequent generation of action potentials (Lowe and Gold, 1993). But not only canonical OSNs exist in the MOE. The olfactory system includes additional subpopulations of OSNs that detect molecular cues different from canonical OSNs. For example, OSNs that belong to the GC-D system express the guanylyl cyclase type D (GC-D) and the channel subunit *Cnga3* that employs cGMP in the signal transduction (Zufall and Munger, 2010), or OSNs that belong to the TAAR system express members of the trace-amine associated receptor family (TAARs) (Liberles and Buck 2006; Pacifico *et al.*, 2012; Johnson *et al.*, 2012; Liberles, 2015). TAAR expressing OSNs determine the olfactory sensitivity towards amines and induce innate responses towards predator derived odors (Ferrero *et al.*, 2011; Dewan *et al.*, 2013). However, they employ the same olfactory signal transduction cascade as OR-expressing OSNs (Zhang *et al.*, 2013).

### 1.1.2 Structure and function of the vomeronasal organ (VNO)

The VNO is a bilaterally symmetrical structure at the ventral site of the nasal cavity located below the nasal septum (Figure 3A). This tubular structure harbors the sensory epithelium (VNE) at its medial aspects, and the non-sensory epithelium at its lateral aspects (Figure 3B). The VNE is a pseudostratified epithelium, which functions in pheromone and semiochemical recognition (Tirindelli *et al.*, 2009; Pérez-Gómez *et al.*, 2015; Wyatt, 2014). The VNO is in contact to the environment through an opening into the nasal cavity, the vomeronasal duct. Three cell types are present in the VNE: Sustentacular cells, progenitor cells, and vomeronasal sensory neurons (VSNs). The morphology of VSNs is similar to that of OSNs, with an apical dendrite and a basal axon. VSN axons project to the accessory olfactory bulb (AOB) and dendritic knobs of VSNs are populated by microvilli instead of cilia as found in OSNs (Münch *et al.*, 2018).

The VNE is divided into two functionally different cell layers, apical and basal (Figure 3), based upon specific ligands, a specific expression of pheromone receptors, and components of the signal transduction cascade, for example the differential expression of the G-protein  $\alpha$ -subunits  $G_i$  (apical VSNs) and  $G_o$  (basal VSNs). Pheromone receptors are expressed on VSN microvilli membranes and mediate pheromone recognition. VSNs belonging to the apical VNE express vomeronasal type 1 receptors (V1R; Rodriguez *et al.*, 2002; Pérez-Gómez *et al.*, 2014) and play a key role as detectors for small volatile substances in urine of conspecifics and sulfated steroid hormones (Leinders-Zufall *et al.*, 2000). In mice, their function is implicated in sexual and social behaviors. For example,

in females, detection of male urine can induce reproductive cyclicity or act on the estrous cycle prolonging the time window for fertilization (Novotny *et al.*, 1999). Basal VSNs mainly express vomeronasal type 2 receptors (V2R; Rodriguez *et al.*, 2002; Pérez-Gómez *et al.*, 2014) and recognize non-volatile protein ligands. For example, major urinary proteins (MUPS), which induce female estrus and male to male aggression (Chamero *et al.*, 2007; Papes *et al.*, 2010; Chamero *et al.*, 2011; Thoß *et al.*, 2019), or the sex-specific exocrine gland-secreted peptide 1 (ESP1), which potentiates female receptive behavior (e.g. lordosis) (Haga *et al.*, 2010). Subpopulations of basal VSNs can furthermore express one member of the nonclassical class I major histocompatibility complex genes (MHC) (Ishii *et al.*, 2003; Loconto *et al.*, 2003). Expression of the MHC-receptor gene H2-Mv is reported to enhance vomeronasal sensitivity towards pheromones (Leinders-Zufall *et al.*, 2014). In addition, a third group of vomeronasal receptors is described in a small subpopulation of VSNs, the N-formylated peptide receptors (FPRs; Liberles *et al.*, 2009; Riviere *et al.*, 2009).



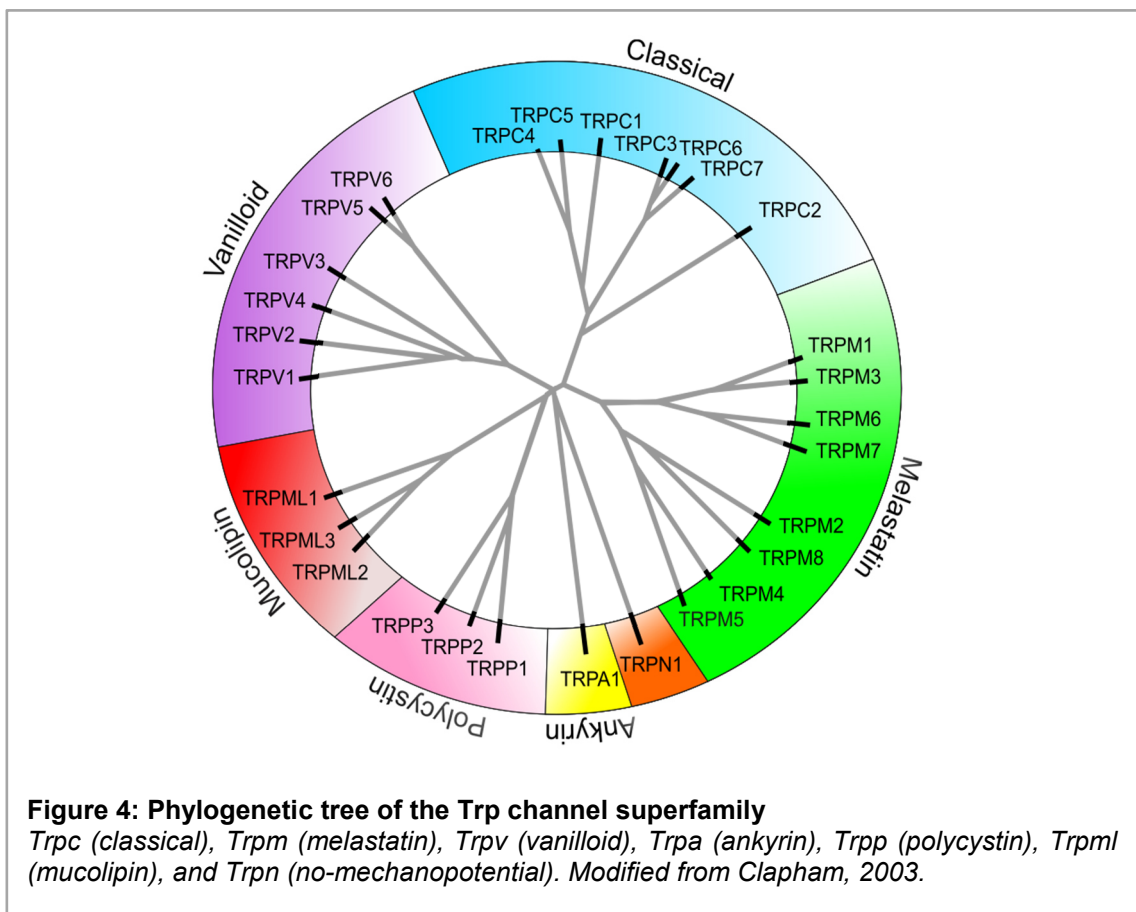
FPR expressing VSNs are thought to be involved in pathogen sensing (Bufe *et al.*, 2012; Dietschi *et al.*, 2017).

The initial steps of pheromone detection are characterized by ligand binding to specific pheromone receptors expressed in VSN microvilli (Figure 3C). Similar to the MOE, receptors are G-protein coupled and ligand binding induces the activation and dissociation of the  $\beta\gamma$ -subunit of the G-protein  $\alpha$ -subunit  $G_i$  (apical VSNs) or  $G_o$  (basal VSNs) (Rodriguez *et al.*, 2002; Chamero *et al.*, 2012). The  $\beta\gamma$ -subunit in turn, activates phospholipase C ( $PLC\beta$ ) to hydrolyze phosphatidylinositol 4,5-bisphosphate ( $PIP_2$ ) to inositol trisphosphate ( $IP_3$ ) and diacylglycerol (DAG) (Lucas *et al.*, 2003; Leinders-Zufall *et al.*, 2018). The key channel of the vomeronasal pheromone transduction machinery is the canonical Trp-channel  $Trpc2$  (Liman *et al.*, 1999; Stowers *et al.*, 2002; Lucas *et al.*, 2003).  $Trpc2$  is activated by DAG and induces  $Ca^{2+}$  and  $Na^+$  influx resulting in a receptor potential (Miller, 2014). Recently,  $Trpc2$  activation by DAG in mouse VSNs has been analyzed by employing photoswitchable DAG (PhoDAG) in combination with  $Ca^{2+}$  imaging, providing a suitable tool for a better understanding of DAG-dependent activation of Trp channels (Leinders-Zufall *et al.*, 2018). The rise in intracellular  $Ca^{2+}$ , induced by  $Trpc2$  activity, leads to an efflux of  $Cl^-$  ions through  $Ca^{2+}$ -activated chloride channels, further potentiating the receptor potential, generating an action potential (Kim *et al.*, 2011; Münch *et al.*, 2018).  $Trpc2$  is expressed in both the apical and the basal layer of the VNO (Liman *et al.*, 1999). Its important function has been shown in  $Trpc2$  knockout mice that displayed impairments in the vomeronasal detection of urinary signals and in sexual behaviors (Leypold *et al.*, 2002; Stowers *et al.*, 2002; Kimchi *et al.*, 2007; Chamero *et al.*, 2007; Haga *et al.*, 2010; Ferrero *et al.*, 2013). Furthermore, several studies have suggested an important and direct role of  $IP_3$  in VSN signal transduction in mammalian and non-mammalian species (Sasaki *et al.*, 1999; Gjerstad *et al.*, 2003) where  $IP_3$  receptor type 3 ( $IP_3R3$ ) is in direct contact with  $Trpc2$  and is implicated in the channels' activation (Brann *et al.*, 2002). However, a recent study on  $IP_3R3$ -knockout mice has shown that  $Trpc2$  activation and primary signal transduction in VSNs is independent from  $IP_3R3$  function (Chamero *et al.*, 2017).

## 1.2 The superfamily of Transient receptor potential channels (Trp)

Trp channels play an important role as physiological sensors towards external environmental stimuli by promoting chemosensation, photosensation, thermosensation, and mechanosensation (Damann, Voets, and Nilius, 2008; Nelson, Beck and Cheng 2011). Of particular interest for this study are Trp-channels and their role in olfaction. For

example, Trpc2 and its role as key component in the vomeronasal pheromone transduction (see also 1.3) (Liman *et al.*, 1999; Stowers *et al.*, 2002; Lucas *et al.*, 2003; Lin *et al.*, 2007; Munger *et al.*, 2009; Zufall, 2014; Bleyemehl *et al.*, 2016; Lopez *et al.*, 2014). The family of transient potential (Trp) channels describes one of the largest families of ion channels that can be categorized into 7 subgroups based on amino acid sequence homology (Figure 4): Trpc (Classical), Trpa (Ankyrin), Trpv (Vanilloid), Trpm (Melastatin), Trpp (Polycystin), Trpml (Mucolipin) and Trpn (no mechanopotential) (Venkatachalam and Montell 2007).

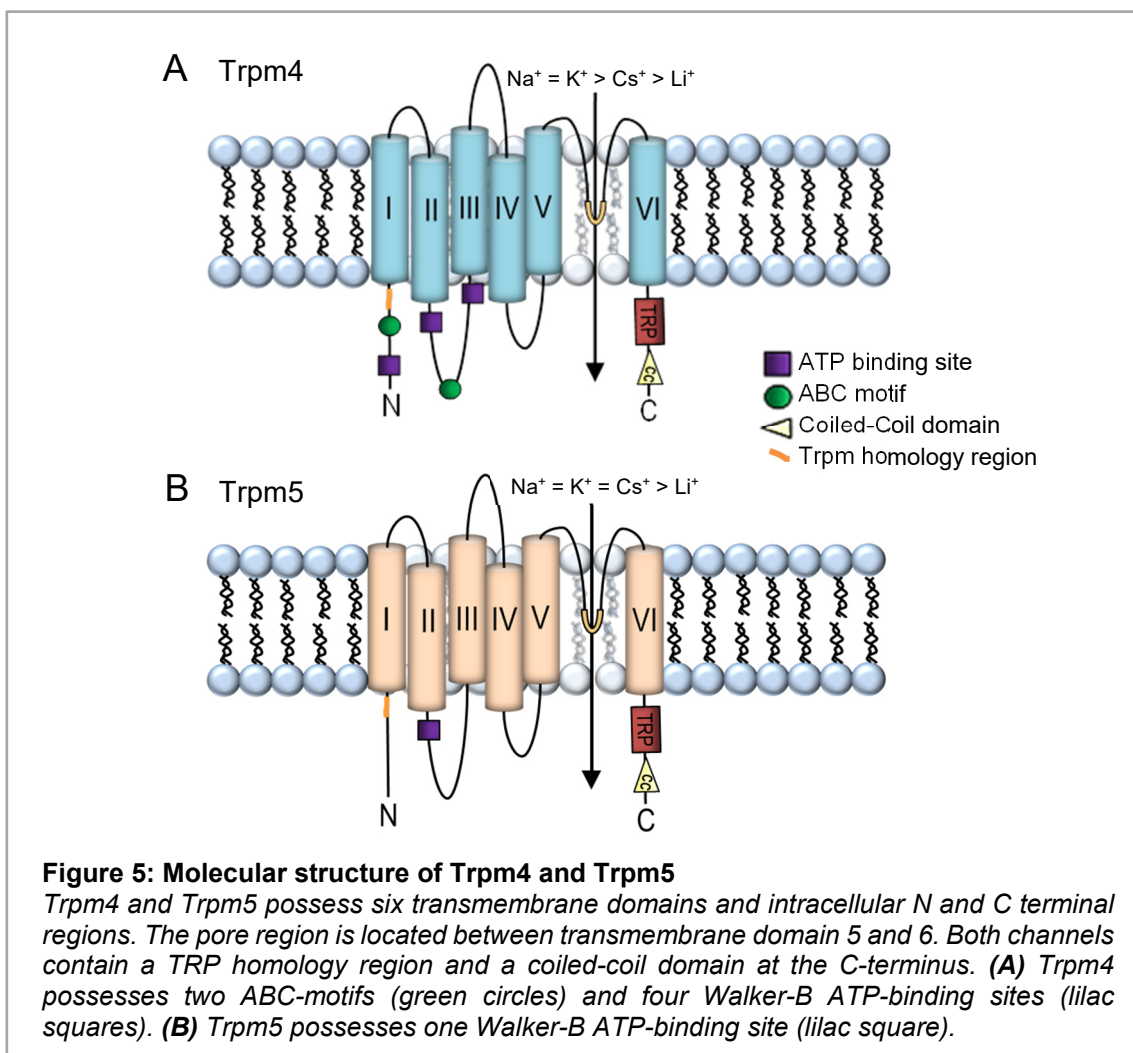


Trp channels possess six transmembrane domains with a pore region between transmembrane domain 5 and 6 and have cytosolic N- and C-termini (Figure 5) (Nelson, Beck and Cheng, 2011). Every functional channel is composed of four subunits, with each monomeric structure contributing to the formation of the selectivity filter and the channel pore (Ramsey, Delling and Clapham, 2006). At the N- and C- termini several commonly present ligand-, channel-, and protein interaction sites are located, such as ankyrin repeats, coiled-coil domains, or the TRP box (Figure 5). Furthermore, characteristic, and unique regions for individual Trp channel families are found at the termini, for example enzymatic or kinase motifs (Nelson, Beck and Cheng, 2011). Most

of the Trp channels permeate  $\text{Ca}^{2+}$  ions, except two members of the transient receptor melastatin family, Trpm4 and Trpm5 (Launay *et al.*, 2002; Prawitt *et al.*, 2003; Nilius *et al.*, 2003). Today, it is believed that almost every cell in both vertebrates and invertebrates expresses a specific subset of different Trp proteins (Owsianik *et al.*, 2006a).

### 1.2.1 Trpm4 and Trpm5

The Trpm family consists of 8 members (Trpm1 to Trpm8), which are grouped into Trpm1/3, Trpm4/5, and Trpm6/7 based on amino acid sequence homology. Trpm2 and Trpm8 are not grouped (Figure 4). Trpms, within this subfamily, have diverse functions and mechanisms of activation. Trpm1 for example contributes to the retinal ON bipolar response pathway and is implicated in melanoma progression (Koike *et al.*, 2010, Hantute-Ghesquier *et al.*, 2018).



Other Trpms like Trpm2, Trpm6 and Trpm7 exhibit enzymatic activities, through domains that act as ADP-ribose pyrophosphatase, and an alpha-kinase domain, implicated in channel regulation (Nilius and Owsianik, 2011). Trpm4 and Trpm5 function in the olfactory system are the focus of my study.

The structure of Trpm4 and Trpm5 is similar to other members of the Trp superfamily with 6 transmembrane domains and an ion conducting pore region between transmembrane domains 5 and 6 (Figure 5) (Montell *et al.*, 2002; Clapham, 2003). However, these two channels are the only members that cannot conduct  $\text{Ca}^{2+}$  ions, but solely monovalent cations, due to the presence of six acidic amino acids in the pore loop region (Launay *et al.*, 2002; Prawitt *et al.*, 2003; Nilius *et al.*, 2003). Furthermore, Trpm4 and Trpm5 are the only members of the Trp-channel family that are activated by a rise in intracellular  $\text{Ca}^{2+}$  concentration (Xu *et al.*, 2001; Launay *et al.*, 2002; Nilius *et al.*, 2003; Prawitt *et al.*, 2003).

In mice, Trpm4 is a 1213 amino acid protein, with its gene located on chromosome 7. Cloning experiments using Trpm4 cDNA revealed the existence of a total of 4 splice variants in mice. Of these only one splice variant, termed Trpm4b, is described to encode the functional Trpm4 ion channel (Xu *et al.*, 2001; Launay *et al.*, 2002; Nilius *et al.*, 2003). Shorter splice variants lacking multiple amino acids at the N-or the C-terminus also exist. However, their exact physiological role has yet to be determined. The gene for the closest relative of Trpm4 with 40% amino acid sequence homology, Trpm5, is also located on mouse chromosome 7. It encodes a protein with a length of 1158 amino acids (Enklaar *et al.*, 2000). Seven shorter splice variants are annotated in the Ensembl genome browser database, however, only the full-length variant containing all of the 1158 amino acids is described to encode a functional channel.

The Trpm4 protein sequence possesses several protein interaction domains located at the N- and C-terminus, such as putative calmodulin binding domains, ATP-binding sites, a  $\text{PIP}_2$  binding site, two ABC motifs and phosphorylation sites for the protein kinases PKA and PKC (Figure 5A, Xu *et al.*, 2001; Launay *et al.*, 2002; Nilius *et al.*, 2003). In contrast, Trpm5 possesses solely one ATP-binding site near transmembrane domain 2 that is likely inaccessible to ATP (Figure 5B) (Ullrich *et al.*, 2005). A common feature of the two channels is the presence of the Trp-typical homology region and the coiled-coil domain at the C-terminus. (Nilius *et al.*, 2005b). Both channels can be modulated by temperature,  $\text{PIP}_2$ , and voltage. Furthermore, modulation of Trpm5 by pH and modulation of Trpm4 by ATP has been reported (Hofmann *et al.*, 2003; Prawitt *et al.*, 2003; Talavera *et al.*, 2005; Wu *et al.*, 2010; Liman, 2014).

The expression of Trpm4 is ubiquitous in a large variety of excitable cells, such as various types of neurons, and vascular and smooth muscle cells (Zufall, 2014). Furthermore, Trpm4 expression has been reported in the murine cochlea, where it may contribute to the signal transduction in inner hair cells (Sakuraba *et al.*, 2014). Trpm4 expression was also described in non-excitabile cells, such as red blood cells, pancreatic cells, mast cells, vascular endothelial cells, adipocytes, and in renal tubule cells (Zufall, 2014).

Trpm5 expression was first described in taste receptor cells of the tongue, driving the sensory transduction for sweet, bitter, and umami detection (Perez *et al.*, 2002; Zhang *et al.*, 2003). In the following years, Trpm5 was also detected in pancreatic tissue, solitary chemosensory cells of the digestive tract, and in the respiratory system (Bezencon *et al.*, 2007; Kaske *et al.*, 2007; Kokrashvili *et al.*, 2009; Lin *et al.*, 2008a; Prawitt *et al.*, 2003; Brixel *et al.*, 2010; Colsoul *et al.*, 2010). In 2017, Banik *et al.*, discovered that besides Trpm5 also Trpm4 is involved in taste-evoked signaling and that detection of bitter, sweet, and umami is disrupted upon deletion of both Trpm4 and Trpm5.

### 1.3 Trp channel expression and function in the olfactory system

Several members of the Trp-family contribute to the function of the main and accessory olfactory system (Zufall, 2014). Trpc2 is so far the most studied Trp in the vomeronasal system (Liman *et al.*, 1999; Leybold *et al.*, 2002; Stowers *et al.*, 2002). Trpc2 is highly expressed in VSN microvilli, suggesting the central role in the process of chemosignal transduction in VSNs (Liman *et al.*, 1999; Menco *et al.*, 2001; Lucas *et al.*, 2003; Zufall *et al.*, 2005). Function of Trpc2 in VSNs was confirmed by deletion of the Trpc2 gene, resulting in severe changes in a large variety of social and sexual behaviors in mice (Leybold *et al.*, 2002; Stowers *et al.*, 2002; Chamero *et al.*, 2007, Kimchi *et al.*, 2007). Male and maternal aggression towards intruders was significantly reduced in knockout animals, whereas mounting behavior was no longer confined to females in Trpc2 mutant males (Leybold *et al.*, 2002; Stowers *et al.*, 2002; Chamero *et al.*, 2007, Kimchi *et al.*, 2007). Nonetheless, there is evidence that function of Trpc2 is not exclusively responsible for the pheromone-induced activation of VSNs and that a mutation of the Trpc2 gene not completely abolishes VNO function (Kelliher *et al.*, 2006; Yang and Delay, 2010; Kim *et al.*, 2011; Yu, 2015). This allows the assumption that other Trp channels besides Trpc2 may be involved in VNO activation. Interestingly, functional analyses suggest a possible role for Trpm4 in VNO function, as Trpm4-like currents were recorded in hamster and murine VSNs (Liman 2003; Spehr *et al.*, 2009). However, no information is available on Trpm4 expression in the olfactory system.

Trpc2 expression was additionally reported in a small subpopulation of OSNs in the MOE, the type B cells (Omura and Mombaerts, 2014; Bleymehl *et al.*, 2016). These cells differ fundamentally from classical OSNs and VSNs. They express the cyclic nucleotide-gated channel subunit Cnga2 in combination with the soluble guanylate cyclase Gucy1b2 but lack expression of odorant receptors, vomeronasal receptors, or trace amine-associated receptors (Omura and Mombaerts, 2014; Omura and Mombaerts, 2015; Saraiva *et al.*, 2015). A recent study discovered a fundamental role of these cells in the detection of low environmental oxygen, supposedly functioning as an early alarm system (Bleymehl *et al.*, 2016). Furthermore, Bleymehl *et al.*, proposed 2017 a new model of OSN signaling for low oxygen detection, in which Trpc2 functions independently from Cnga2, and requires Gucy1b2 and a cGMP-activated protein kinase.

In addition to Trpc2, the Ca<sup>2+</sup>-activated monovalent-selective cation channel Trpm5 was extensively investigated in the olfactory system. Trpm5 is reported to be expressed in a subpopulation of OSNs and MV cells (Lin *et al.*, 2007; Oshimoto *et al.*, 2013). In 2006, the generation of a transgenic mouse line, the Trpm5-GFP mouse, in which enhanced green fluorescent protein (eGFP) is expressed under a partial sequence of the Trpm5 promoter, revealed GFP expression in a large group of cells within the MOE (Clapp *et al.*, 2006). In detail, GFP-positive neurons were detected at the ventro-lateral aspects of the MOE with projections towards the ventral, medial, and lateral MOB (Lin *et al.*, 2007). It was shown that these cells are OMP-positive and contain PLC $\beta$ 2, Cnga2, and the G-protein subunit G<sub>v13</sub>, which are important elements of the cAMP- and PIP<sub>2</sub>-mediated signaling cascade (Lin *et al.*, 2007). Furthermore, to assess whether Trpm5-GFP positive OSNs can function as pheromone sensors in the MOE, functional studies were performed using the putative pheromone 2,5-dimethylpyrazine and the semiochemical (methylthio)methanethiol (MTMT). Both substances are contained in male urine and induce attractive behaviors in female mice (Thompson *et al.*, 2004; Li and Liberles, 2015). These studies propose that Trpm5-GFP positive OSNs may function in pheromonal signal transduction (Lin *et al.*, 2007; Oshimoto *et al.*, 2013; Lopez *et al.*, 2014). To further characterize GFP-positive OSNs from the Trpm5-GFP mouse, Baxter *et al.*, 2019 performed RNA sequencing of these cells. They found that GFP-positive OSNs showed heightened expression levels of transcripts associated with immunity and inflammation, and that number of GFP-expressing OSNs varies depending on environmental conditions (Baxter *et al.*, 2019).

Contrasting these results, *in situ* hybridization analyses of the MOE using the full-length coding region of Trpm5 detected the channel solely in MV cells but not in OSNs (Yamaguchi *et al.*, 2014; Yamashita *et al.*, 2017; Pyrski *et al.*, 2017). Similar results were

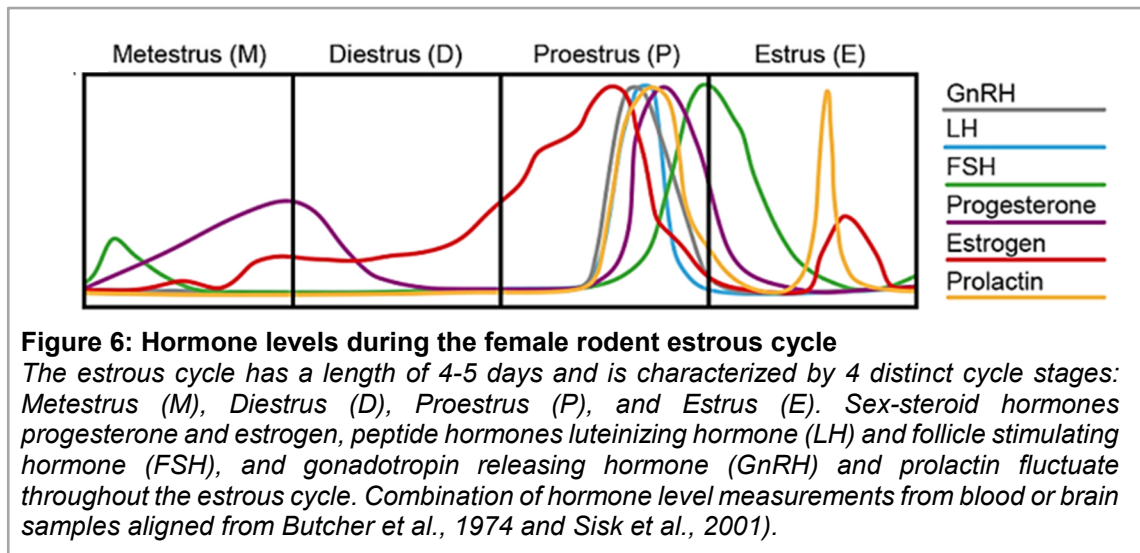
obtained by immunohistochemistry (Kusumakshi *et al.*, 2015). MV cells are described as non-sensory cells as they do not possess any axonal projections which might connect them to the MOB, and as they do not express any specific compounds of the olfactory transduction mechanism (Kaske *et al.*, 2007; Lin *et al.*, 2007; Hansen and Finger 2008; Lin *et al.*, 2008b; Yamaguchi *et al.*, 2014). Instead, some of the Trpm5-positive MV cells are in the immediate vicinity of the trigeminal nerve endings and receive cholinergic input, responding to stimuli like odorous chemicals, bacterial lysates, and ATP (Ogura *et al.*, 2011). Electro-olfactogram measurements in mice lacking Trpm5-MV cells (Lemons *et al.*, 2017) have shown reduced responses towards odors and pheromones after being exposed to high concentration odor chemicals. Thus, these cells may support both the detection of harmful stimuli, and the protection and maintenance of olfactory function by cholinergic modulation (Hansen and Finger 2008; Ogura *et al.*, 2011; Lemons *et al.*, 2017). To this end it is not clear whether OSNs express Trpm5 protein or if its expression is restricted to MV cells.

Another population of MV cells expresses Trpc6 (Elsaesser *et al.*, 2005). These cells are negative for Trpm5, they possess a single basal process protruding towards the basal lamina, and express PLC $\beta$ 2 and IP $_3$ R3 (Hansen and Finger 2008). The Trpc6-positive cells have been shown to respond to odor molecules and to play an important role in adult neurogenesis in the MOE (Hegg *et al.*, 2010). Together, these studies indicate that Trp channels take over a variety of functions in the olfactory system both as indispensable components of neuronal signal transduction, and as putative sensors of harmful stimuli, as well as components in neurogenesis and olfactory function maintenance.

#### **1.4 The interaction between olfaction and female cyclicity**

The female estrous cycle is characterized by 4 distinct cycle stages: metestrus, diestrus, proestrus, and estrus (Figure 6) (Goldman *et al.*, 2007; Caligioni, 2009; Levine, 2015). During these stages, serum level concentrations of the ovarian steroids, estrogen and progesterone, and endocrine peptide hormones, LH, FSH and prolactin fluctuate following a recurring pattern with a time frame of 4 to 5 days during which ovulation occurs. Each estrous cycle is characterized by a slow increase of estrogen levels during metestrus and diestrus, followed by a surge at early proestrus. High levels of estrogen result in elevated gonadotropin releasing hormone (GnRH) release during late proestrus, which in turn stimulates the release of luteinizing hormone (LH) and follicle stimulating

hormone (FSH) (Butcher *et al.*, 1974; Sisk *et al.*, 2001). These processes result in ovulation during early estrus and a subsequent receptive phase during late estrus. After ovulation, the endometrium is prepared for nidation and pregnancy by secretion of progesterone from the corpus luteum (Fata *et al.*, 2001; Lonstein *et al.*, 2015). Thus, the estrous cycle is based on a well-balanced feedback loop between hypothalamic secretion of pituitary hormones and sex-steroid release from the ovaries.



Thus far, many studies have demonstrated that olfaction has a profound impact on female cyclicity and on a large variety of social and reproductive behaviors (Mandiyan *et al.*, 2005). For example, the presentation of odorant cues from a novel, sexually mature male mouse leads to the synchronization of the estrous cycle in group-housed female mice, also called the McClintock effect (McClintock, 1984). Furthermore, the introduction of male cues induces changes in sexual behaviors of young and adult female mice by promoting an earlier onset of puberty and ovulation, also known as the Whitten- and the Vandenberg effect (Whitten *et al.*, 1968; Vandenberg, 1969). However, if the female mouse, exposed to unknown male cues, is newly pregnant, the male signals lead to pregnancy termination due to nidation failure. This effect is called the Bruce effect (Bruce, 1959, 1969).

Furthermore, several studies have shown that the estrous cycle and changes in sex-steroid hormone levels can influence olfactory function, resulting in different sexual output behaviors (Xiao *et al.*, 2004; Moncho-Bogani *et al.*, 2002; Moncho-Bogani *et al.*, 2004, Dey *et al.*, 2015; McCarthy *et al.*, 2018).

Dey *et al.*, have shown in 2015 that depending on estrous cycle stage, odour perception can be altered by changes in VSN activity, resulting in diminished preference behavior of female mice in diestrus towards male urine, compared to females in estrus. Furthermore, it was shown that surgical removal of ovaries (ovariectomy, OVX) also results in diminished preference behavior towards male urine, and that this behavior can be restored by administration of sex-steroid hormones (Moncho-Bogani *et al.*, 2004, McCarthy *et al.*, 2018).

Interestingly, it was also shown that female cyclicity can directly influence gene expression in various organs, for example in specific cell types of the anterior pituitary gland, the gonadotropes (Qiao *et al.*, 2016) and in cells of the human and murine endometrium (DeClercq *et al.*, 2015; DeClercq *et al.*, 2017; Persoons *et al.*, 2018). Most intriguingly, expression levels of several members of the Trp-channel family correlate with changes in hormone levels during the estrous cycle (DeClercq *et al.*, 2015; DeClercq *et al.*, 2017; Persoons *et al.*, 2018).

Taken together, the close interaction between olfaction and the female estrous cycle is characterized by parallel processing of both internal and external information and that these are highly interdependent.

## 1.5 Aims

The olfactory system enables the assessment of and adaptation to the environment through a wide variety of behavioral responses. Several members of the Trp-family were reported to play a crucial role in the function of the main and accessory olfactory system. In particular, in the VNO Trpc2 is shown to be the main key player in the signal transduction machinery. Surprisingly, VSN activity in Trpc2 knockout mice was not completely abolished (Kelliher *et al.*, 2006; Yang and Delay, 2010; Kim *et al.*, 2011; Yu, 2015) and it is yet unknown which channel can be attributed to the observed residual activation. One promising candidate is Trpm4, as Trpm4-like currents have been recorded from hamster and mouse VSNs (Liman 2003; Spehr *et al.*, 2009). In the MOE, activation of Trpm5-GFP positive OSNs using pheromonal cues has been recorded (Oshimoto *et al.*, 2013; Lopez *et al.*, 2014). However, it is still highly debated whether the Trpm5 protein is expressed in OSNs or solely in MV cells (Lin *et al.*, 2007; Oshimoto *et al.*, 2013; Lopez *et al.*, 2014; Yamaguchi *et al.*, 2014; Kusumakshi *et al.*, 2015; Yamashita *et al.*, 2017), and whether the described pheromone-induced activation of OSNs can also be promoted by Trpm4, the functionally closest relative of Trpm5.

In this study, I focus on the two members of the Trpm subfamily, Trpm4 and Trpm5, to answer the question of their expression and their possible function in the olfactory system. Although Trpm4 and Trpm5 play important roles in other sensory systems, e.g. in taste chemo-transduction and in the auditory system, their role in the olfactory system is yet unclear (Trpm5) or even unknown (Trpm4) (Mathar *et al.*, 2014).

To achieve these aims, I proposed the following objectives:

- I. Screening of olfactory tissue for the expression of Trpm4 and Trpm5 channels using molecular, immunohistochemical, and specific mouse models as genetic tools.
- II. Addressing the question whether Trpm4 and Trpm5 may play a role during the development and differentiation of the olfactory system.
- III. Assessment of gender-specific differences in Trpm4 and Trpm5 expression and their potential regulation by sex-specific hormones.

## 2 Materials

### 2.1 Mouse strains

All animal protocols and experimental procedures complied with the ethical guidelines for the care and use of laboratory animals established by the German Government, European Communities Council Directive 2010/63/EU, and the Animal Welfare Committee of Saarland University School of Medicine, approval number H-2.2.4.1.1. The number of mice was minimized in accordance to the animal welfare suggestions. For statistical purpose a minimum of at least 3 mice each experimental group was used. The mice were kept with food and water *ad libitum* in micro-isolator cages under a 12:12-hour light/dark cycle. Mice were regularly tested for pathogens by analysis of sentinel mice via serology and PCR. For the developmental studies, C57BL/6N (Strain #027, Charles River, Sulzfeld, Germany) (referred to as B6) mice of both sexes were used in the experiments at different pre- and postnatal ages from embryonic days (E)15, E17, E18, and E19 to postnatal days (P)1, P7, P14, P21, and 7 weeks (7W). Time-pregnant females were 8-10W of age (Charles River, Sulzfeld, Germany). Surgical procedures were performed in a class IIA laminar flow biosafety cabinet. Results from hormone replacement experiments derived from B6 mice at 6-8W and 70W of age. Colabeling experiments were performed on OMP-GFP mice, in which all cells expressing the olfactory marker protein (OMP) are labeled by GFP (green fluorescent protein, B6; 129P2-Omp<sup>tm3Mom/MomJ</sup>, Jackson Lab, Stock #006667, Potter *et al.*, 2001). Furthermore, colabeling was performed on mice of the Trpm5-IRES-Cre knockin strain (Trpm5-IC, Kusumakshi *et al.*, 2015, kindly provided by U. Boehm, Department of Experimental Pharmacology, Saarland University, Germany) and Trpm4-IRES-Cre knockin strain (Trpm4-IC, kindly provided by R. Vennekens, Department of Cellular and Molecular Medicine, KU Leuven, Belgium), each crossed with the ROSA26 reporter strain (eR26- $\tau$ GFP, Gt(ROSA)26Sor<sup>tm1(CAG-Mapt/GFP)Uboe</sup>, Wen *et al.*, 2011, kindly provided by U. Boehm, Department of Experimental Pharmacology, Saarland University, Germany). The resulting offspring were heterozygous for Cre recombinase and  $\tau$ GFP. Global Trpm5- and Trpm4 knockout mouse lines (Trpm5-null, *-/-*, Damak *et al.*, 2006, Trpm4-null, *-/-*, Trpm4<sup>tm1.1Mfre</sup>, Vennekens *et al.*, 2007) served as a control for the specificity of the antibodies used.

## 2.2 Chemicals and enzymes

**Table 1: Chemicals and enzymes**

<b>Chemical</b>	<b>Manufacturer</b>
17 $\beta$ -estradiol implants (E2-M/30)	Belma Technologies
Acetic acid	Roth
Agarose	Sigma-Aldrich
Ammonium bicarbonate (NH <sub>4</sub> HCO <sub>3</sub> )	Fluka
Ammonium sulphate ((NH <sub>4</sub> ) <sub>2</sub> SO <sub>4</sub> )	Roth
Calcium chloride (CaCl <sub>2</sub> )	AppliChem
Carprofen, Rimadyl	Pfizer
Citric acid (C <sub>6</sub> H <sub>8</sub> O <sub>7</sub> )	Roth
Colorless GoTaq reaction buffer	Promega
Concanavalin A	Sigma-Aldrich
D (+)-Glucose (C <sub>6</sub> H <sub>12</sub> O <sub>6</sub> )	Merck
Disodium carbonate (Na <sub>2</sub> CO <sub>3</sub> )	Roth
DNase I	Thermo Scientific
dNTP mix	Agilent Technologies
DMEM	Invitrogen
DPBS	Thermo Scientific
EDTA	Thermo Scientific
Ethanol (C <sub>2</sub> H <sub>6</sub> O)	Roth
Ethidium bromide	Roth
Exemestane	Sigma-Aldrich
Hoechst 33342	Invitrogen
Hydrochloric acid (HCL)	Merck
Hydrogen peroxide (H <sub>2</sub> O <sub>2</sub> ), for analysis, 35 wt. % solution in water	Acros Organics
Ketamine	Pharmacia GmbH
L-cysteine hydrochloride	Sigma-Aldrich
Magnesium chloride (MgCl <sub>2</sub> )	AppliChem
Methanol (CH <sub>3</sub> OH)	Merck
2-Methylbutane	Merck
Monosodium phosphate (NaH <sub>2</sub> PO <sub>4</sub> )	Roth
Sodium carbonate (NaHCO <sub>3</sub> )	Roth
Sodium chloride (NaCl)	Roth
O.C.T. compound, Tissue-Tek	Miles Scientific
Papain	Worthington
Paraformaldehyde (OH(CH <sub>2</sub> O) <sub>n</sub> H)	AppliChem
Potassium chloride (KCl)	Roth
Placebo implants (E2-M/P)	Belma Technologies
Potassium dihydrogen phosphate (KH <sub>2</sub> PO <sub>4</sub> )	AppliChem
RNA later	Ambion
Progesterone	Sigma Aldrich
Progesterone implants (P4-M/30)	Belma Technologies
Sesame oil	Sigma-Aldrich
Sodium hydrogen carbonate (NaHCO <sub>3</sub> )	Roth

Sodium dodecyl sulphate ( $\text{CH}_3(\text{CH}_2)_{11}\text{OSO}_3\text{Na}$ )	Roth
Sodium hydroxide (NaOH)	Grüssing GmbH
Sucrose ( $\text{C}_{12}\text{H}_{22}\text{O}_{11}$ )	Roth
Testosterone (T4-M/30)	Belma Technologies
Tris ( $\text{C}_4\text{H}_{11}\text{NO}_3$ )	Roth
Triton X-100 ( $\text{C}_{14}\text{H}_{22}\text{O}(\text{C}_2\text{H}_4\text{O})_n$ )	Sigma-Aldrich
tRNA	Sigma-Aldrich
Urea ( $\text{CH}_4\text{N}_2\text{O}$ )	Roth
Xylazine	Bayer Health Care

### 2.3 Antibodies and sera

**Table 2 : Antibodies and sera**

Primary antibodies	Dilution	Manufacturer (RRID, Cat. #)
Goat-anti-OMP, 544-10001	1:2000	Wako, RRID: AB_664696, #544-10001
Rabbit-anti-Trpm5, polyclonal	1:1000	V.Flockerzi, #1050; N/A
Rabbit-anti-Trpm5, polyclonal	1:500	Kaske <i>et al.</i> , 2007, #321; N/A
Rabbit-anti-Trpm4, polyclonal	1:100	Alomone, RRID: AB_2040250, #ACC-004
Chicken-anti-Trpm4, polyclonal, whole serum	1:300	Osenses, RRID: N/A, #OST00370W
Rabbit-anti-Trpc2, polyclonal	1:2000	Liman <i>et al.</i> , 1999, N/A
Mouse-anti-Gap-43, polyclonal	1:1000	Millipore, RRID: AB_2107282, #AB5220
Chicken-anti-GFP, polyclonal	1:1000	Abcam, RRID: AB_300798, #ab13970
Secondary antibodies	Dilution	Manufacturer (RRID, Cat. #)
Goat-anti-rabbit Alexa488	1:1000	Invitrogen, RRID: AB_2576217, #A-11034
Goat-anti-chicken Alexa 488	1:1000	Invitrogen, RRID: AB_2534096, #A-11039
Goat-anti-mouse Alexa 488	1:1000	Invitrogen, RRID: AB_2535771, #A-21131
Donkey-anti-rabbit Alexa 555	1:1000	Invitrogen, RRID: AB_162543, #A-31572
Goat-anti-rabbit Alexa 633	1:1000	Invitrogen, RRID: AB_2535732, #A-21071
Goat-anti-rabbit Fab-fragments	1:50	Rockland; RRID: AB_218909, #811-7102,
Sera		Manufacturer (Cat. #)
Normal Horse Serum (NHS)		Vector Labs, #S-2000
Fetal calf serum (FCS)		Sigma-Aldrich, #12238C

### 2.4 Solutions

Alkaline buffer	pH 9.5
Tris-HCl	100 mM
NaCl	100 mM
MgCl <sub>2</sub>	5 mM

---

<u>Blocker</u>	pH 7.4
Normal serum (horse or rabbit)	2% - 4% (v/v)
In Permeabilization solution	

<u>Cell dissociation (for IHC)</u>	pH 7.0 - 7.3
Papain	15 U/ml
DNase I	1 U/ml
In DPBS	

<u>Cell dissociation (for RT-PCR)</u>	pH 7.4
Papain	0.22 U/ml
EDTA	1.1 mM
L-cysteine hydrochloride	5.5 mM
In 1 ml PBS	

<u>Paraformaldehyde solution</u>	pH 7.0
Paraformaldehyde (PFA)	2% - 4% (w/v)
In PBS	

PFA is added to preheated H<sub>2</sub>O<sub>dest</sub> (60°C). To dissolve the PFA, 1 N NaOH is added dropwise until the solution clears. 10 x PBS is added to reach a final concentration of 1 x PBS. The final solution is cooled down to 25°C, and the pH is adjusted to pH 7.0.

<u>Phosphate buffered saline (10x)</u>	pH 7.4
Phosphate buffer (0.2 M)	
Na <sub>2</sub> HPO <sub>4</sub>	28.38% (w/v)
NaH <sub>2</sub> PO <sub>4</sub> *H <sub>2</sub> O	27.6% (w/v)
In H <sub>2</sub> O <sub>dest</sub>	

The ready to use solution is prepared by dilution 1:10 (v/v) with H<sub>2</sub>O<sub>dest</sub> and finalized by pH correction to pH 7.4.

<u>Saccharose solution (30%)</u>	pH 7.4
Saccharose	30% (w/v)
Na-azide	0.01% (w/v)
in PBS	

<u>S2 solution</u>	pH 7.3
NaCl	145 mM
KCl	5 mM
HEPES	10 mM
MgCl <sub>2</sub>	1 mM
CaCl <sub>2</sub>	1 mM
Glucose	10 mM

TAE-buffer	pH 8.3
Tris	40 mM
Acetic acid	20 mM
EDTA	1 mM
In deionized H <sub>2</sub> O	
Tissue Permeabilization	pH 7.4
Triton X-100	0.1% - 0.3% (v/v)
in PBS	

## 2.5 Critical commercial kits and compounds

**Table 3: Critical commercial kits and compounds**

Product name	Manufacturer
AMV reverse transcriptase	NEB
innuPREP RNA mini kit	Analytik Jena AG
iTaq™ Universal SYBR® Green Supermix	BioRad
Phusion High Fidelity DNA polymerase	Thermo Scientific
Phusion Got Start II High-Fidelity PCR master mix	Thermo Scientific
RNase inhibitor	Promega
SMARTer PCR cDNA synthesis kit	Clontech
QIAquick MinElute Kit	Qiagen
QIAquick PCR-Purification Kit	Qiagen

## 2.6 Oligonucleotides

**Table 4: Oligonucleotides**

Trpm5			
	variant specificity	Binding site	primer sequence (5'- 3')
1	Trpm5-1	5'-UTR	(F) CTCATGCAGTCCAAGGCACTGA
2	Trpm5-1+2	1.ATG	(F) ATGCAAACAACCCAGAGCTCCT
3a	Trpm5-1-4	Exon 10	(F) CATGGCCGAGTTCTTGACCTATG
3b	Trpm5-1-4	Exon 10	(R) AGGTCAAGAACTCGGCCAT
4a	Trpm5-1-4+6	Exon 13	(F)TTCTCAGAGTGCTACGGCAACAGT
4b	Trpm5-1-4+6	Exon 13	(R)ACTGTTGCCGTAGCACTCTGAGAA
5a	Trpm5-1-4+6	Exon 15	(F)ATGGACCTAGAAGATCTGCAGGAGC
5b	Trpm5-1-4+6	Exon 15	(R)GCTCCTGCAGATCTTCTAGGTCCAT
6a	Trpm5-9	Intron 19/20	(F) GTTTGCATCCCATCTGAGAGCA
6b	Trpm5-9	Intron 19/20	(R) TGCTCTCAGATGGGATGCAAAC
7a	Trpm5-9	Intron 19/20	(F)TGTTGGCTTGGTGTAACTAGGGCT
7b	Trpm5-9	Intron 19/20	(R)AGCCCTAGTTACACCAAGCCAACA
8	Trpm5-1-4+9	Exon 20	(F) CTGGAAAGCTCGGCTTCCTG
9	Trpm5-2+9	Intron 20/21	(R) CTGCAGGTCCAGCCCCTG
10	Trpm5-2+9	Intron 20/21	(R)TGTAGACCCATCTTCTTCTTAACAG
11a	Trpm5-1-5+7+8	Exon 22	(F) TGCTGAGGAAAACGGCAC

11b	Trpm5-1-5+7+8	Exon 22	(R) GTGCCGTTTTCTCAGCA
12	Trpm5-1-5+7+8	Exon 24	(R)CCAGTGTATCCGTCATAGAGGACAA
13	Trpm5-1-5	Exon 25	(R) GGTGTCAGAGGGTGGCAAGC
14	Trpm5-1+3+5	Exon 25	(R) GAAGGTTGATGTGCCCAAAAA
15	Trpm5-8	3'-UTR	(R) TGATGCTGGGTCATTCCACTG
16	Trpm5-7	3'-UTR	(R) GAGACTGGACAGGACCGAATCC
<b>Trpm4</b>			
1		Exon 1	(F)GGCCGGAGAAGGAGCA
2		Exon 25	(R)GGATGCAAACACCTAGACATCCA
3 Q		Exon 22	(F)TCGGGACAAGCGAGACAGTGA
4 Q		Exon 24	(R)AGGCAGCAAGGCAGAGTGGCTAA
<b>Omp</b>			
1		Exon 1	(F)ATGGCAGAGGATGGGCC
2		Exon 1	(R)GAGCTGGTTAAACACCACAGAGGC
<b>Gapdh</b>			
1 Q		Exon2	(F)TGAACGGATTTGGCCGTATTGG
2 Q		Exon 3	(R)TGCCGTTGAATTTGCCGTGAG
<b>cDNA synthesis</b>			
CDS primer-Clontech			AAGCAGTGGTAACAACGCAGAGTACTT TTTTTTTTTTTTTTTTTTTTTTTTTTTTT
Smart II primer-Clontech			AAGCAGTGGTATCAACGCAGAGT

## 2.7 Consumables and equipment

**Table 5: Consumables and equipment**

Consumables	Product name	Manufacturer
Capillary Glass, 8250, Filament, 1.50/0.86, 75 mm or 150 mm		Science Products GmbH
Cellstar Tubes 15 ml, 50 ml		Greiner Bio-one
Cover glass Ø 12 mm		Thermo Fisher
Cover glass 24 x 40 mm		Roth
Cover glass 24 x 50 mm		VWR
Disposable Pasteur Pipettes		Chase Instruments
Disposable Spatulas		VWR
Eppendorf tubes 1.5 ml, 2 ml, 5 ml		Eppendorf
Needle-suture combination USP 4/0,1,5 Metric (3/8 19 mm)		Eickemeyer
8 Strip 0.2ml PCR Tubes		Eppendorf
Quality Pipette Tips 10 µl, 20 µl, 200 µl, 1000 µl		Sarstedt AG
Reaction tubes (1.5 ml, 2 ml, 5 ml)		Eppendorf
Safe Seal Tips Professional 10 µl, 20 µl, 200 µl, 1000 µl		Biozym
Single Edge Carbon Steel Razorblade		ElectronMicroscopy Sciences
Sterile needle, 0.45 x 13 mm		BD Microlance
Sterile Syringe 1 ml Omnifix®-F		Braun
Superfrost Plus glass slides		Thermo Scientific
Weighing Paper		Thermo Scientific

<b>Equipment Product name</b>	<b>Manufacturer</b>
Well plates (96)	VWR
Bright field microscope, SZT300	VWR
Bright field microscope, LCD Micro 5MP DM 750	Leica
CO <sub>2</sub> -incubator, CB210-UL	Bochem Instr. GmbH
Cryostat HM525	Microm
Electrophoresis chamber	Biozym
Electrophoresis power supply (PowerPac 300)	BioRad
Fluorescent microscope BX50WI	Olympus
Fluorescent microscope BX61, DP71 camera	Olympus
Gradient cycler, MyCycler	BioRad
Hormone implant injector	Eickemeyer
Magnet Stirrer	Thermo Fisher
LSM 880/ConfoCor-3 confocal microscope	Zeiss
Microwave, MW 1243 CB	Bomann
My-iQ-cycler	BioRad
peristaltic pump, Peri-star™ Pro	WPI
pH Meter, PHM240	MeterLab™
Precision Balance 572	Kern & Sohn GmbH
Single Channel Pipettes (0.5-10 µl, 10-200 µl, 100-1000 µl)	VWR
Spectrophotometer (Ultraspec 2100 pro)	Amersham Biosciences
Spectrosil, 5 mm, super sub micro cuvette	Amersham Biosciences
UV trans illuminator (ChemiDoc XRS+ system)	BioRad
Vortex Genie 2	Scientific Industries

## 2.8 Software

**Table 6: Software**

<b>Product name</b>	<b>Manufacturer</b>
CorelDRAW Graphics Suite X7	Corel Corporation
ImageJ	Wayne Rasband, NIH
iQ5 Software	BioRad
Microsoft Excel	Microsoft Corporation
Microsoft Word	Microsoft Corporation
Origin Pro 2017G	OriginLab Corporation
Photoshop Elements 10	Adobe Photoshop
Zen Black 2.3	Zeiss

## 3 Methods

### 3.1 Nucleic acid techniques

#### 3.1.1 RNA extraction from olfactory tissue

Total RNA was obtained from B6 MOE and VNO tissue of 8-12 weeks old or six pooled embryos at E18. First, the tissue was dissected and stored in RNA later at  $-80^{\circ}\text{C}$ . The total RNA was extracted using the innuPREP RNA mini kit according to the manufacturer's protocol. As a control for RNA quality and integrity gel electrophoresis was performed and the RNA was eluted in RNase free water. RNA concentration was measured with a spectrophotometer using a spectrosil, 5 mm, super sub micro cuvette. The absorption was determined at a wavelength of 260 nm. The  $\text{OD}_{260\text{nm}}$  of 1 represents 40  $\mu\text{g/ml}$  RNA (Gallagher and Desjardins, 2008). To assess the purity of the RNA, the ratio of absorbance at 260 nm and 280 nm was measured and RNA samples with an  $\text{OD}_{260\text{nm}}/\text{OD}_{280\text{nm}}$  ranging from 2.0 to 2.2 were accepted as pure and used for further analyses.

#### 3.1.2 RNA extraction from isolated cells

To obtain RNA of isolated cells, olfactory tissue of 8 to 12 weeks old *Trpm5-IC/eR26- $\tau$ GFP*, *Trpm4-IC/eR26- $\tau$ GFP*, and *OMP-GFP* mice was used. First, the VNO and the MOE were stripped from their bony capsules, and washed in dissociation buffer (1 ml of PBS, 0.22 units/ml papain, 1.1 mM EDTA, 5.5 mM L-cysteine hydrochloride) at  $4^{\circ}\text{C}$  and then incubated for 20 min at  $37^{\circ}\text{C}$ . For OSN dissociation 40 mM urea was added to the dissociation solution. Next, the cell suspension was transferred into 1 ml of DNA digestion solution containing 600  $\mu\text{l}$  PBS, 400  $\mu\text{l}$  Colorless GoTaq reaction buffer, and 50 units of DNase I and incubated for 5 min at RT. Addition of 10 ml of DMEM containing 10% (v/v) fetal calf serum (FCS) stopped the DNA digestion. The cell suspension was centrifuged for 5 min at  $1000 \times g$  at  $4^{\circ}\text{C}$ , the supernatant discarded, and the cell pellet resuspended by gentle extrusion with a glass pipette in 50  $\mu\text{l}$  DMEM supplemented with 10% (v/v) FCS. Subsequently, cells were seeded on concanavalin-A covered (0.5 mg/ml) glass coverslips and placed into a cell culture incubator for 60 min at  $37^{\circ}\text{C}$  and 5%  $\text{CO}_2$ . Examination of the cell suspension by fluorescent microscopy enabled selection and manual collection of individual  $\tau$ GFP-positive or GFP-positive VSNs, OSNs, and MV cells. Discrimination of the different cell types was possible due to differences in cell size and cell morphology. Each cell type sample used for cDNA synthesis contained

approximately 5-10 cells that were manually collected in glass capillaries (5-10  $\mu\text{m}$  tip size) in a volume of 2-3  $\mu\text{l}$  S2 solution. Cells were immediately shock-frozen in liquid nitrogen and stored at  $-80^{\circ}\text{C}$  until further use.

### 3.1.3 cDNA synthesis

Total RNA was used for the synthesis of first strand complementary DNA (cDNA). 0.5  $\mu\text{g}$  total RNA was mixed with 1.5  $\mu\text{l}$  of CDS primer (10  $\mu\text{M}$ ), 1.5  $\mu\text{l}$  Smart II primer (10  $\mu\text{M}$ ) (Table 4), in a total volume of 7.5  $\mu\text{l}$  with DEPC-treated water. The RNA-primer mix was incubated for 2 min at  $65^{\circ}\text{C}$  and immediately cooled down for 2 min on ice. Next, 1.5  $\mu\text{l}$  dNTP mix (10 mM), 0.5  $\mu\text{l}$  RNase inhibitor (20 U/ $\mu\text{l}$ ), 1.5  $\mu\text{l}$  10  $\times$  AMV buffer, and 1.5  $\mu\text{l}$  AMV reverse transcriptase (10 U/ $\mu\text{l}$ ) were added and the cDNA synthesis was performed using the following protocol in a gradient cycler:

**Table 7: cDNA synthesis**

Cycles	Duration	Temperature	Cycle step
1	30 min	$42^{\circ}\text{C}$	
1	10 min	$45^{\circ}\text{C}$	
1	10 min	$50^{\circ}\text{C}$	
1	10 min	$55^{\circ}\text{C}$	
1	5 min	$65^{\circ}\text{C}$	Final denaturation

The volume of cDNA synthesized from tissue was adjusted to 50  $\mu\text{l}$ . cDNA synthesis from isolated cells was performed using the same protocol. The cell solution (3–5  $\mu\text{l}$  S2) was directly added into the reaction mixture instead of the total RNA and the final volume of the cDNA was adjusted to 20  $\mu\text{l}$ .

### 3.1.4 RT-PCR

Reverse transcription-polymerase chain reactions (RT-PCR) were performed using Phusion High Fidelity DNA polymerase according to the manufacturer's protocol with the following components:

**Table 8: RT-PCR reaction solution content**

2x Phusion HSII Master Mix	10 $\mu\text{l}$
Forward primer	0.5 $\mu\text{M}$
Reverse primer	0.5 $\mu\text{M}$
Template cDNA	0.5 $\mu\text{l}$
H <sub>2</sub> O	ad 20 $\mu\text{l}$

Gene specific primers were used to identify the full-length *Trpm4* ([https://www.ncbi.nlm.nih.gov/nucore/NM\\_175130.4](https://www.ncbi.nlm.nih.gov/nucore/NM_175130.4); 4,234 bp amplicon) and the full-length *Trpm5* ([https://www.ncbi.nlm.nih.gov/nucore/NM\\_020277](https://www.ncbi.nlm.nih.gov/nucore/NM_020277); 4,123 bp amplicon) (Table 4). A total of 16 different primers covering specific regions of the *Trpm5* mRNA were used to identify possible *Trpm5* splice variants expressed in the MOE (Table 4). Eight different splice variants for *Trpm5* are annotated in the Ensembl database ([www.ensembl.org](http://www.ensembl.org), ENSMUSG00000009246). To identify the full-length *Trpm5-2* splice variant primer 2 in combination with 9 and 10 was used (Table 4). Furthermore, various segments at the N-terminus of *Trpm5-1*, *Trpm5-2*, *Trpm5-3*, *Trpm5-4*, and *Trpm5-5* cDNA were analyzed using primers 1, 2 in combination with 3b, 4b, 5b (Table 4). C-terminal stretches were amplified using primers 3a, 4a, 5a, 8, 11a in combination with 13. To identify the splice variants *Trpm5-7*, *Trpm5-8*, and *Trpm5-9* primers 6a, 7a, 8 were used in combination with 9 and 10, and 11a was used in combination with 16 and 15 (Table 4). The PCR reactions were performed using the following PCR protocol in a gradient cycler:

**Table 9: RT-PCR**

Cycles	Duration	Temperature	Cycle step
1	15 s	98°C	Initial Denaturation
	10 s	98°C	Denaturation
39	10 s	60°C, 68°C	Annealing
	15 s/kb	72°C	Extension
	5 min	72°C	Final Extension
1	hold	4°C	Storage

The expected product sizes for *Trpm4* and *Trpm5-1* were obtained using an annealing temperature of 60 °C and 68 °C, respectively, with an extension time of 60 s for both products. Products for *Trpm5-9*, *Omp*, and *GapdH* were obtained upon annealing at 60 °C and an extension time of 20 s.

For the cellular identification of OSNs and VSNs, primers specific for *Omp* with an amplicon length of 489 bp were used (Table 4). As an internal control, primers resulting in a 225 bp amplicon, specific for the housekeeping gene *GapdH* were used (Table 4). Furthermore, omitting of the reverse transcriptase during cDNA synthesis served as control for genomic contamination. At least three different experiments for each PCR were performed. PCR products were purified using the QiaQuick PCR-Purification Kit and confirmed by direct sequencing (Seqlab).

### 3.1.5 Rapid amplification of cDNA ends (RACE)

As starting material 0.5  $\mu$ l cDNA was used for all RACE-PCRs in combination with the Phusion Go Start II High-Fidelity PCR master mix according to the manufacturer's protocol. In brief, the RACE reaction solution contained an adapter primer and gene specific primers each recognizing a known sequence in the gene of interest for both the 5' and 3' RACE-PCR. The splice variant *Trpm5-1* was analyzed via 5'-RACE-PCR and the splice variant *Trpm5-9* was analyzed via 3'-RACE-PCR. For *Trpm5-1* a gene specific primer binding to exon 13 of *Trpm5* (Table 4, primer 4) and for *Trpm5-9* a gene specific primer binding to exon 21 of *Trpm5* (Table 4, primer 9) was used.

The Rapid amplification of cDNA ends (RACE) is used to identify full length cDNA ends to reveal the starting and terminal sequences of mRNA by amplification of the transcripts of interest by reverse transcription. Unknown sequences at either the 5' or the 3' end of the mRNA are targeted by a combination of gene specific primers and adapter primers. RACE-PCR was performed using the following amplification protocol in a gradient cycler:

**Table 10: RACE-PCR**

Cycles	Duration	Temperature	Cycle step
1	30 s	98°C	Initial Denaturation
35	10 s	98°C	Denaturation
	10 s	60°C, 64°C, 68°C	Annealing
	40 s	72°C	Extension
	5 min	72°C	Final Extension
1	hold	4°C	Storage

PCR products were size-separated by gel electrophoresis, isolated by gel extraction (QiaQuick MinElute Kit), and analyzed by direct sequencing (Seqlab).

### 3.1.6 Quantitative real-time RT-PCR

Quantitative real-time RT-PCR (qRT-PCR) was performed on a My-iQ-cycler using iTaq™ Universal SYBR® Green Supermix on total VNO samples of B6 males, and on the VNO of B6 females at different estrous cycle stages (diestrus and estrus). Gene specific forward and reverse primers for *Trpm4* are listed in Table 4. The housekeeping gene *GapdH* served as control. The reactions were performed according to the manufacturer's protocol. In brief, 100 ng of cDNA were mixed with 0.5  $\mu$ M forward and 0.5  $\mu$ M reverse primer. iTaq™ Universal SYBR® Green Supermix (2x) was added and

the volume was adjusted to a total reaction volume of 20  $\mu$ l by H<sub>2</sub>O. The PCR parameters were as follows:

**Table 11: qRT-PCR**

Cycles	Duration	Temperature	Cycle step
1	3 min	95°C	Initial Denaturation
39	30 s	95°C	Denaturation
	20 s	64°C	Annealing
	30 s	72°C	Extension
1	hold	4°C	Cooling

qRT-PCR reactions were performed as triplicates on 96-well plates. Each sample contained the equivalent of the VNO of two animals. The results were analyzed using the iQ5 Software. The specificity of PCR products was confirmed by direct DNA sequencing. Controls for RNA isolation, PCR conditions and the linearity of amplification were evaluated according to MIQE guidelines (Bustin *et al.*, 2009). To assess the copy number, a calibration curve for the primer sets used, with a defined amount of copies as starting material was generated. Yeast tRNA (100 ng/ml) was added to the reaction solution to prevent the nucleic acid of interest from attaching to the reaction tube walls. tRNA functions as a carrier molecule and adheres to nucleic acid binding sites in the reaction tube.

### 3.1.7 Gel electrophoresis

Following all RT-PCR reactions PCR products were separated by size and analyzed by gel electrophoresis on 1% agarose gels. Agarose (w/v) was dissolved in TAE-buffer (40 mM Tris, 20 mM acetic acid, and 1 mM EDTA). To visualize the PCR products ethidium bromide was added to agarose gels and the electrophoresis buffer to 0.5  $\mu$ g/ml final concentration. PCR samples were prepared by addition of 6 x Loading dye, and as a size marker 3  $\mu$ l (12 ng) of FastRuler™ Middle Range DNA Ladder was loaded on the gel. Subsequently, the gel was run at 100 V for 10-30 min, depending on the size of the products and the separated DNA fragments were documented by an UV transilluminator.

## 3.2 Immunohistochemical methods

### 3.2.1 Transcardial perfusion and olfactory tissue preparation

Mice were deeply anaesthetized by intraperitoneal injection of PBS containing 165 mg/kg body weight ketamine and 11 mg/kg body weight xylazine. Deep anesthesia was confirmed by the absence of reactions towards noxious stimuli (toe pinches) and the loss of “Stellreflex”. The tissue preparation was initiated by an incision through the skin along the thoracic midline at the level of the xiphoid process and the removal of the ribcage to expose the heart. A 0.45 x 13 mm needle connected to a single-tubed peristaltic pump was inserted into the left ventricle. Subsequently, the right atrium was cut open, and the perfusion was initiated at the first sign of blood flow. Transcardial perfusion was conducted using PBS until the perfusate was clear of blood. Tissue fixation followed by perfusion with 2 ml/g bodyweight ice-cold PFA, 2% w/v or 4% w/v in PBS. Then the mouse was decapitated, and the cranium was skinned. To expose the brain and the OB, the cranium was cut open along the mid-sagittal suture and the parietal and frontal bones were removed. Additionally, to expose the VNO, the lower jaw was removed, and the palatal cartilage was peeled off. Deboning of the nasal tissue was performed as described (Dunston *et al.*, 2013). Following dissection, the tissue was post fixed for 2 hours in 2% PFA solution for Trpm4, or 4% PFA for Trpm5 at 4°C. Time-pregnant females were generated to obtain olfactory tissues from mouse embryos and from the females at the desired day of pregnancy. Therefore, breeding pairs were kept together overnight. On the next morning females exhibiting a vaginal plug were considered pregnant (embryonic day 1, E1). On the required day of pregnancy, females were sacrificed by an overdose of ketamine and xylazine (300 mg/kg body weight, 22 mg/kg body weight). Embryos were removed from the uterus, decapitated, and their heads were rinsed in PBS and fixed in 4% PFA overnight. Cryopreservation was achieved by incubation of the obtained tissues in 30% sucrose solution for 48 hours at 4°C. The dissected tissue was embedded in O.C.T. compound, snap frozen by immersion in a dry-ice/2-methylbutane bath and stored at -80°C until further use.

### 3.2.2 Cryostat sections

Frozen sections of olfactory tissues (12-16 µm) were cut on a cryostat and collected on Superfrost Plus glass slides. Sections were collected either consecutively or as sets for the representation of the whole VNO, MOE, and MOB. Tissues were cut in both coronal and sagittal planes. Cryostat sections were stored at -80°C until further use or directly

subjected to immunohistochemical procedures following an incubation time of at least 10 min at -20°C.

### 3.2.3 Immunohistochemistry

All immunohistochemical procedures were performed at room temperature if not otherwise noted. Sections were rinsed in PBS, incubated in blocking solution containing 0.3 % Triton X-100 and 4 % horse serum in PBS for 1 h, followed by incubation in blocking solution containing the primary antibody overnight at 4 °C. All primary antibodies are listed in Table 2. In brief, primary antibodies were: rabbit-anti-Trmp4 (1:100; rabbit polyclonal), Trpm4 (1:300; chicken polyclonal), OMP (1:2000, goat polyclonal), Trpc2 (1:2000, rabbit polyclonal), and GFP (1:1000, chicken polyclonal). For double-labeling experiments of Trpm4 and Trpc2, a rabbit block was included between applications of the primary antibodies, to prevent cross-reactivity. After the first immunostaining, an incubation of the sections for 1 h in blocking solution containing 2% normal rabbit serum was performed. Next, tissue sections were washed in PBS and incubated for 1 h in goat-anti-rabbit Fab-fragments in PBS (1:50). For the detection of Trpm5 two distinct anti-Trpm5 antisera were used: Trpm5 (1:1000, rabbit polyclonal, #1050) and Trpm5 (1:500, rabbit polyclonal, #321). For the immunostaining using anti-Trpm5 antiserum #1050, tissue sections were incubated for 90 min in alkaline buffer (100 mM Tris-HCl, 100 mM NaCl, 5 mM MgCl<sub>2</sub>, pH 9.5). Furthermore, primary antibody for Gap-43 (1:1000, mouse monoclonal) was used in this study. For the Gap-43 immunostaining a pretreatment with goat-anti-mouse Fab-fragments for 1 h (1:50 in PBS) was performed, to block unspecific antibody binding. Following incubation in the primary antibody solution, the tissue was washed three times for 10 min in PBS and incubated in secondary antibody solution for 1 h in the dark. All secondary antibodies were used in a dilution of 1:1000 and are listed in Table 2. Secondary antibodies were: Alexa Fluor 488 goat anti-rabbit, Alexa Fluor 488 goat anti-chicken, Alexa Fluor 488 goat anti-mouse, Alexa Fluor 555 donkey anti-rabbit, and Alexa Fluor 663 goat anti-rabbit. The tissue sections were rinsed in PBS, the nuclei counterstained in Hoechst 33342 (1:10000) for 10 min and tissue sections were cover-slipped using DAKO mounting medium.

### 3.2.4 Dissociation of VSNs and immunocytochemistry

Adult, 6-8 weeks old B6 mice were sacrificed by CO<sub>2</sub> inhalation. The dissociation protocol was adapted from Lucas *et al.*, 2003. In brief, the VNO was dissected and the

vomeroneasal epithelium was submerged in DPBS containing 15 U/ml papain and 1 U/ml DNase I, and was incubated for 25 min at 37°C. The tissue was then transferred to PBS, gently triturated, and centrifuged at 500 rpm for 10 min at 8°C. The supernatant was discarded, and the cells were resuspended in 50 µl of fresh PBS and plated on concanavalin-A (0.5 mg/ml) coated coverslips. Subsequently, coverslips were incubated for 15 min at 4°C and the cells were fixed with 2% PFA in PBS (w/v) for 10 min at RT. After 3 washes with PBS, the cells were incubated in blocking solution containing 0.1% Triton X-100 and 4% normal horse serum in PBS for 15 min, followed by incubation in blocking solution containing primary antibody for 1 hour at RT. Primary and secondary antibodies are listed in detail in Table 2 and were: Trmp4 (1:100; rabbit polyclonal) and Trpc2 (1:2000, rabbit polyclonal). Cells were then washed three times 5 min in PBS and incubated in secondary antibody solution for 30 min in the dark. Secondary antibodies were: Alexa Fluor 488 goat anti-rabbit (1:1000) and Alexa Fluor 555 donkey anti-rabbit (1:1000, see Table 2). The cells were rinsed in PBS, the nuclei counterstained with Hoechst 33342 (1:10000) for 5 min, and cover slipped using DAKO fluorescence mounting medium.

### 3.2.5 Cell counts

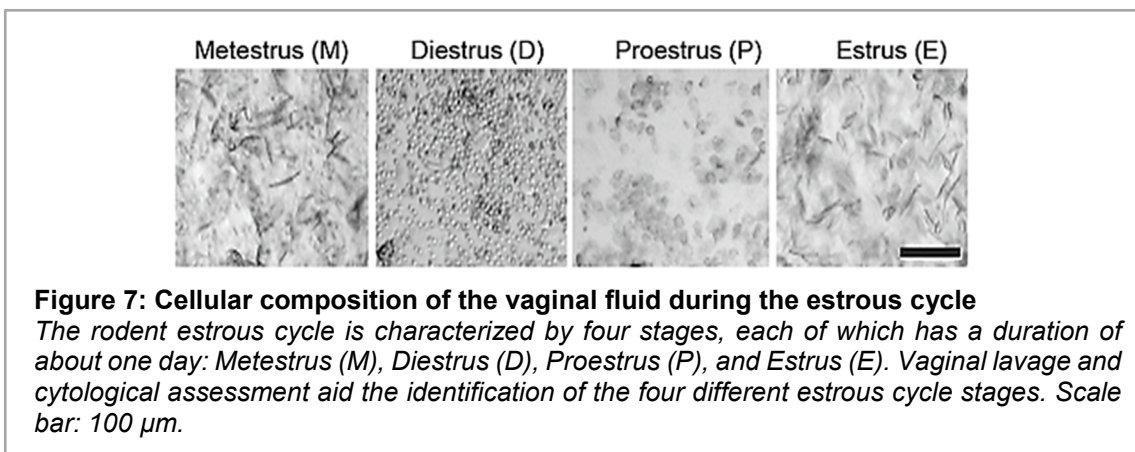
Mouse embryos deriving from three different litters of B6 and of Trpm5-IC/eR26-τGFP mice were analyzed for Trpm5-immunoreactivity (ir) and GFP-ir in the MOE. For this purpose, the entire embryonic olfactory tissue was cut into 16 µm sections and the Trpm5- or GFP- immunoreactive OSNs were manually counted using a fluorescence microscope. Trpm5 cell counts were performed at five different age stages: E15, E17, E18, E19 and P1 (n = 2 for E15 and P1, n = 3 for all other ages). GFP cell counts were performed at embryonic stage E18. Data are depicted as means ± SEM. Furthermore, to determine the proportion of total GFP fluorescence accounted by the different cell types in Trpm5-IC/eR26-τGFP mice, GFP-ir cell types were manually counted from fluorescence images acquired using a confocal Zeiss LSM 880/ConfoCor-3 microscope. Cells were counted at the tips of endoturbinates 1 and 2 along the anterior-to-posterior extent (n = 3 adult 7 weeks old Trpm5-IC/eR26-τGFP mice). Two photomicrographs were taken of each turbinate, resulting in a total of 4 images per mouse used for analysis.

### 3.2.6 Fluorescence and confocal imaging microscopy

Fluorescence images were taken with a BX61 epifluorescence microscope (Olympus) equipped with appropriate excitation and emission filters: Alexa 488 (Excitation: 480 nm / 20 nm; Emission: 530 nm / 40 nm), Alexa 555 (Excitation: 535 nm / 30 nm; Emission: 580 nm IF), DAPI (Excitation: 365 nm / 10 nm; Emission: 440 nm / 40 nm), and Alexa 633 (Excitation: 635 nm / 30 nm; Emission: 655 nm LP). All confocal images were taken with a Zeiss LSM 880/ConfoCor-3 microscope equipped with a 32-channel GaAsP-PMT and 2-channel PMT QUASAR detector using bandpass barrier filters for DAPI (Excitation: 365 nm / 30 nm; Emission: 445 nm / 50 nm), Alexa 488 (Excitation: 470 nm / 40 nm; Emission: 525 nm / 50 nm), Alexa 555 (Excitation: 545 nm / 25 nm; Emission: 605 nm / 70 nm), and Alexa 633 (Excitation: 640 nm / 30 nm; Emission: 690 nm / 50 nm). Acquired digital images were minimally adjusted in brightness and contrast using Photoshop Elements 10 (Adobe Photoshop).

### 3.3 Estrous cycle assessment

Changes of blood concentrations of ovarian hormones induce changes in morphology of the vaginal epithelium. The cytological composition of the epithelium was evaluated by vaginal smear examination. As exemplified by Caligioni 2009, and Byers *et al.*, 2012, the estrous cycle is 4-5 days long and is composed of the stages proestrus (primarily nucleated epithelial cells), estrus (predominantly cornified epithelial cells), metestrus (all three cell types) and diestrus (mostly leucocytes) (Figure 7). Vaginal smears were obtained daily at 0900 h from mature virgin B6 female mice. Phosphate-buffered saline (PBS, 20  $\mu$ l) was used to gently flush the vagina. Subsequently, the vaginal fluid was examined under a bright field microscope. Each estrous cycle phase (Figure 7) was identified according to the criteria described above.

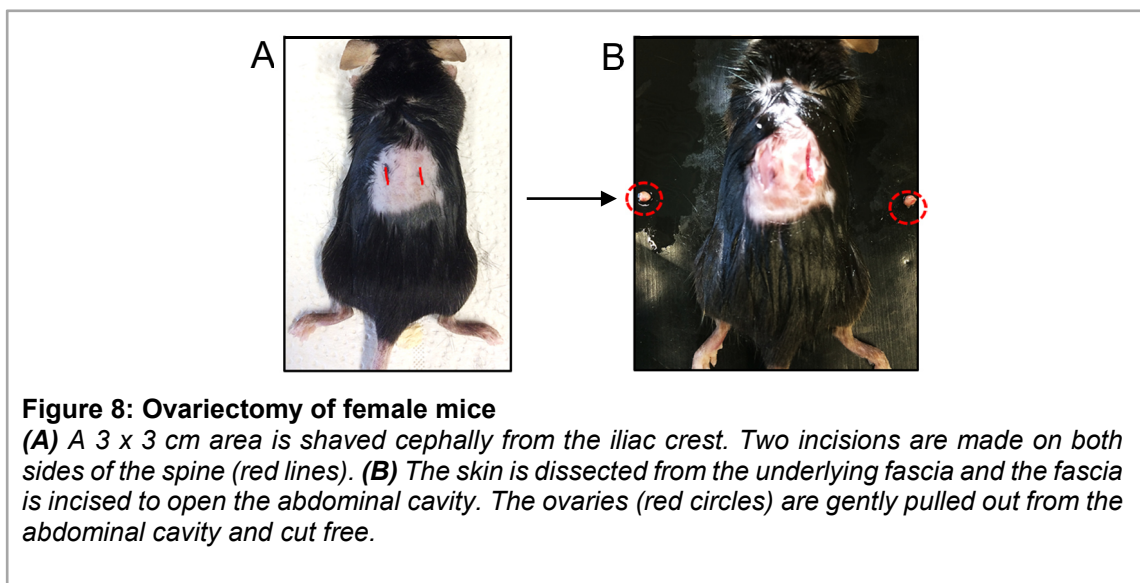


### 3.4 Surgical procedures and hormone replacement

#### 3.4.1 Ovariectomy

At 8-weeks of age, B6 females were deeply anesthetized using an intraperitoneal injection of 100 mg/kg body weight ketamine and 6 mg/kg body weight xylazine. To prevent drying of the eyes Bepanthen eye cream was applied. The dorsal lumbar region was shaved and disinfected with an iodine solution. The surgery was performed using a dorsal approach (Figure 8).

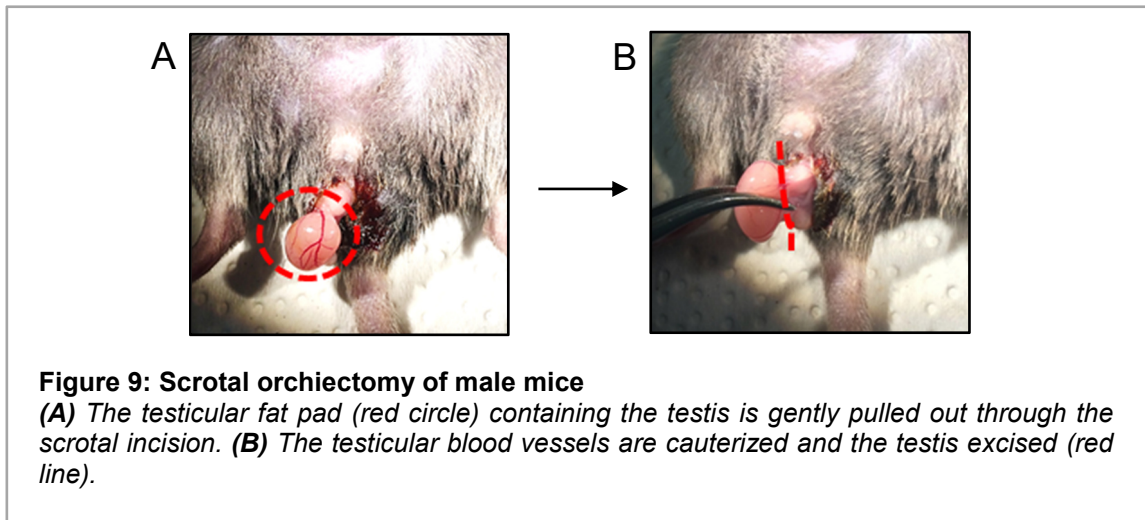
A small incision at the abdominal wall was made at each side of the spinal cord to excise the ovaries (Figure 8A,B). The skin incision was subsequently sutured and disinfected. Analgesia was provided by administration of 5 mg/kg bodyweight Carprofen. The success of the surgery was confirmed by daily cytological examination of vaginal lavage one week after recovery.



#### 3.4.2 Scrotal orchietomy

Adult, 8 weeks old B6 males were deeply anaesthetized by intraperitoneal injection of ketamine-xylazine (100 mg/kg body weight and 6 mg/kg body weight, respectively). To prevent the eyes from drying out, Bepanthen eye cream was applied. The scrotum was disinfected with iodine solution (Betaisadona) and opened by a small incision at the midline.

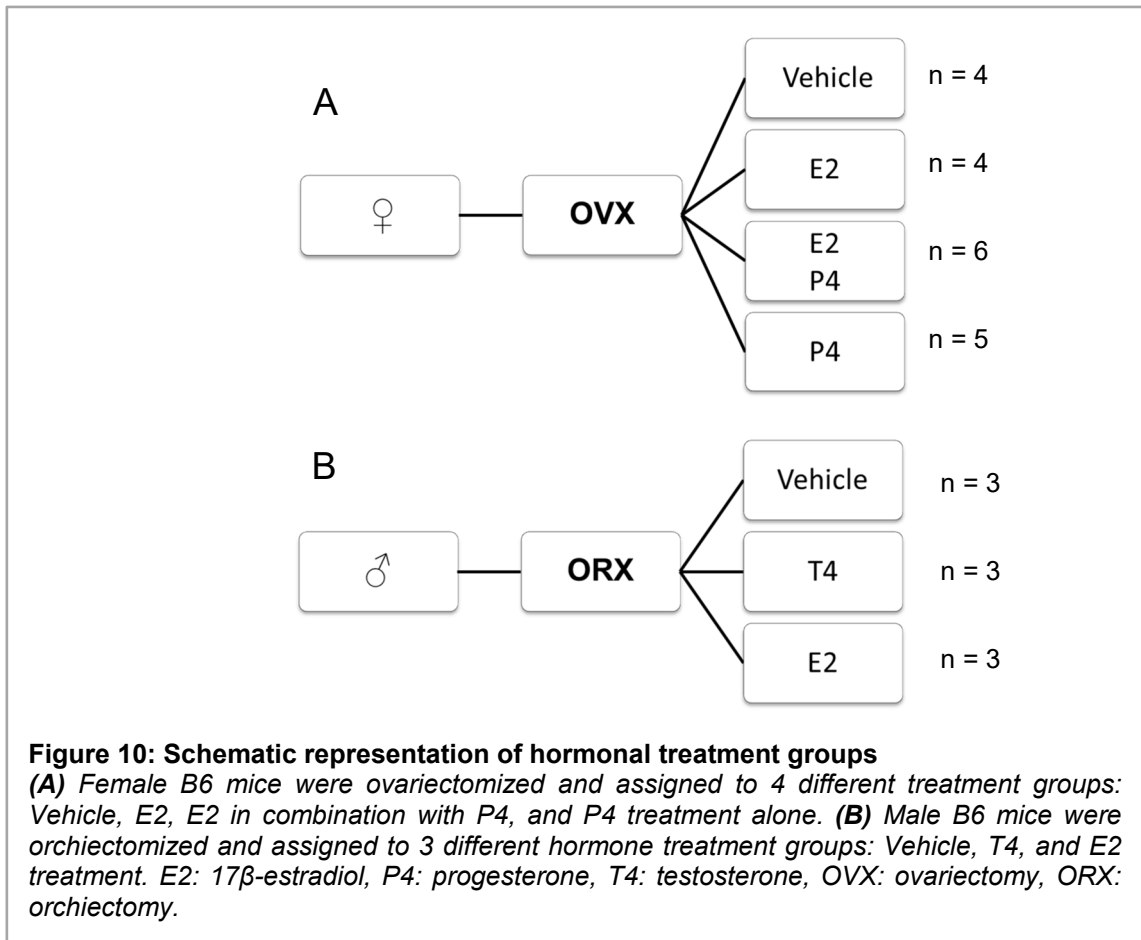
The testicular content including the testis, cauda epididymis, and the testicular blood vessels were gently pulled out using blunt forceps (Figure 9A). The testes were excised bilaterally, and the blood vessels were cauterized (Figure 9B). Subsequently, the abdominal skin was sutured and disinfected. Analgesia was provided by administration of 5 mg/kg bodyweight Carprofen.



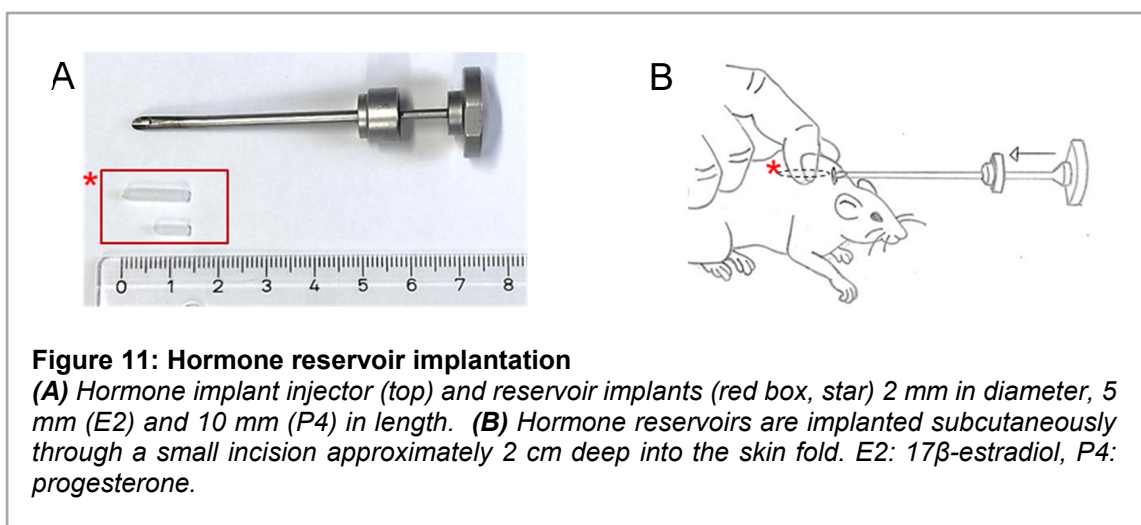
### 3.4.3 Hormone replacement

Seven days after ovariectomy, female mice were randomly assigned to 4 hormonal treatment groups (Figure 10A). Group 1 females (n = 4) served as controls and received vehicle implants. Group 2 females (n = 4) received 17 $\beta$ -estradiol implants (ME2-30). Group 3 females (n = 6) were injected intraperitoneally with progesterone (P4) (4  $\mu$ g/g bodyweight) dissolved in sesame oil, two weeks after E2 implantation. These females were sacrificed by transcardial perfusion with 2% PFA at 6 hours and at 24 hours after P4 injection. Group 4 females (n = 5) received progesterone implants (MP4-30) (Figure 10A). The estrous cycle was monitored throughout the whole experiment (37 days) for all females.

Males were assigned to 3 hormonal treatment groups 7 days after orchietomy (Figure 10B). Group 1 males (n = 3) served as controls and received vehicle implants, group 2 males (n = 3) received testosterone implants (MT4-30), and group 3 males received 17 $\beta$ -estradiol implants (ME2-30).



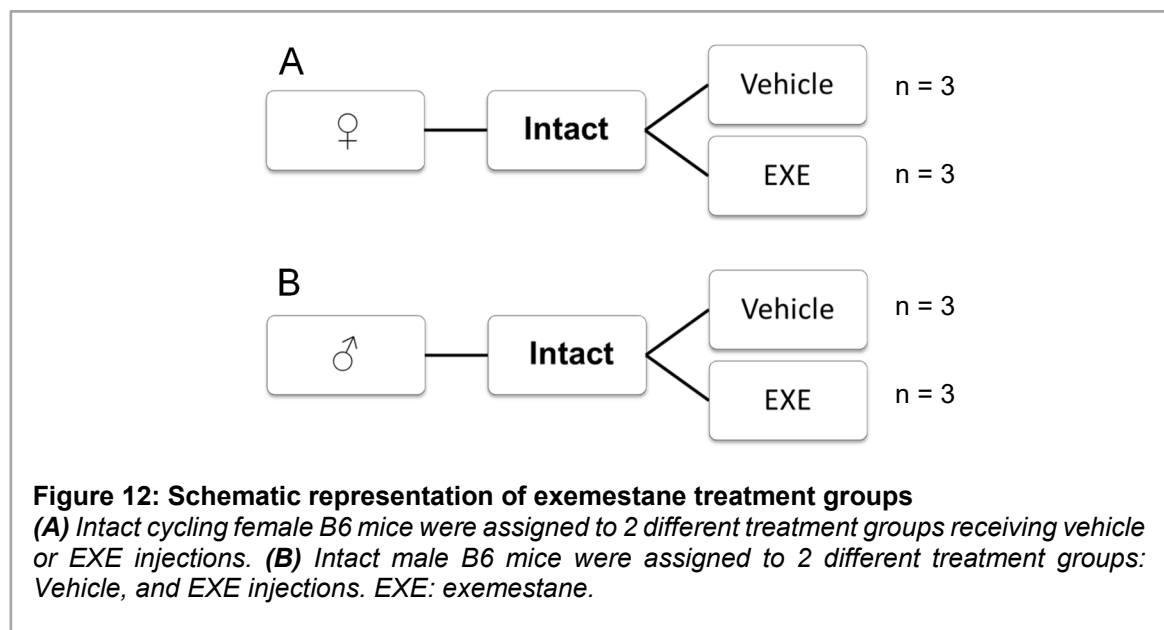
Reservoir implants (2 mm  $\varnothing$ , 5-10 mm length, Figure 11A) were subcutaneously implanted under short-term anaesthesia. The insertion of the implants was performed using an injector (Table 5, Figure 11). The skin between the scapulae was raised and the implant was ejected approximately 2 cm deep into the skin fold (Figure 11B).



The used implants are designed to release daily doses of hormone that were shown to achieve physiological plasma concentrations of progesterone (~15 ng/ml) and 17 $\beta$ -estradiol (60 pg/ml) corresponding to ovulatory plasma concentrations (Wood *et al.*, 2007). Analgesia was provided by administration of 5 mg/kg body weight Carprofen. After 14 days of hormone administration, mice were sacrificed and VNO tissue was collected for immunohistochemical analyses.

#### 3.4.4 Systemic block of aromatase activity

Adult B6 female and male mice (8 weeks, each gender n = 3) were treated i.p. once a day on 5 consecutive days with the aromatase inhibitor exemestane (EXE; 6-methylideneandrosta-1,4-diene-3,17-dione in 5% DMSO in sesame oil) at a dose of 5 mg/kg bodyweight or with vehicle only (n = 3; 5% DMSO in sesame oil). The estrous cycle in females was monitored daily during the whole duration of the experiment (19 days).



#### 3.5 Statistics

Quantitative PCR data were examined with the software Origin Pro 2017G. All data sets were tested for normal distribution and uniformity of variance. Given a parametric distribution, significance of difference between two distributions was measured using the unpaired Student's t-test. Data are shown as mean  $\pm$  SD (standard deviation). The value of  $p \leq 0.05$  was considered as statistically significant.

## 4 Results

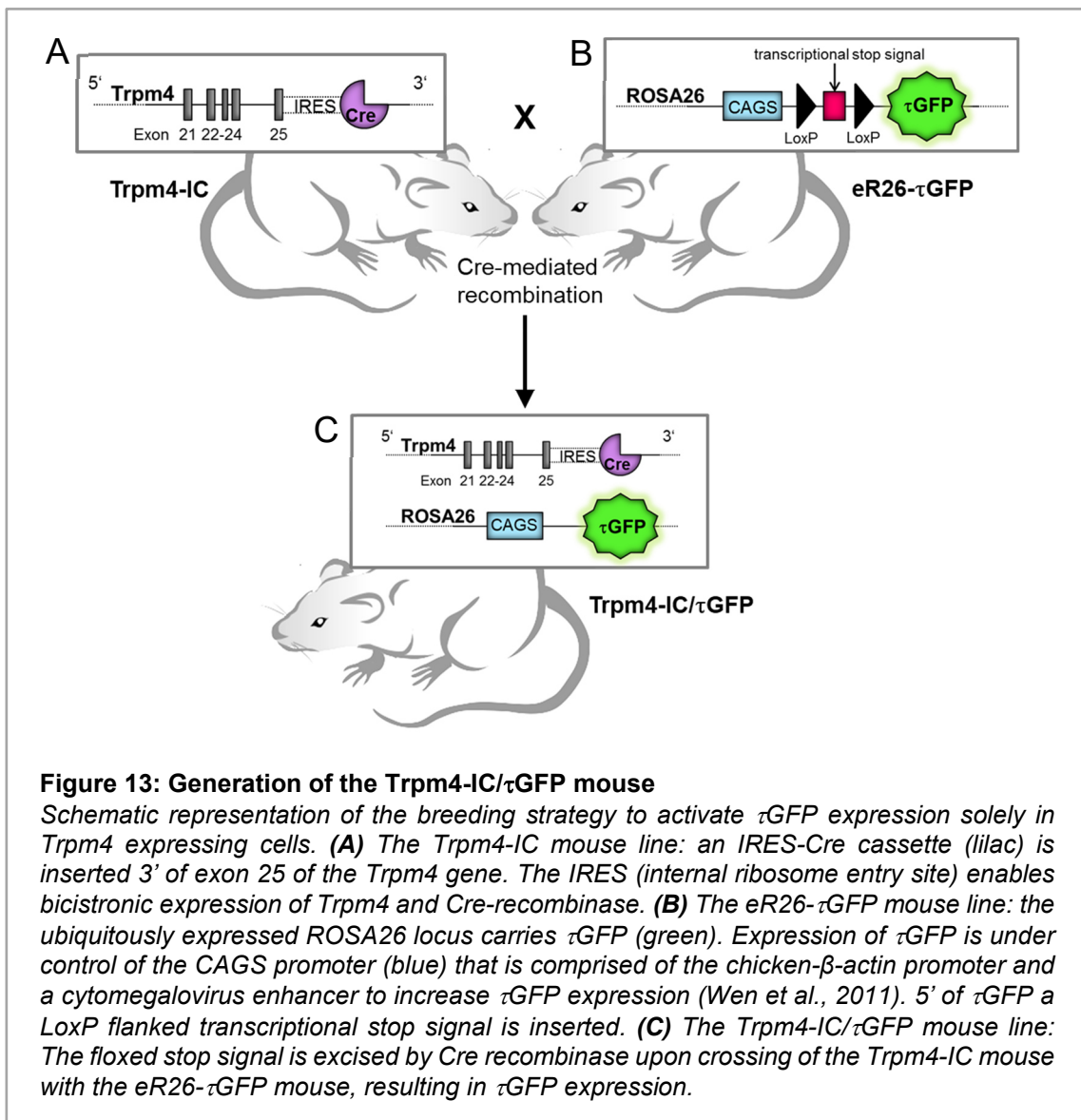
### 4.1 Trpm4

#### 4.1.1 Trpm4 expression and distribution in the murine olfactory system

To address the function of Trpm4 in the murine olfactory system, I performed a systematic analysis of Trpm4 expression in two different mouse strains, the fluorescent Trpm4-reporter mouse line Trpm4-IC/ $\tau$ GFP (Eckstein *et al.*, in preparation, Figure 13), and the global Trpm4 knockout mouse (Trpm4<sup>-/-</sup>, Vennekens *et al.*, 2007), in which exons 15 and 16 have been excised. To identify the cell types expressing Trpm4, I analyzed cryostat sections derived from the four different partitions of the olfactory system for the  $\tau$ GFP reporter in combination with IHC for the Trpm4 protein.

#### 4.1.2 The Trpm4-IC/ $\tau$ GFP reporter mouse line

To examine Trpm4 expression in the murine olfactory system, a novel mouse line, the Trpm4-IC/ $\tau$ GFP mouse (Eckstein *et al.*, in preparation) was generated employing the Cre-Lox recombination strategy through classical breeding of two mouse lines, the Trpm4-IRES-Cre (Trpm4-IC) knock-in mouse (kindly provided by R. Vennekens) and the eR26- $\tau$ GFP mouse (Wen *et al.*, 2011, kindly provided by U. Boehm). The Trpm4-IRES-Cre mouse carries an IRES (internal ribosome entry site) - Cre cassette downstream to the stop sequence of the Trpm4 gene (Figure 13A), which results in the bicistronic expression of Trpm4 and Cre-recombinase. In the eR26- $\tau$ GFP mouse line (Wen *et al.*, 2011, kindly provided by U. Boehm) (Figure 13B), the reporter gene  $\tau$ GFP that is comprised of the microtubule-associated protein  $\tau$  and GFP has been inserted into the ubiquitously expressed ROSA26 locus. To ensure that  $\tau$ GFP expression is restricted to Trpm4-Cre-expressing cells, a transcriptional stop sequence that is flanked by LoxP sites has been inserted 5' of the GFP reporter gene (Figure 13B). In the offspring chimera of these two lines, Cre-recombinase excises the floxed stop sequence, resulting in  $\tau$ GFP expression (Figure 13C). In these mice,  $\tau$ GFP expression is present in cells that acutely express Trpm4 and in cells where the Trpm4 promoter was active during the past.



#### 4.1.3 $\tau$ GFP expression in the MOE of *Trpm4*-IC/ $\tau$ GFP mice

To verify the successful generation of the *Trpm4*-IC/ $\tau$ GFP mouse, I first analyzed coronal cryosections of the MOE for  $\tau$ GFP expression. For this analysis, I used tissue sections from different MOE regions of adult, 7 weeks old *Trpm4*-IC/ $\tau$ GFP mice. The *Trpm4*-IC/ $\tau$ GFP reporter mouse showed abundant expression of  $\tau$ GFP in OSNs (Figure 14A).  $\tau$ GFP labeled OSNs were distributed throughout the depth of the MOE (Figure 14A, overview, and high magnification image, green). Despite strong GFP labeling, no *Trpm4*-ir was detected in the MOE of adult mice (Figure 14A,C).

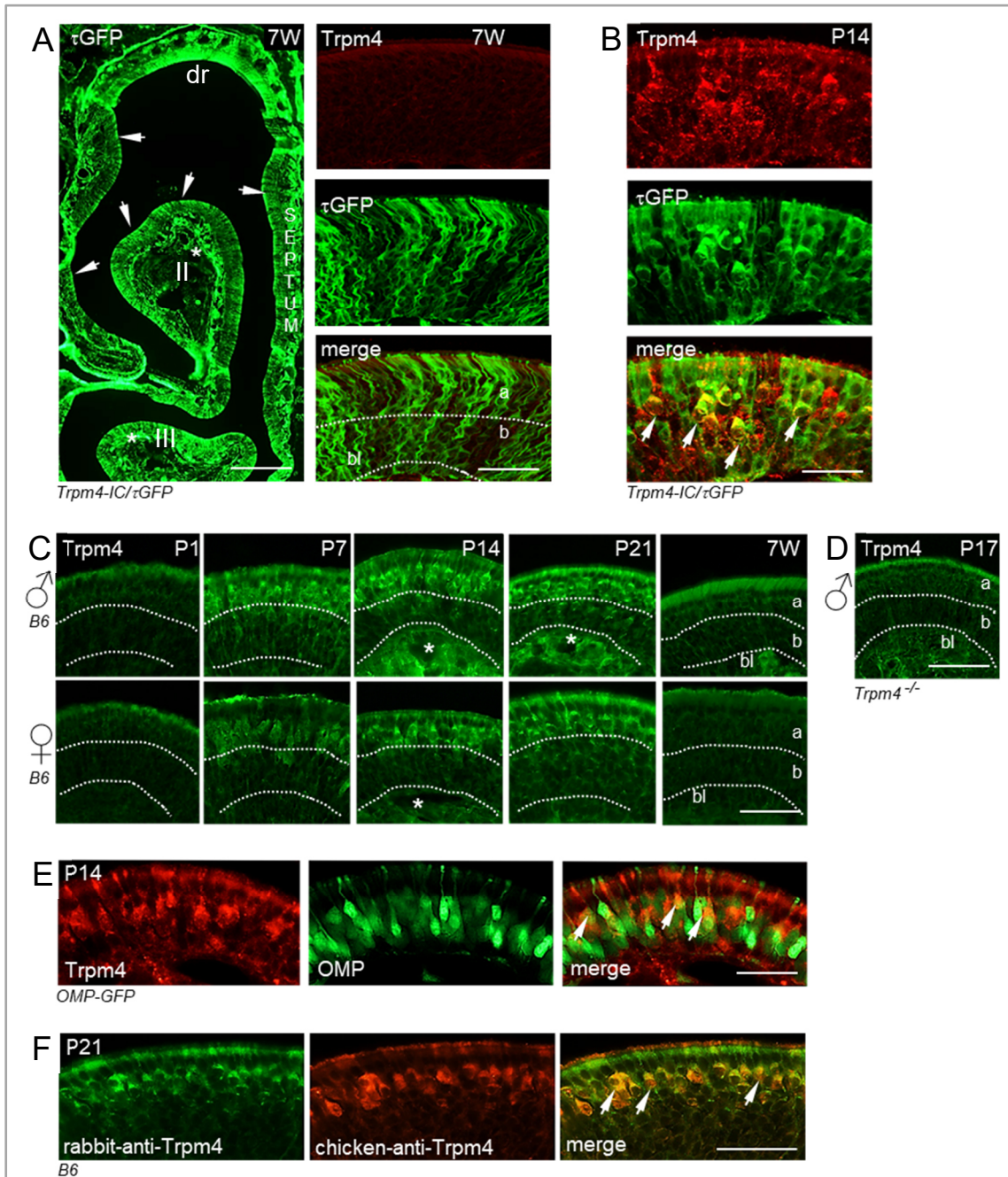


**Figure 14: Transient expression of Trpm4 during MOE development**

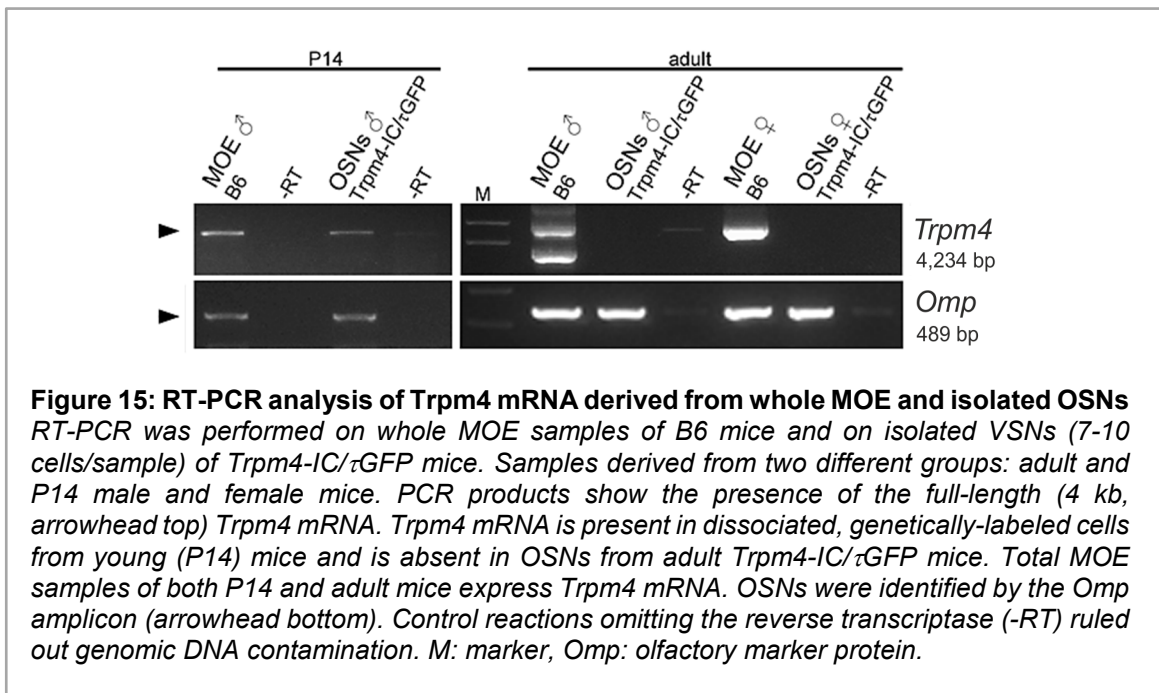
(A) Immunohistochemistry for Trpm4 (red) and  $\tau$ GFP (green) in the right nasal cavity of an adult, 7 weeks old Trpm4-Ic/ $\tau$ GFP mouse. Cells expressing  $\tau$ GFP are dispersed throughout the whole MOE (arrows). High magnifications show absence of Trpm4-ir in the adult MOE. (B) Immunohistochemistry for Trpm4 and  $\tau$ GFP in a Trpm4-Ic/ $\tau$ GFP mouse at 2 weeks of age shows coexpression of both Trpm4 (red) and  $\tau$ GFP (green) in the majority of OSNs (arrows). (C) Immunohistochemistry for Trpm4 in coronal sections of the olfactory epithelium (endoturbinates II) of male (top) and female (bottom) B6 mice at postnatal day (P) 1, P7, P14, P21, and 7 weeks of age. Trpm4-ir (green) is evident in OSN somata and dendrites between P7 and P21 but absent in the early postnatal (P1) and in the adult MOE (7W). (D) Specificity of the Trpm4 staining was verified by the absence of Trpm4-ir in age matched (P17) Trpm4<sup>-/-</sup> mice. (E) The vast majority of Trpm4-positive OSNs (red) colocalizes with the olfactory marker protein (Omp, green, arrows), a marker for mature OSNs. (F) Double labeling IHC for Trpm4 in the VNO of an adult B6 mouse using two different Trpm4 antibodies from two different species (rabbit and chicken). Rabbit-anti Trpm4 (green) and chicken-anti Trpm4 (red) label the same cells (arrows). a: apical MOE layer; b: basal MOE layer; bl: basal lamina; dr: dorsal roof; II, III: endoturbinates. Scale bars A: 200  $\mu$ m, magnification: 20  $\mu$ m; B, C, D: 20  $\mu$ m; E, F: 50  $\mu$ m.

Thus, Trpm4 expression takes place at an earlier time of development. To determine the onset of Trpm4 protein expression in the MOE, I performed a systematic analysis of the postnatal expression pattern of Trpm4. This analysis comprised different developmental ages in male and female B6 mice (postnatal day (P)1, P7, P14, P21, 7W; Figure 14C). These age groups were chosen based on important developmental events that take place at those particular time points: Shortly after birth (around P1), neonates are exposed to volatile olfactory inputs and have to use the olfactory system in order to breast feed (Latham and Mason, 2004; Al Ain *et al.*, 2013). Around P7, ears, and at P14, eyes begin to open, resulting in increased exploratory behaviors (Theiler, 1972; Williams and Scott, 1954). Finally, at P21, juvenile mice undergo weaning and change their diet from milk to solid food (Le Roy *et al.*, 2001). As representation for the entire MOE, a high magnification of endoturbinates II is shown in Figure 14C. Analysis of Trpm4 expression in the developing MOE revealed that in contrast to the adult MOE, strong Trpm4-ir was present in OSNs in the young MOE. Trpm4 expression in OSNs displayed dynamic and transient characteristics. At P1, OSNs were devoid of any Trpm4-ir (Figure 14C, left panel). Trpm4 expression emerged around the first postnatal week with a few Trpm4 positive OSNs at P7. At P14, cell density of Trpm4-positive OSNs increased and reached its maximum. At P21, the number of Trpm4-positive OSNs started to decline and was below detection threshold reaching adulthood at 7 weeks of age. I detected Trpm4-ir in the apical half of the MOE, where the majority of mature OSNs are located (Figure 14C). The basal, immature half of the MOE, however, showed no Trpm4-ir at any developmental age analyzed (Figure 14C). Trpm4 expression pattern did not differ between male and female mice during development (Figure 14C). As control for antibody specificity, I performed experiments on tissue from age matched (P17) global Trpm4<sup>-/-</sup> knockout mice. The knockout tissue was devoid of any Trpm4-ir (Figure 14D).

To verify that Trpm4 labeled OSNs in the apical MOE are indeed mature cells, I performed IHC for Trpm4 in the MOE of OMP-GFP mice (Potter *et al.*, 2001) (Figure 14E). OMP-GFP mice express GFP under the promoter of the olfactory marker protein (OMP), thereby labeling only mature OSNs. Robust immunostaining for Trpm4 was evident only in OMP-positive OSN somata and dendrites, identifying Trpm4 positive cells exclusively as mature OSNs. Double labeling of Trpm4 and  $\tau$ GFP in 2 weeks old Trpm4-IC/ $\tau$ GFP mice showed that  $\tau$ GFP and Trpm4 are coexpressed in OSNs during MOE development (Figure 14B) and that with age the acute expression of Trpm4 in OSNs declines, whereas  $\tau$ GFP expression is maintained. In summary, in the developing MOE,  $\tau$ GFP reports acute Trpm4 expression, and in the adult MOE,  $\tau$ GFP reports the history of Trpm4 expression and in the developing MOE. Identical results were obtained using

a second anti-Trpm4 antibody, deriving from another species (chicken-anti-Trpm4, Osenses) (Figure 14F, Table 2).

This result was further confirmed by RT-PCR on mRNA using isolated from manually collected single OSNs of Trpm4-IC/ $\tau$ GFP mice, identified by GFP fluorescence and morphology. mRNA from whole MOE tissue of B6 mice served as positive control. Samples derived from juvenile male mice at P14, and from adult male and female mice at 7 weeks of age (Figure 15).

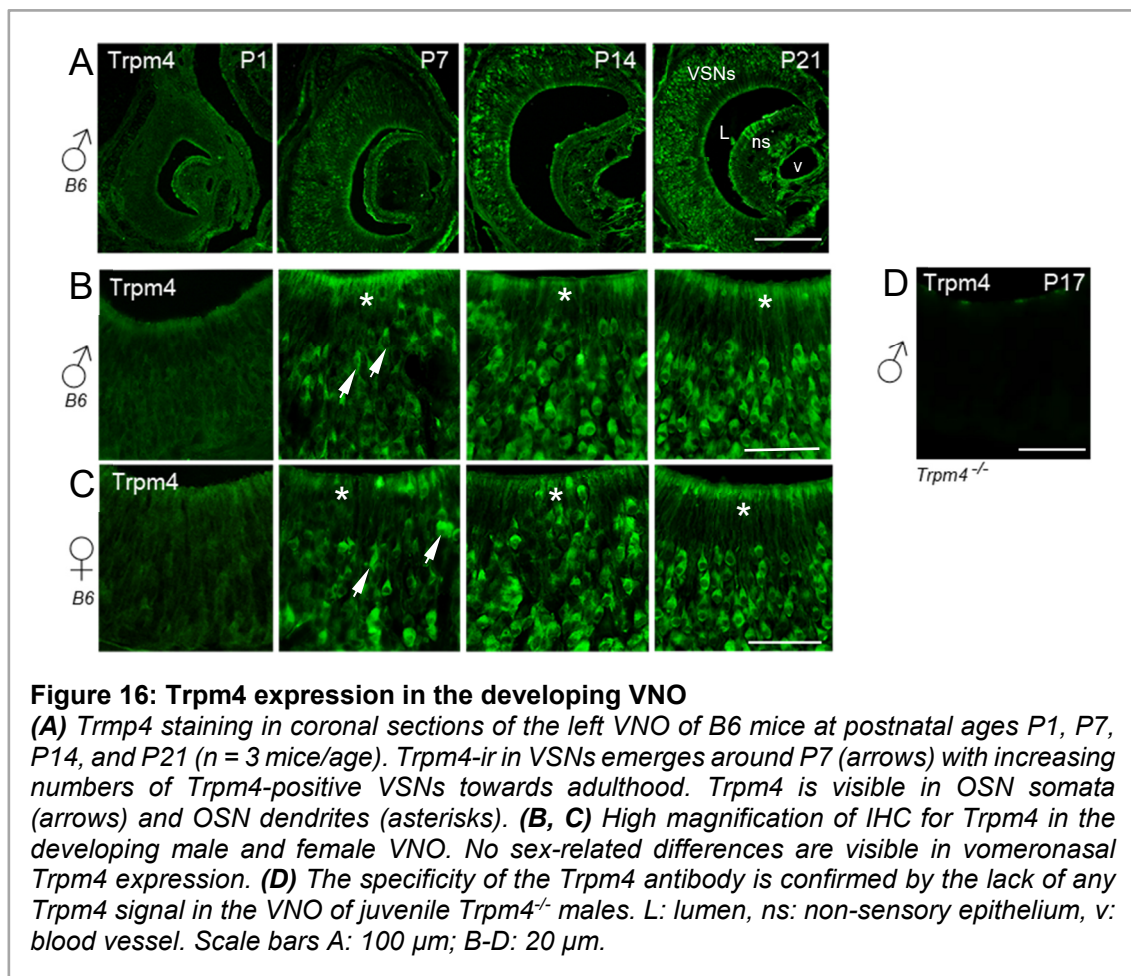


RT-PCR primers (Table 4) were designed to amplify the full-length *Trpm4* as annotated in the Ensembl genome browser database (ENSMUSG00000038260, www.ensembl.com). The RT-PCR for *Trpm4* revealed that whole tissue samples of both P14 and 7 weeks old mice, as well as of adult male and female mice were positive for *Trpm4* mRNA. Consistent with the IHC data depicted in Figure 14C, collected OSNs of adult Trpm4-IC/ $\tau$ GFP mice yielded no product for *Trpm4*, whereas OSNs of Trpm4-IC/ $\tau$ GFP mice at P14 were positive for *Trpm4* mRNA (Figure 15). Purified PCR products were confirmed by direct sequencing (Seqlab), and showed that the identified PCR products correspond to the full length 4,234 bp *Trpm4* encoding the functional channel. The presence of *Trpm4* in whole tissue samples can be explained by the widespread expression of *Trpm4* in endothelial cells (Mathar *et al.*, 2014) and the presence of such in the samples is attributed to the method of tissue preparation. Altogether, the results

reveal that *Trpm4* is expressed in OSNs and that its expression is developmentally regulated.

#### 4.1.4 Expression of *Trpm4* during postnatal development of the VNO

Having shown that *Trpm4* is developmentally regulated in the MOE, I also analyzed *Trpm4* expression in the VNO at the same developmental time points by IHC. VNO sections derived from B6 mice at postnatal days 1 (P1), P7, P14, and P21 (Figure 16).



*Trpm4*-ir in VSNs emerged at P7 with increasing numbers of positive cells towards the time of weaning (P21).

To quantify the changes in *Trpm4*-ir in VSNs, I performed cell counts using *Trpm4*-IHC on coronal cryosections of the VNO at different ages, counterstained by the nuclear dye Hoechst 33342. At P1 VSNs were devoid of any *Trpm4*-ir, whereas at P7 32%, at P14 48%, and at P21 73% of all analyzed VSNs were positive for *Trpm4* ( $n = 3$  mice for each

developmental stage). Male and female mice did not show any obvious differences in vomeronasal Trpm4 expression during the first 3 postnatal weeks (Figure 16B,C).

#### 4.1.5 Sexually dimorphic Trpm4 expression in VSNs of adult mice

To correlate  $\tau$ GFP expression with the expression of the Trpm4 protein, I performed double-labeling IHC for Trpm4 and  $\tau$ GFP on coronal cryosections of the VNO of adult, 7 weeks old, sexually mature Trpm4-IC/ $\tau$ GFP mice (Figure 17). These analyses showed that virtually all VSNs were positive for  $\tau$ GFP. In addition, supporting cells and cells of the non-sensory epithelium showed strong  $\tau$ GFP fluorescence (Figure 17A). Double-labeling experiments for Trpm4 protein and  $\tau$ GFP revealed that  $\tau$ GFP coincides with acute Trpm4 protein expression in virtually all VSNs of both males and females (Figure 17B). Profound Trpm4 staining was observed in VSN somata at all depths of the sensory epithelium with no zonal restrictions to  $G\alpha_i/G\alpha_o$  layers (Figure 17B). Furthermore, I detected Trpm4-ir in dendrites and dendritic knobs (Figure 17B, asterisks). Double-labeling experiments in OMP-GFP mice identified Trpm4 positive VSNs as mature (Figure 17D). Interestingly, Trpm4-IHC in OMP-GFP mice revealed that Trpm4 is not expressed in axon bundles. As a control for the antibody specificity, age-matched male Trpm4<sup>-/-</sup> mice were used and the VNO was devoid of any Trpm4 signal (Figure 17E). Surprisingly, I observed that around 50% of adult females were devoid of acute Trpm4 expression in VSNs and solely exhibited  $\tau$ GFP fluorescence (Figure 17C), whereas no such variations of Trpm4 expression occurred in any of the males analyzed (n = 6) (Figure 17B).

Similar to the MOE, Trpm4 protein expression in VSNs was confirmed using two different anti-Trpm4 antibodies. I performed double labeling experiments using anti-Trpm4 antiserum #ACC-044 (rabbit-anti-Trpm4, Alomone Labs), in combination with a second anti-Trpm4 antiserum, made in chicken (chicken-anti-Trpm4, Osenses) (Figure 17F, Table 2). IHC experiments using the chicken-anti-Trpm4 antiserum yielded identical results to the rabbit antiserum with strong Trpm4 staining of VSN dendrites and somata (Figure 17F). Furthermore, both Trpm4 antisera labeled the exact same cells (Figure 17F, merge).

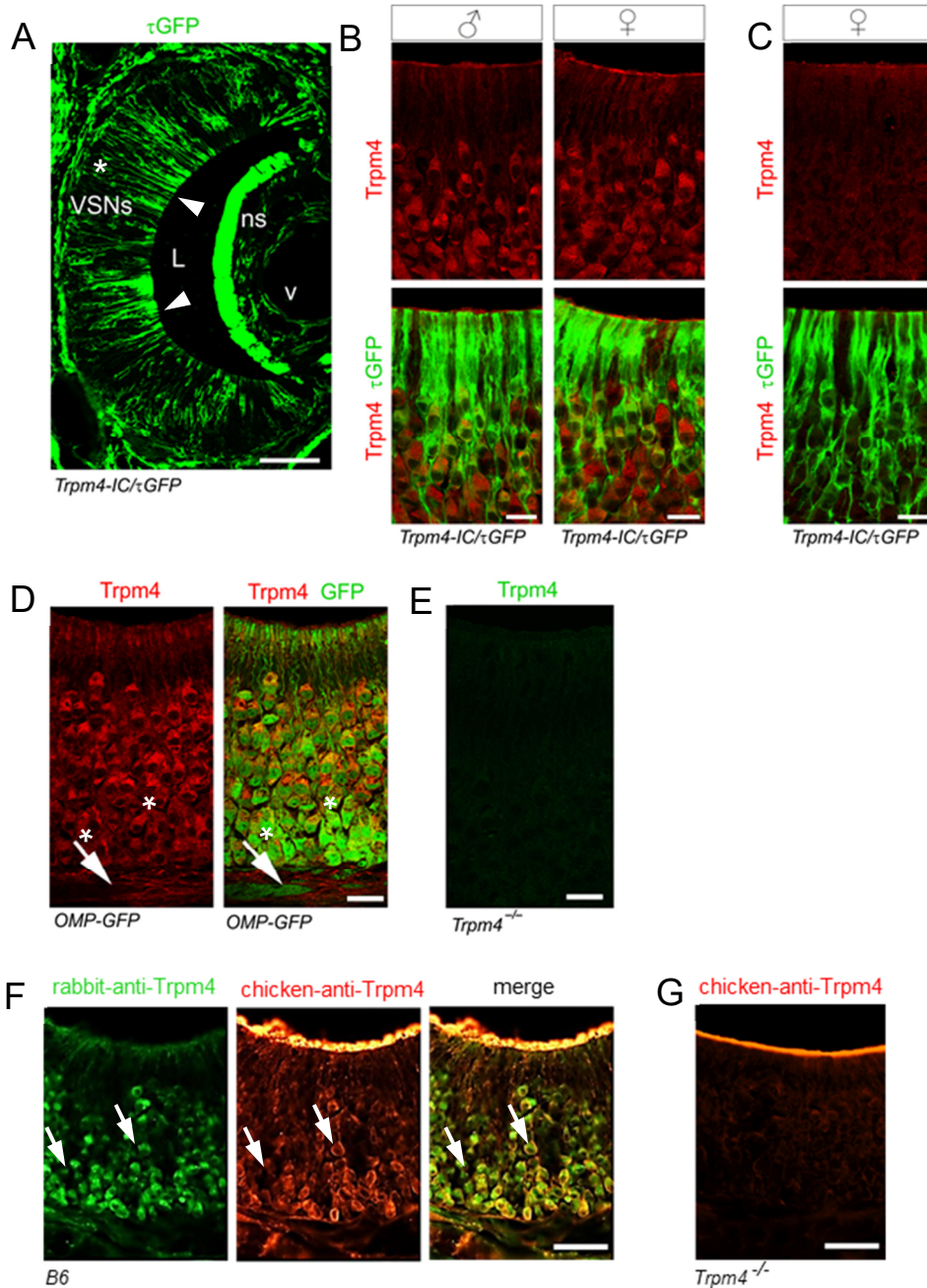


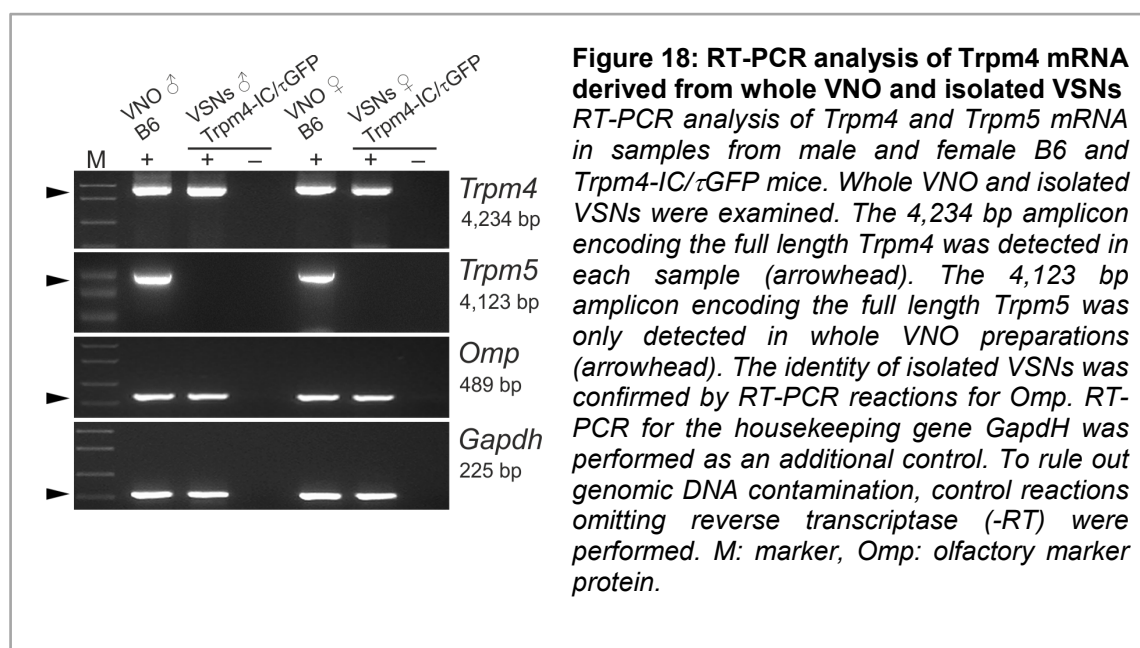
**Figure 17: *Trpm4* expression in the vomeronasal organ**

(A) IHC for  $\tau$ GFP in a coronal cryosection of the left VNO of an adult, 7 weeks old, male *Trpm4-IC/\tau*GFP mouse.  $\tau$ GFP is visible throughout the VNO in sensory neurons (asterisk) and in supporting cells (arrowheads), but also in cells of the non-sensory epithelium (ns), and in vascular endothelial cells (v). (B) Both male and female VNO of *Trpm4-IC/\tau*GFP mice show abundant *Trpm4* protein expression (red) colocalizing with  $\tau$ GFP in OSNs. *Trpm4-ir* is absent in supporting cells. (C) Despite abundant  $\tau$ GFP expression, about 50% of female VNO lacked *Trpm4-ir*. (D) *Trpm4* and OMP-GFP colocalize in somata of VSNS, but not in axon bundles (arrow) of OMP-GFP mice. (E) The specificity of the *Trpm4* antibody is confirmed by the lack of *Trpm4* signal in the VNO of *Trpm4*<sup>-/-</sup> mice. (F) Double labeling IHC for *Trpm4* in the VNO of an adult B6 mouse using two different *Trpm4* antibodies from two different species (rabbit and chicken). Rabbit-anti *Trpm4* (green) and chicken-anti *Trpm4* (red) label the same cells with a strong signal in VSN dendrites and somata (merge). Chicken-anti *Trpm4* additionally labels VSN microvilli (asterisks). (G) Control experiments on the VNO of *Trpm4*<sup>-/-</sup> mice depict an unspecific signal of chicken-anti *Trpm4* in microvilli (asterisk). L: lumen, ns: non-sensory epithelium, v: blood vessel, Scale bars A: 200  $\mu$ m; B-E: 20  $\mu$ m; F, G: 50  $\mu$ m.

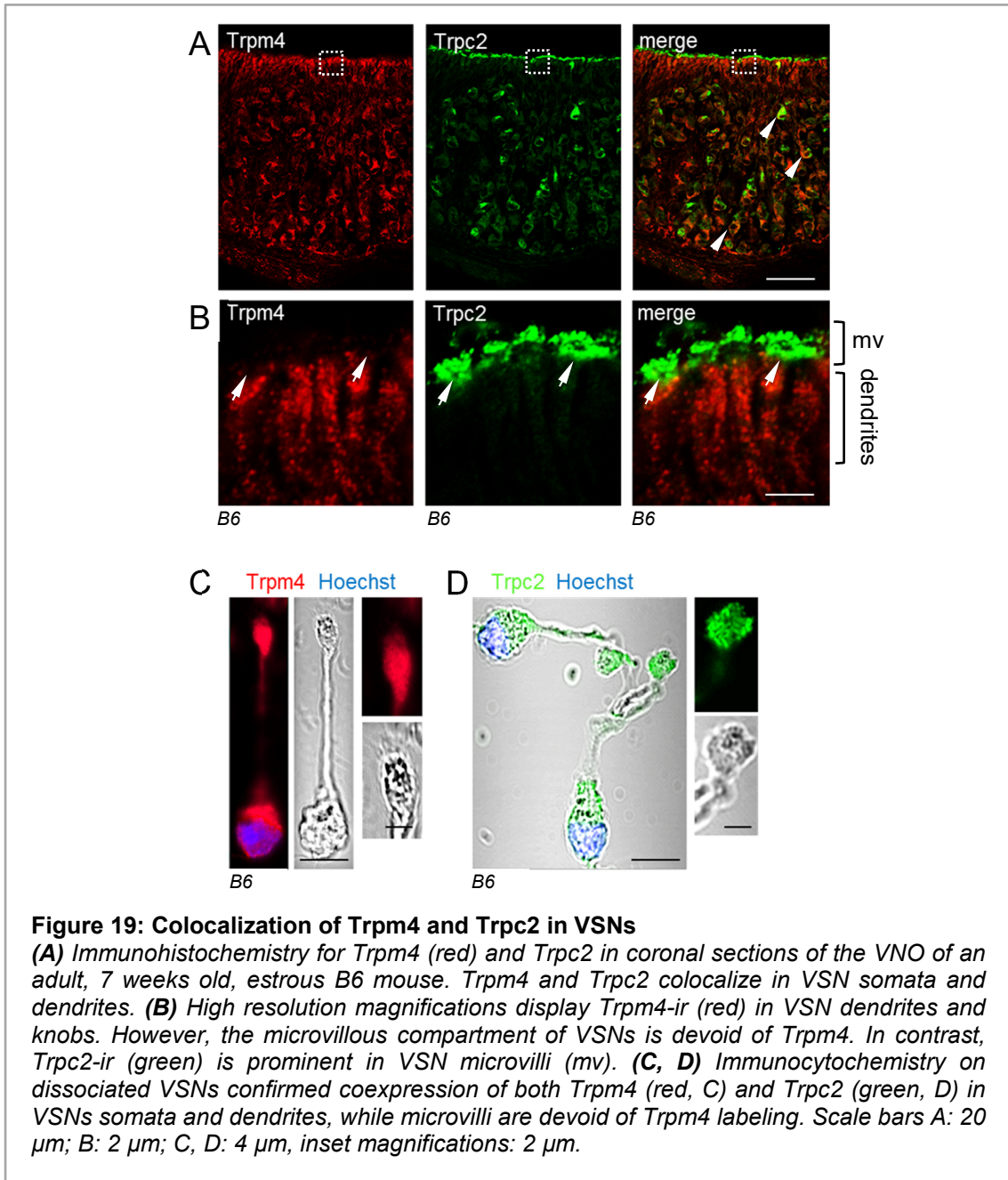
However, strong microvillar Trpm4-ir was solely visible when employing the chicken-anti-Trpm4 antiserum. Control experiments using VNO cryosections of Trpm4<sup>-/-</sup> mice showed that the microvillar signal is unspecific, as it was also present in the Trpm4<sup>-/-</sup> tissue (Figure 17G). This unspecific labeling was not evident using rabbit-anti-Trpm4 (Figure 17E).

To further analyze the possibility that Trpm4 expression is sexually dimorphic, I performed RT-PCR experiments on mRNA isolated from whole MOE tissue of male and female B6 mice, and from manually collected single OSNs of Trpm4-IC/ $\tau$ GFP mice (Figure 18). Here, I employed a primer set that covers the full length 4234 bp *Trpm4* amplicon (Table 4). Even though Trpm4-IHC revealed that 50% of females were devoid of vomeronasal Trpm4 expression, the RT-PCR experiment demonstrated that mRNA of single VSNs and of the whole VNO of adult animals contained the full length *Trpm4* (Figure 18).

I also performed RT-PCR for *Trpm5*, a second Ca<sup>2+</sup> activated cation channel, using gene-specific primers flanking the complete coding region the *Trpm5* mRNA, (Table 4). This experiment revealed that  $\tau$ GFP labeled VSNs of the Trpm4-IC/ $\tau$ GFP strain are negative for *Trpm5* mRNA (Figure 18). In contrast, cDNA deriving from total VNO samples contained *Trpm5* mRNA, as a subpopulation of cells of the non-sensory vomeronasal epithelium expresses Trpm5 (Kaske *et al.*, 2007; Kusumakshi *et al.*, 2015).



To further characterize the subcellular localization of Trpm4, double-labeling of Trpm4 and Trpc2, the key channel involved in the vomeronasal signaling transduction, was performed on VNO sections of B6 mice (Figure 19A). As seen before, Trpm4-ir was mainly localized to VSN dendrites, dendritic knobs and somata (Figure 19A, arrowheads), but not to VSN microvilli (Figure 19B, arrows).



In contrast, I detected strong Trpc2-ir in VSN microvilli (Figure 19B, arrows). This result was particularly obvious in dissociated cells (Figure 19C, D high magnification of VSN microvilli). Thus, due to the different compartmental expression of Trpc2 and Trpm4, both channels may serve different functions in VSNs. As the microvilli are the main

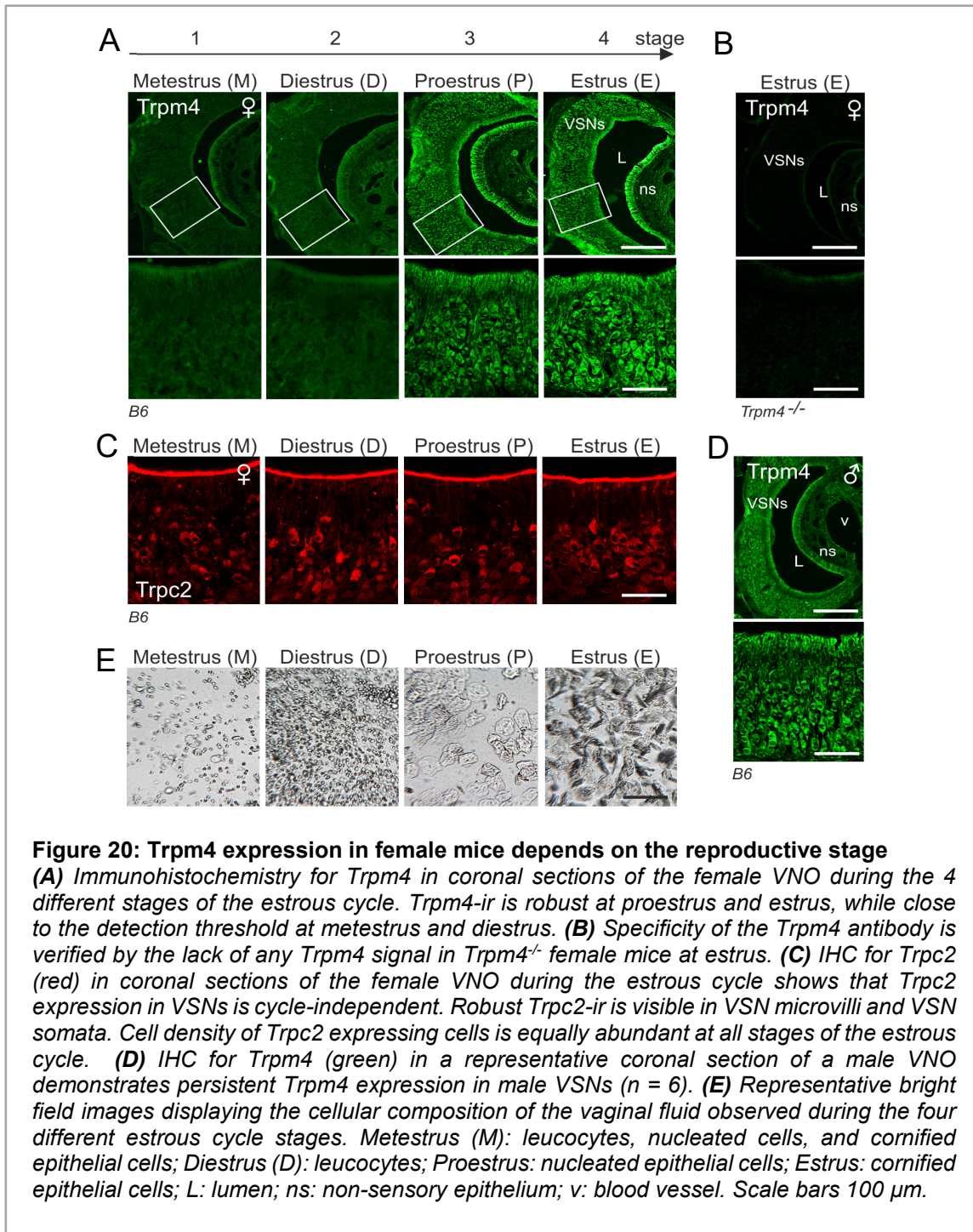
compartment for VSN signal transduction, the absence of Trpm4 may coincide with a more downstream regulatory function of Trpm4 in the olfactory signal transduction of VSNs.

#### 4.1.6 Trpm4 expression in VSNs is estrous cycle dependent

As stated earlier (4.1.5), Trpm4 protein expression was absent in about 50% of female VNOs although *Trpm4* mRNA was evident. Since females undergo hormonal changes during their estrous cycle, I addressed the idea that vomeronasal expression may coincide with female cyclicity and hormonal changes during this time period. Therefore, I performed Trpm4-IHC on coronal cryosections of the VNO of adult female B6 mice at different estrous cycle stages. The murine estrous cycle has a length of 4-5 days and each of the four different stages, metestrus (M), diestrus (D), proestrus (P), and estrus (E) (Figure 20A) is characterized by a unique cellular composition of the vaginal fluid. For the identification of the cycle stage, vaginal cytology was assayed (Figure 20E). Additionally, I analyzed VNO sections of randomly chosen adult males to verify that males display steady Trpm4 expression in VSNs (Figure 20D).

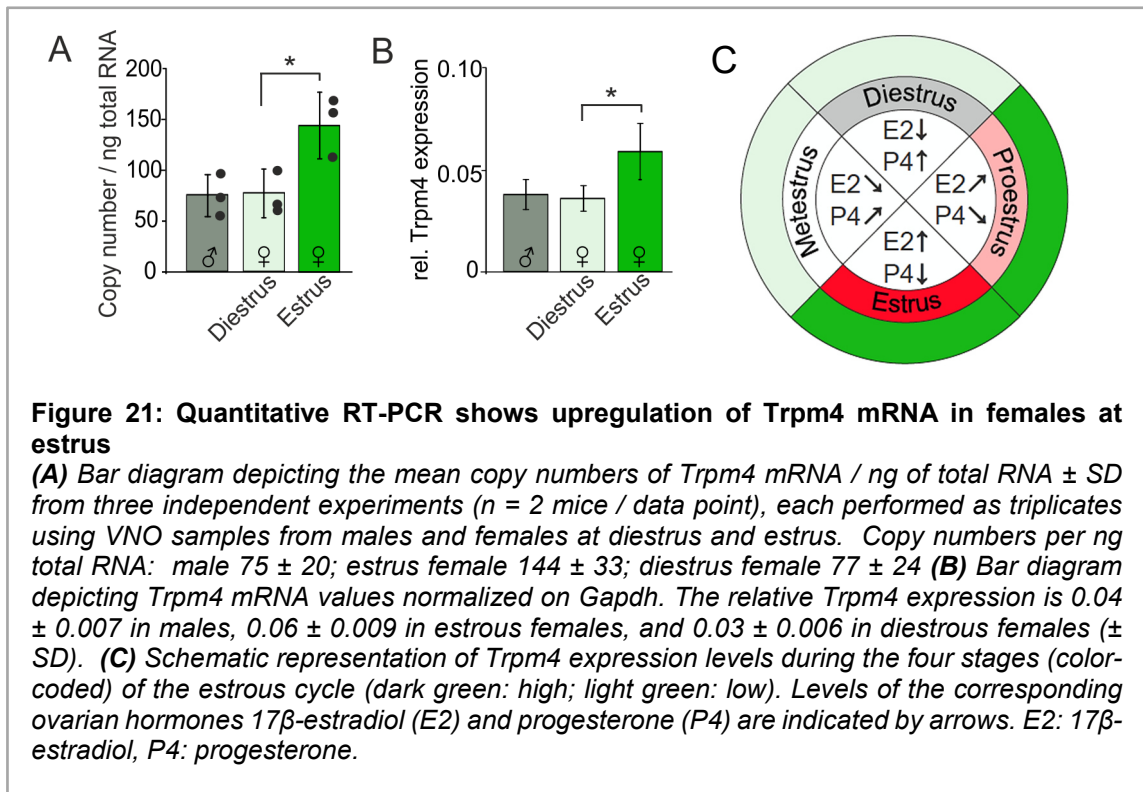
The results showed that in fact, only 50% of females exhibited robust Trpm4-ir in VSNs (Figure 20A). In detail, females prior to ovulation, in proestrus and estrus, displayed strong and robust Trpm4-ir in VSN somata, dendrites and dendritic knobs (Figure 20A, third and fourth panel). In contrast, postovulatory females, in metestrus and diestrus, showed Trpm4 expression that was close to the detection threshold (Figure 20A, first and second panel). In comparison, Trpm4-IHC on the VNO of randomly picked adult male mice showed equally abundant Trpm4-ir in VSNs in all mice analyzed (n = 6, Figure 20D). In addition, control experiments conducted on tissue from estrous global *Trpm4*<sup>-/-</sup> knockout females that exhibit a normal estrous cycle of 4 days, were devoid of any Trpm4-ir during the ovulatory phase (Figure 20B).

To further extend the impact of the estrous cycle on Trp channel expression, I also performed IHC analyses for Trpc2 in VSNs during the four different estrous cycle stages (Figure 20C). In these experiments, Trpc2-ir did not display any differences in fluorescence intensity, or in subcellular localization throughout the entire estrous cycle (Figure 20C). This shows that unlike Trpm4, Trpc2 expression is independent of the estrous cycle in the female VNO. Altogether, these results demonstrate a specific estrous cycle-dependent regulation of Trpm4 expression in VSNs that might coincide with the hormonal changes during the different estrous cycle stages.



To understand whether the cycle dependent regulation of *Trpm4* expression in VSNs is based on changes in mRNA levels or in protein levels, I analyzed mRNA levels by quantitative real-time RT-PCR (qRT-PCR) using gene-specific primers for *Trpm4* (Table 4, Figure 21). I used total RNA samples from the VNO of adult, 7 weeks old, male, and female B6 mice to compare *Trpm4* mRNA levels.

Female VNO samples were collected during the ovulatory phase (estrus) and the post-ovulatory phase (diestrus), in which the strongest differences in vomeronasal *Trpm4* expression were observed (4.1.6). qRT-PCR for *GapdH* served as internal control. Three independent experiments comprising 6 animals each group revealed that *Trpm4* mRNA is upregulated two-fold during the ovulatory phase in comparison to the post-ovulatory phase or to males (estrus female:  $144 \pm 33$  copies/ ng total RNA, diestrus female:  $77 \pm 24$  copies/ ng total RNA; male:  $75 \pm 20$  copies/ ng total RNA, Figure 21A).

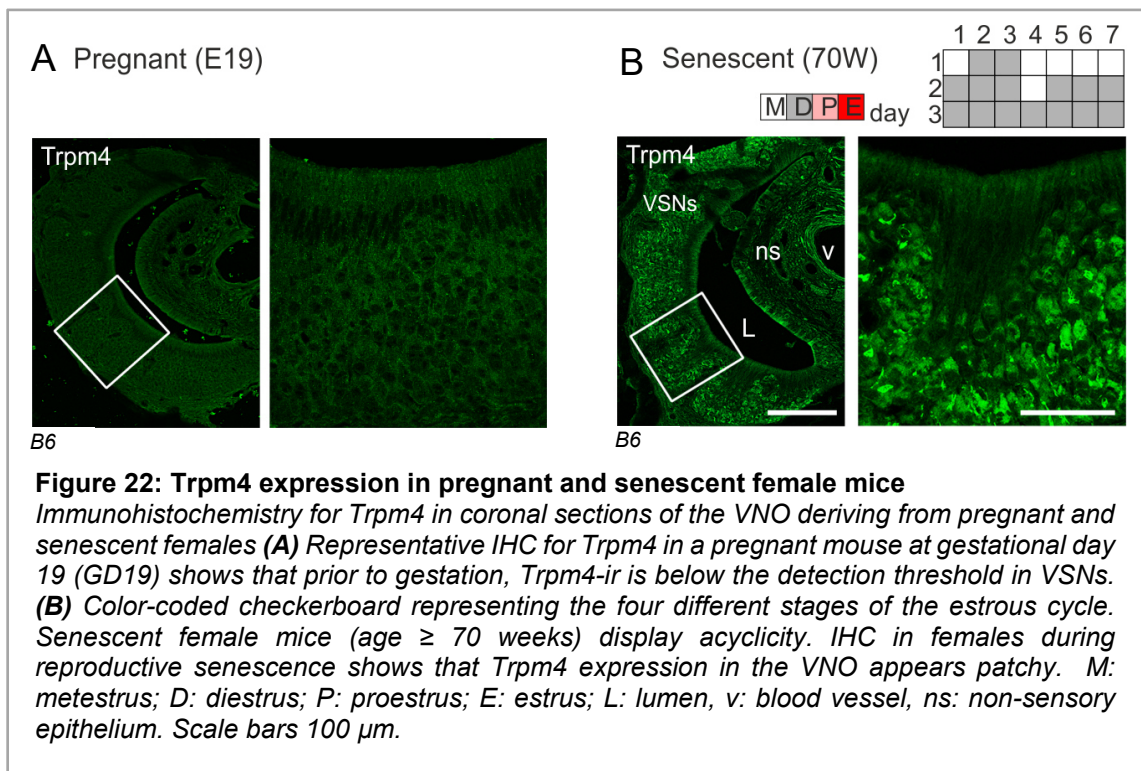


This result was also true when copy numbers were normalized to the housekeeping gene *GapdH* (Figure 21B). Relative expression of *Trpm4* in the estrous VNO is two-fold higher in comparison to diestrus VNO or to males (estrous female:  $0.06 \pm 0.009$ , diestrus female:  $0.03 \pm 0.006$ , male:  $0.04 \pm 0.007$ , Figure 21B).

Thus, the qPCR experiments suggest that *Trpm4* protein expression in the female VNO may be regulated at the mRNA level in a cycle dependent manner. This also raises the idea that gonadal hormones, such as  $17\beta$ -estradiol and progesterone, which guide the estrous cycle and female receptivity, may correlate with *Trpm4* expression in VSNs (Figure 21C).

#### 4.1.7 Regulation of Trpm4 expression in pregnant and aged females

The results described so far point out a relation between the female estrous cycle and Trpm4 expression in the VNO. Female cyclicity is characterized by repetitive changes of blood serum levels of various hormones (steroid hormones like  $17\beta$ -estradiol and progesterone, and peptide hormones such as LH and FSH). Interruptions of the estrous cycle can occur by events such as pregnancies or natural aging, which guide the females into anestrous phases. The first natural state that leads to cycle arrest is pregnancy, which is characterized by exceedingly high levels of serum progesterone until parturition after 3 weeks (Lonstein *et al.*, 2015). The second natural cycle disturbance is reproductive aging, which describes the process that guides the female mice from regular to irregular cycles and finally to acyclicity. This transition is driven by the neuroendocrine system resulting in diminished Gonadotrope releasing hormone (GnRH) output to the pituitary gland while ovaries of aged female mice are still able to exert moderate amounts of gonadal hormones and contain viable follicles until a very old age (Brinton, 2012; Koebele and Bimonte-Nelson, 2016).



To determine whether Trpm4 expression in VSNs is also influenced by pregnancy or reproductive senescence, I performed IHC analysis of Trpm4 expression in the VNO of two groups of B6 females differing in age and hormonal status (Figure 22). The first group included pregnant B6 mice ( $n = 3$ ), 2 days before delivery at gestational day 19. Most

interestingly, Trpm4-IHC on VNO sections of these animals showed weak and close to the detection threshold Trpm4-ir in VSNs (Figure 22A).

The second group of analyzed animals included 70 weeks old B6 females in natural reproductive senescence (n = 3). These mice showed an anestrous, acyclic phenotype, as identified by vaginal cytometry (Figure 22B, top). Furthermore, IHC on VNO sections of aged females showed a patchy Trpm4 expression with few but strongly labeled VSNs, and a larger fraction of unlabelled VSNs, compared to estrous females (Figure 22B).

Combining the results of pregnant and senescent females with the finding that Trpm4-ir in VSNs is high during proestrus and estrus and low during metestrus and diestrus, it appears that vomeronasal Trpm4 expression is downregulated during natural, non-receptive conditions.

#### **4.1.8 Cyclic regulation of Trpm4 expression depends on ovarian hormones**

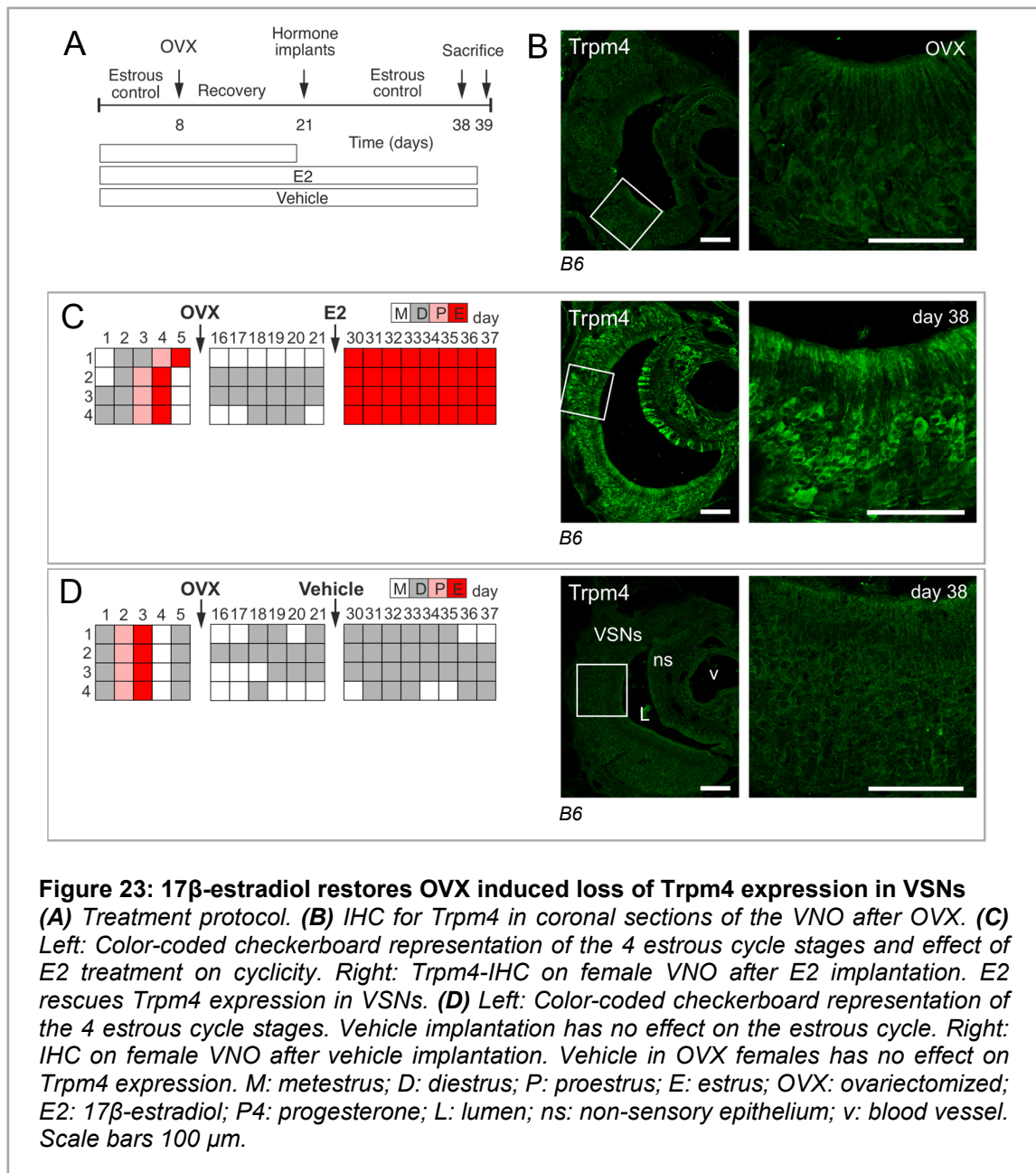
##### **4.1.8.1 Ovariectomy causes loss of Trpm4 expression in the female VNO**

To analyze the potential effects of  $17\beta$ -estradiol (E2) and progesterone (P4), the major gonadal hormones, on the cyclic regulation of vomeronasal Trpm4 expression in more detail, the female sex-steroid hormone production was disrupted by ovariectomy (OVX). Adult, 6-8 weeks old, intact cycling B6 females were used in this experiment and in all cases OVX resulted in cycle arrest (n = 30, Figure 23, Figure 24). OVX females displayed notably lower cell densities in vaginal smears. Furthermore, the vaginal opening in OVX females was closed and very dry and pale in appearance compared to sham-operated females.

Intriguingly, Trpm4-IHC on VNO cryosections revealed that OVX abolished Trpm4 expression (n = 12; Figure 23B). This result suggests that intact ovaries play a major role in reporting the estrous state of a female to the VNO and thereby regulate Trpm4 expression in VSNs. To verify the specificity of the observed effect, I performed rescue experiments by implanting subcutaneous reservoir pellets containing  $17\beta$ -estradiol (E2) into OVX females (Figure 23A). E2 hormone implants were designed to maintain physiological levels of circulating E2 corresponding to ovulatory plasma concentrations of ~60 pg/ml (Wood *et al.*, 2007).

The estrous cycle of each individual female was monitored throughout the experiment. *Trpm4*-ir in VSNs was analyzed after 38 days of treatment (Figure 23C,D). Mice that received E2 switched from OVX-induced acyclicity to a persistent estrus and displayed a dramatic increase in *Trpm4*-ir in VSNs ( $n = 4$ ; Figure 23C) compared to mice receiving placebo implants ( $n = 4$ ; Figure 23D).

This result shows that E2 plays an important role in the cycle-dependent *Trpm4* regulation in female VSNs.



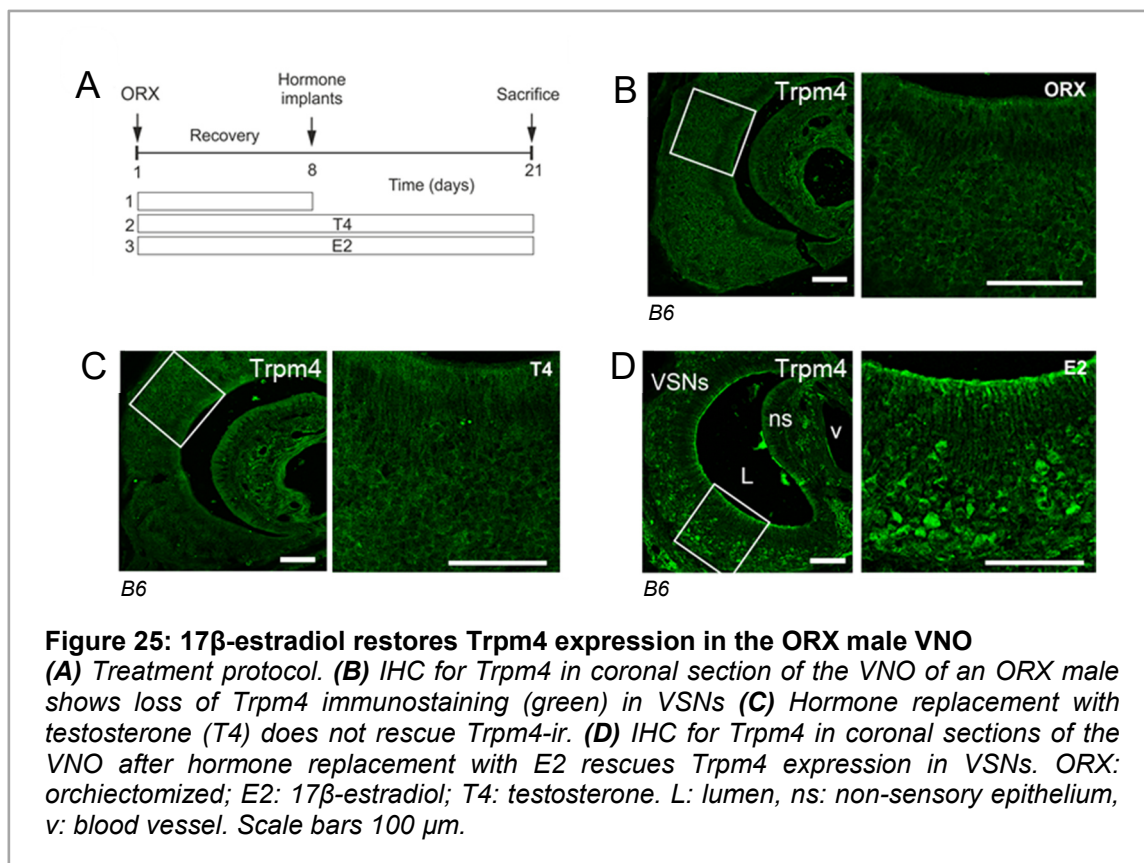


The IHC results show that the E2-induced upregulation of Trpm4-ir was reduced 6 h and 24 h after intraperitoneal injection of P4 (Figure 24B). Furthermore, P4 implantation alone shifted the estrous cycle of OVX mice to a persistent diestrus and did not elicit any Trpm4 signal comparable to the effect of E2 treatment in VSNs (Figure 24C).

In summary, systemic E2 but not P4 treatment rescues Trpm4 expression in the female VNO upon OVX. This effect is dampened by P4, which suggests that P4 acts antagonistically to E2 in the cycle-dependent regulation of vomeronasal Trpm4 expression.

#### 4.1.8.3 17 $\beta$ -estradiol restores Trpm4 expression in the ORX male VNO

The results point out so far, that the ovarian hormone 17 $\beta$ -estradiol is crucial for Trpm4 expression in the VNO of females. But what happens to Trpm4 expression in the male VNO when they are devoid of or supplemented with circulating gonadal hormones? Although testosterone is described as the predominant hormone in males, estrogen has been reported to be important in fluid homeostasis of the male reproductive tract (Hess, 2003).

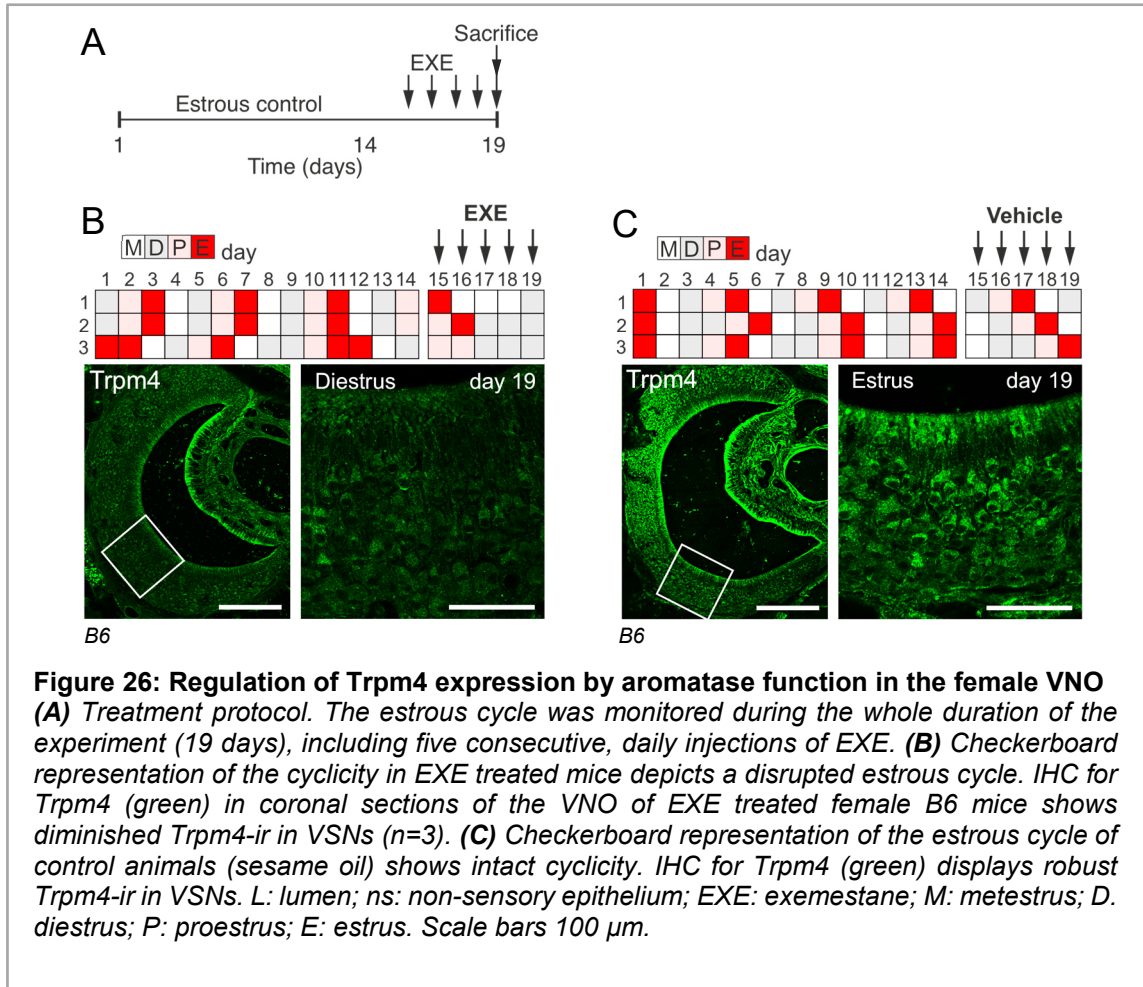


Therefore, male mice were orchietomized (ORX) and possible effects of hormone supplementation were analyzed (Figure 25). In the intact male VNO (Figure 17B, Figure 20D) Trpm4 staining is prominent in the somata and dendrites of VSNs. One week after ORX, the VNO was devoid of any Trpm4 signal (Figure 25B). This is likely to be attributed to the loss of gonadal hormones. Surprisingly, two weeks of constant testosterone treatment did not restore Trpm4-ir (Figure 25C). In contrast, two weeks of  $17\beta$ -estradiol supplementation rescued Trpm4 expression in VSNs of male ORX mice (Figure 25D).

Thus, the results reveal that  $17\beta$ -estradiol but not testosterone can induce Trpm4 expression in VSNs after ORX.

#### **4.1.8.4 Pharmacological block of endogenous $17\beta$ -estradiol synthesis diminishes Trpm4 expression in VSNs of both males and females**

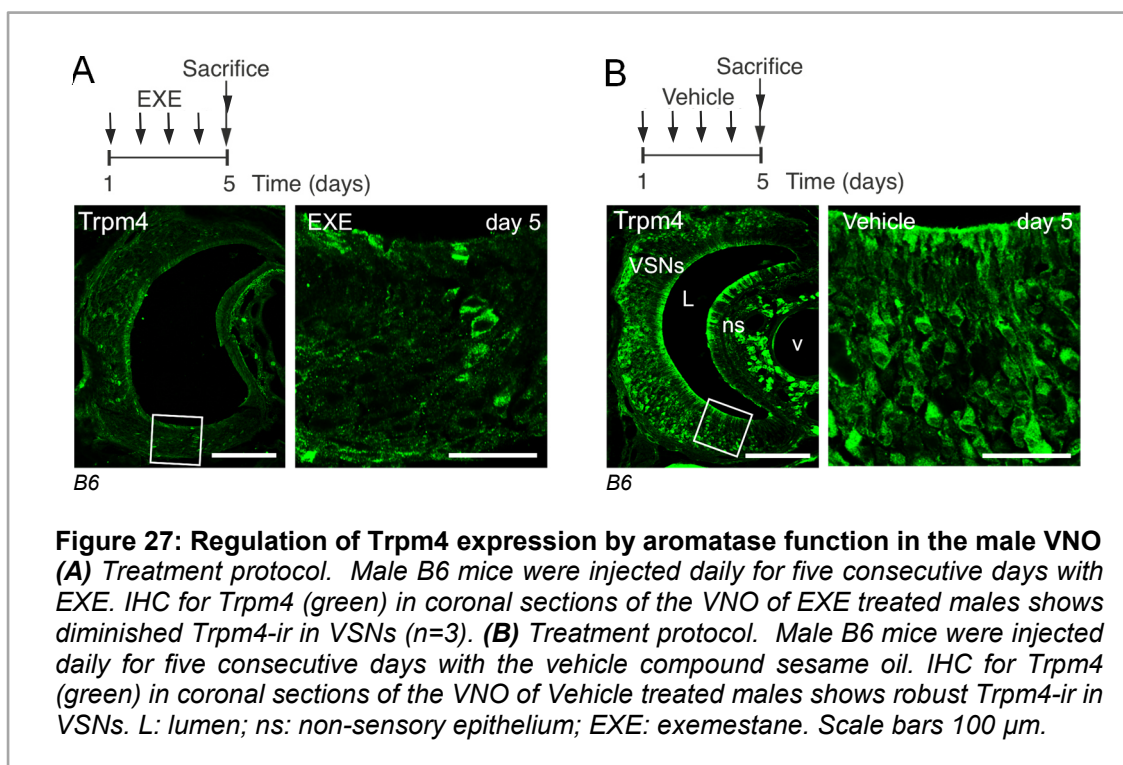
$17\beta$ -estradiol is synthesized and excreted in the reproductive tract, the brain, and the pituitary gland. The synthesis is accomplished by the function of the estrogen-synthesizing enzyme aromatase (Santen *et al.*, 2009). Aromatase (CYP19) belongs to the family of cytochrome P450 and is localized to the endoplasmic reticulum membrane where it acts with the co-enzyme NADPH-cytochrome P450 reductase to irreversibly convert androgens to estrogens. As revealed in 4.1.8.1 and 4.1.8.2, Trpm4 expression in VSNs is regulated by the interaction of the gonadal hormones E2 and P4. Thus, the question arises whether the endogenous production of E2 itself, through the activity of aromatase, is required for Trpm4 upregulation in VSNs? To answer this question, female mice were systemically injected with the synthetic steroid exemestane (EXE; 6-methylideneandrosta-1,4-diene-3,17-dione) that inhibits aromatase activity by irreversibly binding to the enzyme (Di Salle *et al.*, 1992). I administered EXE on five consecutive days with one daily intraperitoneal injection with an injection dose of 5 mg/kg bodyweight (Figure 26A). The estrous cycle was monitored during the whole experiment and as final step the Trpm4-ir in VSNs was analyzed (Figure 26). Control mice received injections with the vehicle compound sesame oil. All mice ( $n = 6$ ) exhibited a normal estrous cycle prior to EXE or vehicle administration (Figure 26B,C). After two days of EXE treatment, mice experienced estrous cycle disturbances and by the fifth day of EXE administration all mice entered a persistent diestrus (Figure 26B, top). Furthermore, in addition to the estrous cycle arrest, Trpm4-ir was not detectable in VSNs of EXE treated mice (Figure 26B, bottom). In contrast, control animals showed a normal estrous cycle during the injection period, accompanied by a robust Trpm4-ir in VSNs when sacrificed during estrus (Figure 26C).



To further support the radical effect of pharmacological block of endogenous aromatase function on VSN-Trpm4 expression, I injected intact male B6 mice with EXE and analyzed Trpm4-ir (Figure 27). EXE was administered on five consecutive days, with one daily intraperitoneal injection of 5 mg/kg bodyweight in addition to vehicle treatment (Figure 27A,B, top).

Trpm4-IHC in the VNO showed that VSN Trpm4-ir was strongly diminished after 5 days of EXE injections (Figure 27A, bottom). In contrast, control animals showed a robust Trpm4-ir in VSNs (Figure 27B, bottom).

Taken together, these results suggest that not only the external administration of E2 to OVX females and ORX males is crucial for vomeronasal Trpm4 expression, but also that the endogenous conversion from testosterone to  $17\beta$ -estradiol by the enzyme aromatase in intact females and males plays a fundamental role in the regulation of Trpm4 expression in VSNs.

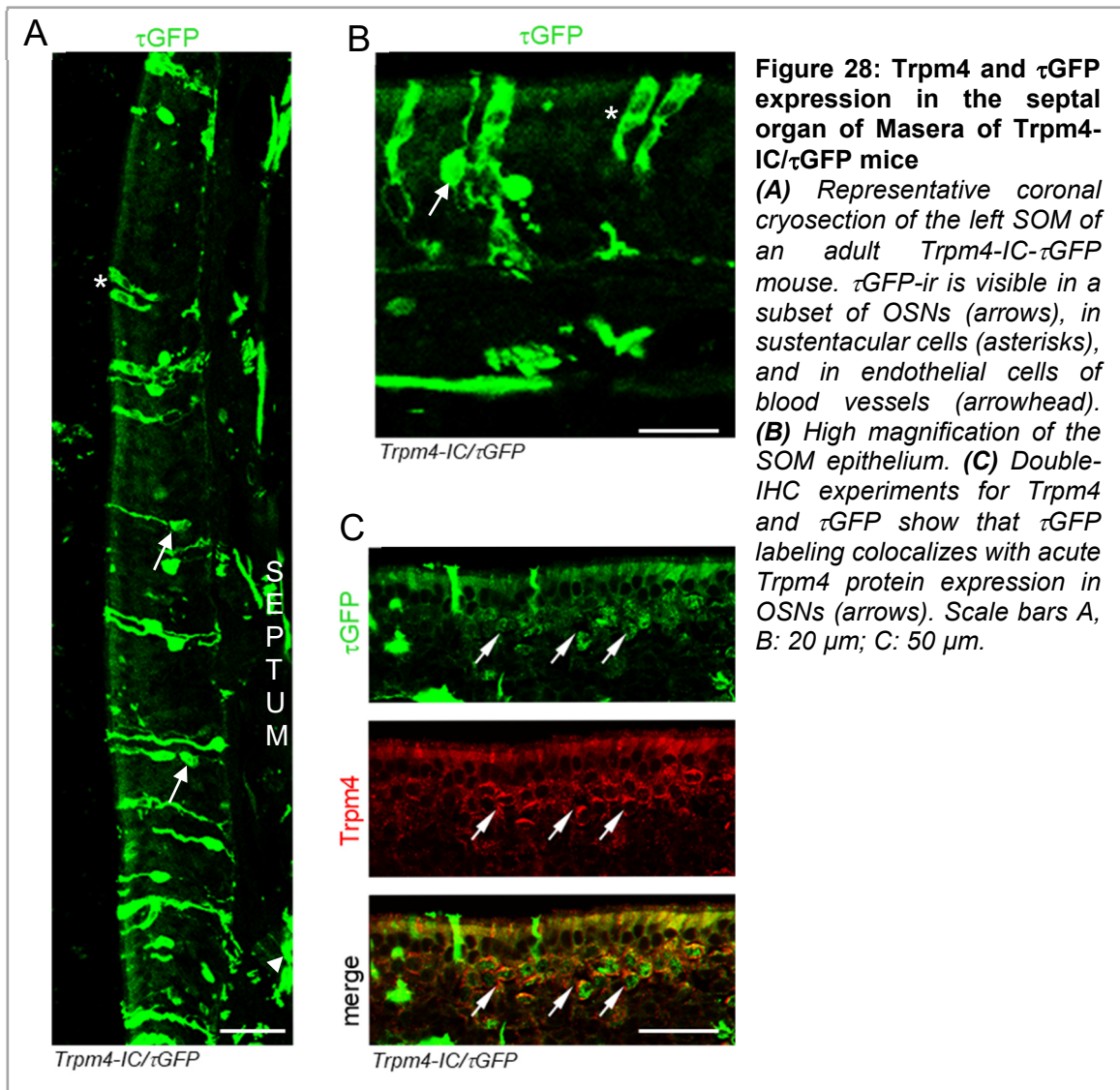


#### 4.1.9 Trpm4 expression in the SOM and in the GG

The septal organ of Masera (SOM) is a separated island of the main olfactory epithelium and similar to the MOE detects volatile odorants (Ma *et al.*, 2003; Tian and Ma, 2004). This raises the question whether Trpm4 and reporter gene expression is similar to that observed in the MOE (see Figure 14). To answer this question, I performed IHC for Trpm4 and  $\tau\text{GFP}$  on coronal cryosections of the SOM in adult, 7 weeks old Trpm4-IC/ $\tau\text{GFP}$  mice (Figure 28). I detected  $\tau\text{GFP}$  expression in different types of cells that were identified based on their morphology: OSNs (Figure 28, arrows), sustentacular cells (Figure 28A, C asterisks), and endothelial cells, lining blood vessels (Figure 28A arrowhead). In comparison to  $\tau\text{GFP}$  expression in the MOE, numbers of  $\tau\text{GFP}$  positive cells were lower in the SOM, as visually estimated.

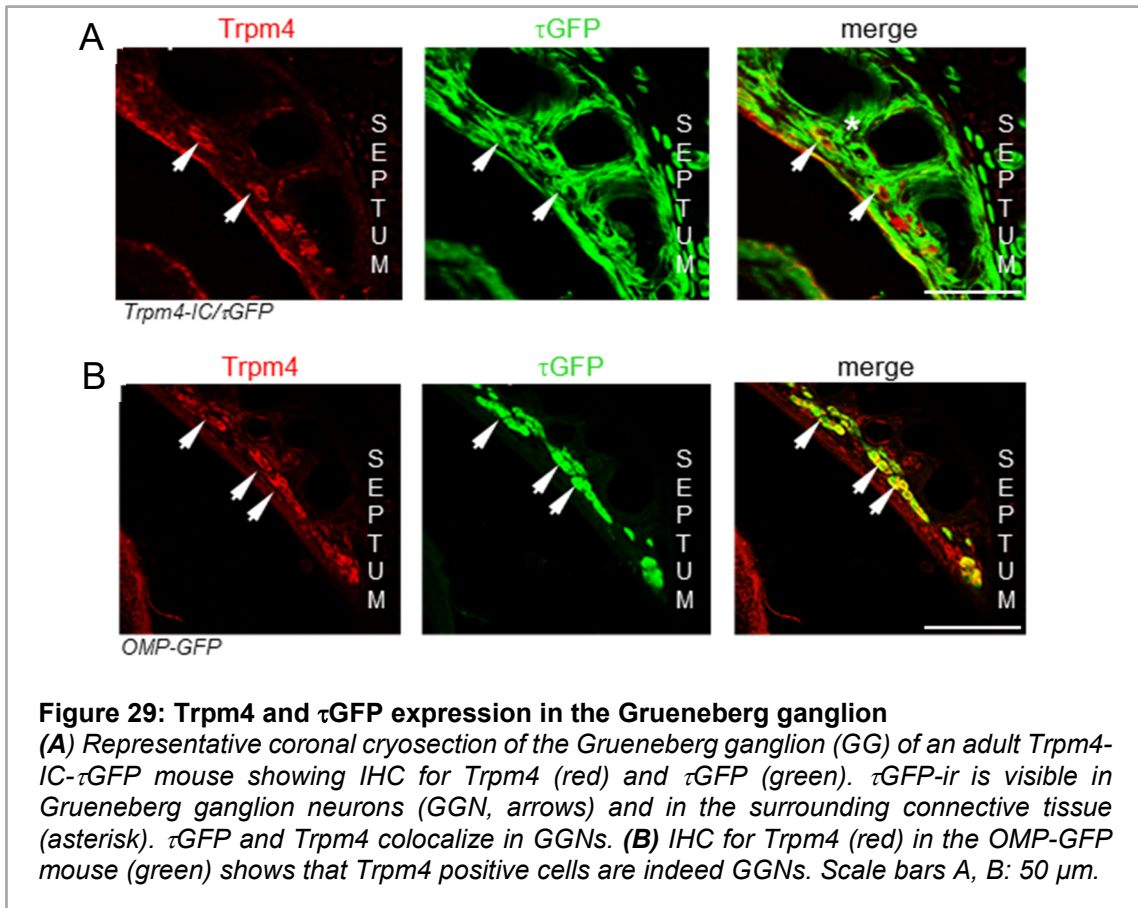
To assess acute Trpm4 expression in the SOM, I performed double-labeling IHC for  $\tau\text{GFP}$  and Trpm4 (Figure 28C). This experiment unveiled the most striking difference between the MOE and the SOM, as OSNs located in the SOM of adult Trpm4-IC/ $\tau\text{GFP}$  mice showed Trpm4-ir, whereas OSNs in the adult MOE were devoid of TRPM4 (Figure 14). Comparing the distribution of  $\tau\text{GFP}$ -positive cells with antibody staining for Trpm4, it is

evident that the acute Trpm4 expression only takes place in the OSNs, but not in sustentacular cells (Figure 28B, arrows).



The Grueneberg ganglion (GG) is located at the very anterior tip of the nose (Grueneberg, 1973). To tackle the question whether Trpm4 is expressed in all peripheral olfactory subsystems, I performed double-labeling IHC for  $\tau$ GFP and Trpm4 on coronal cryosections of adult, 7 weeks old Trpm4-IC/ $\tau$ GFP mice (Figure 29). Strong  $\tau$ GFP-ir was detectable in Grueneberg ganglion neurons (GGN) (Figure 29A, B). These neurons are embedded in the underlying connective tissue and covered by a keratinized epithelial cell layer, which also showed a high level of  $\tau$ GFP fluorescence. The comparison of  $\tau$ GFP-ir to acute Trpm4 expression revealed that both Trpm4 and  $\tau$ GFP are co-expressed in virtually all GGNs (Figure 29A). As the GG is presumed to be already functional at birth, unlike the other olfactory systems, all GGNs are mature and express

OMP (Matsuo *et al.*, 2012). However, the OMP-GFP mouse is suitable to confirm the neuronal identity of Trpm4 positive cells. Therefore, I performed Trpm4-IHC in OMP-GFP mice, in which all mature olfactory neurons are labeled by GFP. This experiment verified Trpm4 positive cells as GGNs (Figure 29B).



#### 4.1.10 *Trpm4* and $\tau$ GFP expression in the olfactory bulb

One advantage of the *Trpm4-IC- $\tau$ GFP* mouse is that  $\tau$ GFP visualizes OSNs axonal projections, which can be followed to the olfactory bulb (OB). In the OB, synapses between OSNs and second order neurons, the mitral and tufted cells, are formed in regions of dense neuropil called glomeruli (Mombaerts *et al.*, 1996). As shown in Figure 30A, robust endogenous  $\tau$ GFP fluorescence was visible in a whole mount preparation of the OB from an adult, 7 weeks old *Trpm4-IC- $\tau$ GFP* mouse.  $\tau$ GFP-ir was present at the medial and dorso-lateral aspects of the MOB. To further dissect the expression of  $\tau$ GFP, I analyzed sagittal MOB cryosections (Figure 30B), which confirmed  $\tau$ GFP expression in the nerve layer (NL) and in glomeruli (GL). Interestingly,  $\tau$ GFP signal intensity varied among glomeruli.

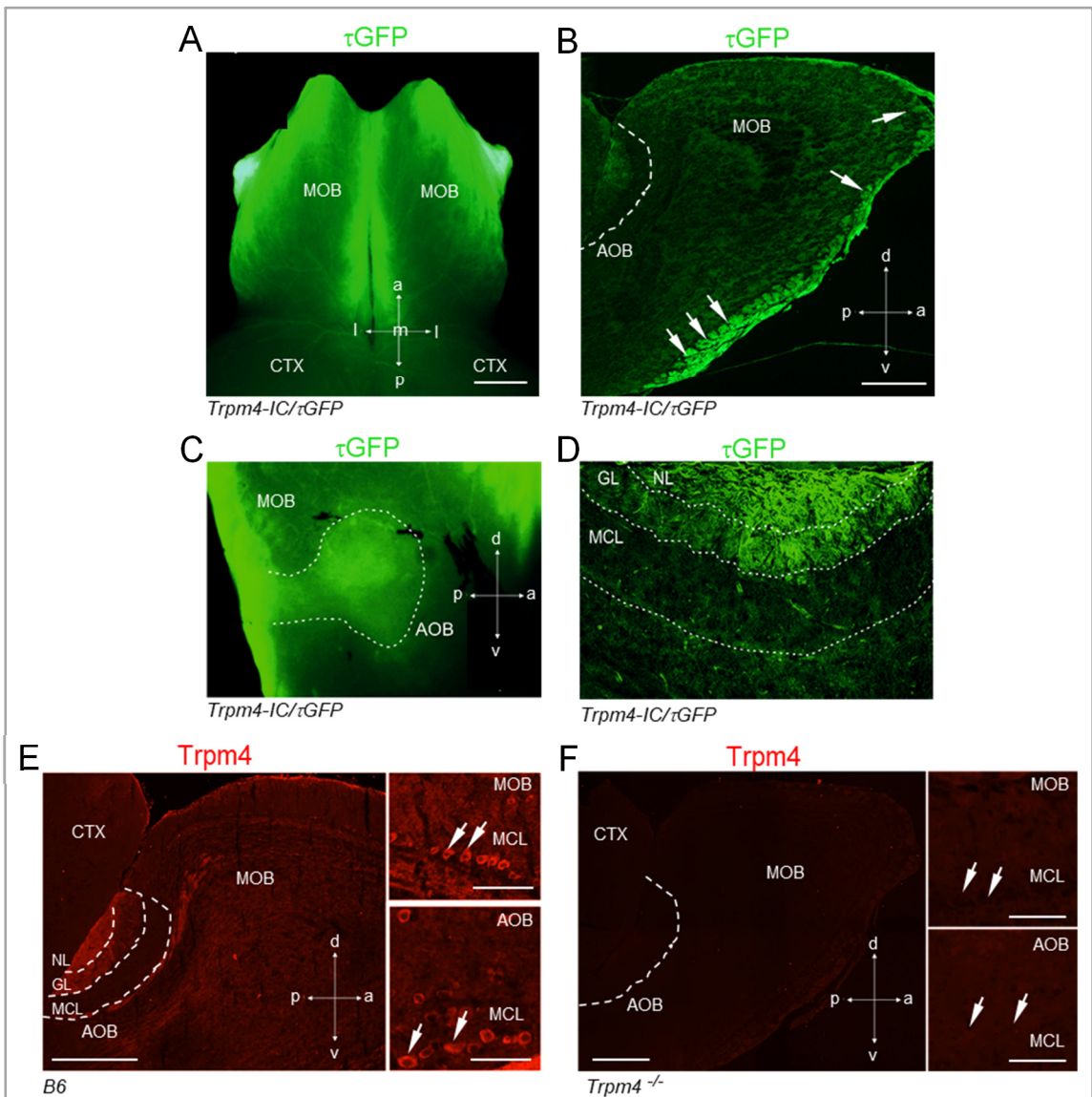


**Figure 30: Trpm4 and  $\tau$ GFP expression in the olfactory bulb**

(A) Whole mount preparation of the main olfactory bulb (MOB) of an adult, 7 weeks old *Trpm4-IC/τGFP* reporter mouse. Strong endogenous  $\tau$ GFP expression (green) is visible at the medial and anterior-lateral aspects. (B) Representative sagittal cryosection of an adult, 7 weeks old *Trpm4-IC/τGFP* mouse shows robust  $\tau$ GFP-ir in the nerve layer (NL) and in glomeruli (GL) (arrows) in the MOB. (C) Higher magnification of the accessory olfactory bulb (AOB) shows a robust  $\tau$ GFP signal (green) in the AOB nerve layer (dotted line). (D) Representative sagittal cryosection of an adult, 7 weeks old *Trpm4-IC/τGFP* mouse shows the level of AOB glomerular innervation by  $\tau$ GFP positive VSN axons. (E) *Trpm4*-IHC (red) on a sagittal cryosection of an adult, 7 weeks old B6 mouse. Robust *Trpm4*-ir is detected in the NL and GL of the AOB (dotted line). MOB glomeruli are negative for *Trpm4*. Inset magnification shows *Trpm4* positive cells within the mitral cell layer of the MOB (top, arrows) and AOB (bottom, arrows). (F) *Trpm4* antibody specificity was verified by the lack of *Trpm4*-ir in *Trpm4*<sup>-/-</sup> tissue. MOB: main olfactory bulb; AOB: accessory olfactory bulb; NL: nerve layer; GL: glomerular layer; MCL: mitral cell layer; CTX: cortex; a: anterior; p: posterior; d: dorsal; v: ventral; m: medial; l: lateral. Scale bars A: 1 mm; B: 500  $\mu$ m; C: 250  $\mu$ m; D: 100  $\mu$ m; E, F: overviews 250  $\mu$ m, magnifications 50  $\mu$ m.

---

The strongest glomerular labeling was observed in the ventral MOB (Figure 30B). Whole mount preparations of the olfactory bulb of Trpm4-IC/ $\tau$ GFP mice also showed a strong  $\tau$ GFP signal in the AOB (Figure 30C). This result was confirmed by the analysis of sagittal AOB cryosections, which resulted in a strongly  $\tau$ GFP labeled AOB nerve layer and glomeruli (Figure 30D).

More interestingly, acute Trpm4 expression in the olfactory bulb of adult, 7 weeks old mice (Figure 30E) showed robust Trpm4-ir in the nerve layer and glomeruli of the AOB. Trpm4-ir was absent in adult MOB glomeruli. These results are consistent with the absence of Trpm4-ir in the adult MOE (Figure 14) and the strong Trpm4 expression in virtually all VSNs (Figure 17). Furthermore, I observed similar to Shpak *et al.*, 2012, a robust Trpm4-ir in mitral cells of the main and accessory olfactory bulb (Figure 30E, arrows). The specificity of the antibody was verified in OB tissue of Trpm4<sup>-/-</sup> mice, that were devoid of any staining (Figure 30F).

## 4.2 Trpm5

### 4.2.1 Trpm5 expression and distribution in the murine olfactory system

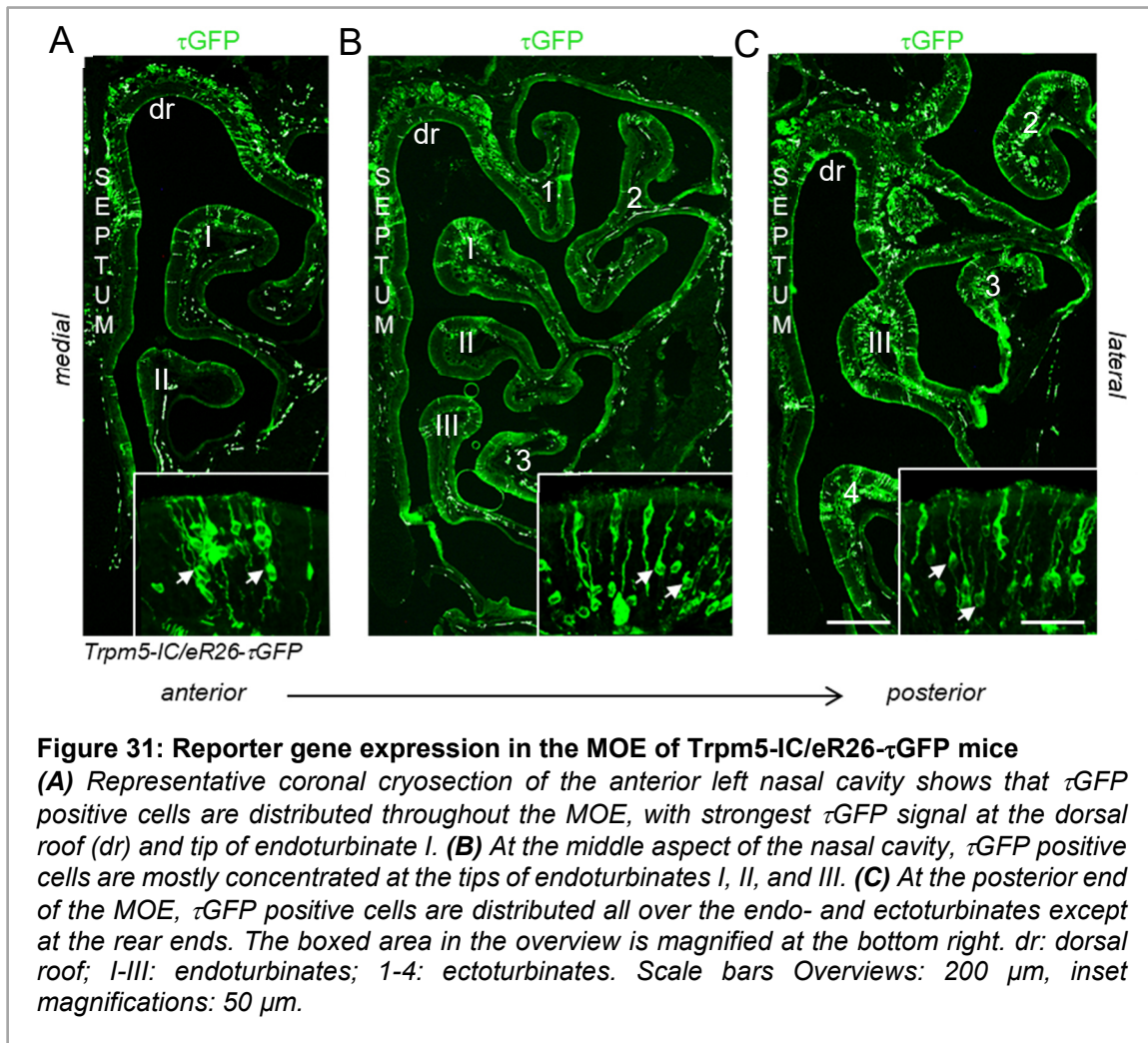
Trpm5 is an established key component in chemosensory transduction of the taste system (Perez *et al.*, 2002; Zhang *et al.*, 2003). However, the expression and function of Trpm5 in the olfactory system remains unclear and is still debated (Lin *et al.*, 2007; Oshimoto *et al.*, 2013; Lopez *et al.*, 2014; Yamaguchi *et al.*, 2014, Kusumakshi *et al.*, 2015, Yamashita *et al.*, 2017).

In 2015, Kusumakshi *et al.*, generated a Trpm5 reporter mouse, the Trpm5-IC/eR26- $\tau$ GFP mouse line, to study Trpm5 expression in various oral and extra-oral tissues. This mouse line relies, like the Trpm4-IC/ $\tau$ GFP mouse, on the Cre-Lox mediated recombination system. The green fluorescent protein  $\tau$ GFP labels the cells which acutely express Trpm5 or at one point have expressed the protein. Kusumakshi *et al.*, have furthermore shown in 2015, that the Trpm5 protein expression takes place in microvillar (MV) cells of the MOE, and that OSNs are solely expressing the reporter gene  $\tau$ GFP in the Trpm5-IC/eR26- $\tau$ GFP mouse line but not the Trpm5 protein. To ascertain whether Trpm5 protein is expressed in OSNs, I performed a thorough analysis of the murine olfactory system using RT-PCR and immunohistochemical procedures.

### 4.2.2 $\tau$ GFP expression in the MOE of Trpm5-IC/eR26- $\tau$ GFP mice

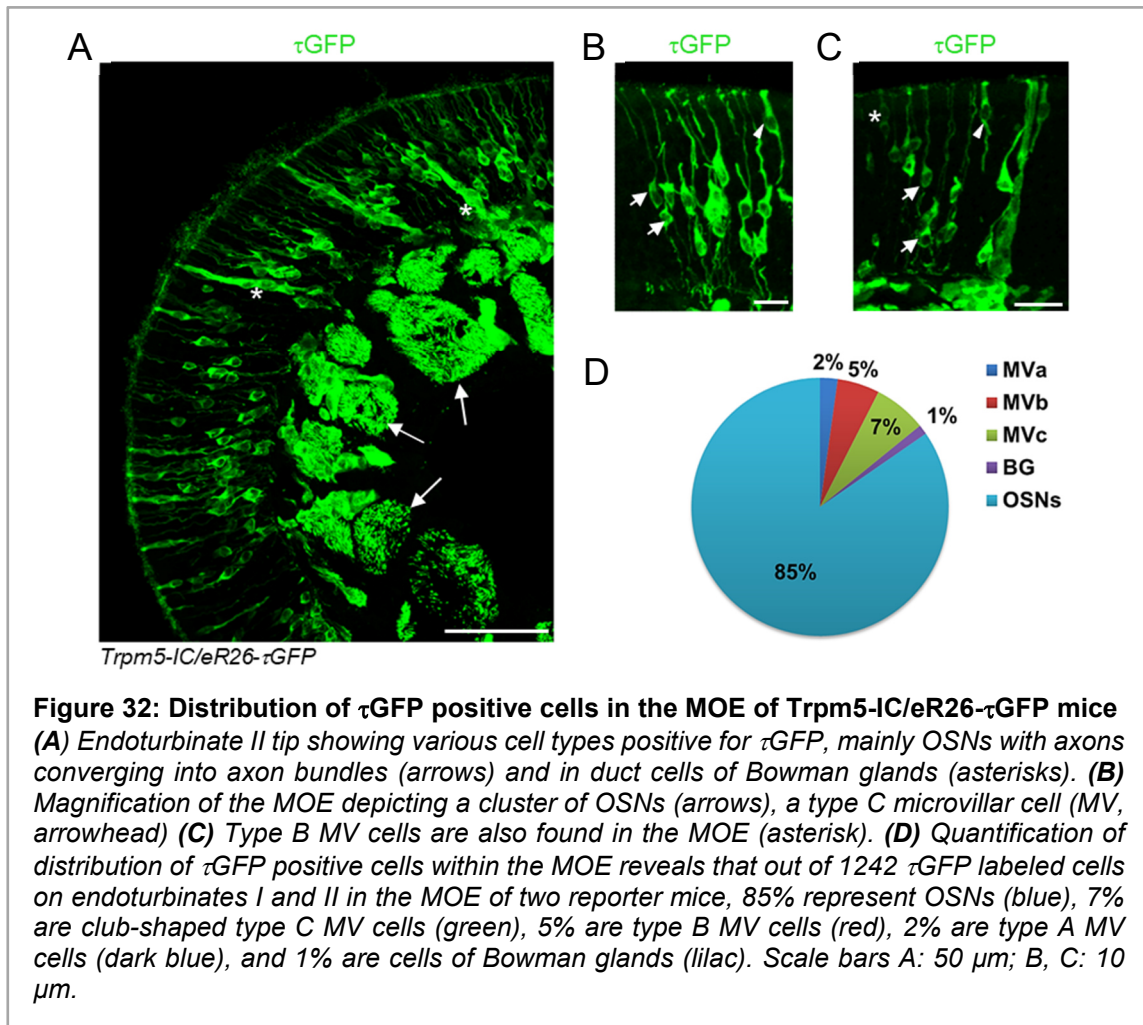
To determine the localization of Trpm5 in the MOE, I first analyzed coronal cryosections of the MOE for  $\tau$ GFP expression. Tissue sections derived from adult, 6-8 weeks old Trpm5-IC/eR26- $\tau$ GFP mice. Both genders were used in these analyses. I detected abundant  $\tau$ GFP expression, with labeled cells present throughout the whole MOE along its anterior-to-posterior extend (Figure 31). No obvious zonal organization of  $\tau$ GFP cells was observed, instead,  $\tau$ GFP labeled cells appeared scattered over the dorsal, ventral, and lateral endo- and ectoturbinates, as well as on the nasal septum. Higher magnifications showed  $\tau$ GFP positive cells at all depths of the epithelial layer, both single cells and clustered in small groups (Figure 31, inset magnifications). Interestingly,  $\tau$ GFP positive cells were not homogeneously distributed along the anterior to the posterior extent of the MOE. In the anterior MOE,  $\tau$ GFP positive cells mainly localized to the dorsal roof and the dorsal aspects of endoturbinates (Figure 31A).

In the posterior MOE, the localization of  $\tau$ GFP positive cells extended to ventral aspects of the endoturbinates as well (Figure 31C). On the basis of their morphology and location within the MOE, various  $\tau$ GFP positive cell types were identified (Kusumakshi *et al.*, 2015). The first group of  $\tau$ GFP positive cells is a subpopulation of OSNs, with strong  $\tau$ GFP expression in cilia, dendrites and dendritic knobs, somata, and axons (Figure 32B,C, arrows).



OSN axons converge into bundles located below the basal lamina (Figure 32A, arrows). The second group of  $\tau$ GFP expressing cell types comprises 3 different types of MV cells, residing in the uppermost layer of the MOE (Figure 32B,C). The “A-type MV cells”, characterized by cell bodies of about 20  $\mu$ m length and the “B-type MV cells”, characterized by a short, droplet shaped soma with a length of about 10  $\mu$ m, both previously identified by *Trpm5-IHC* (Kaske *et al.*, 2007, Hansen and Finger 2008).

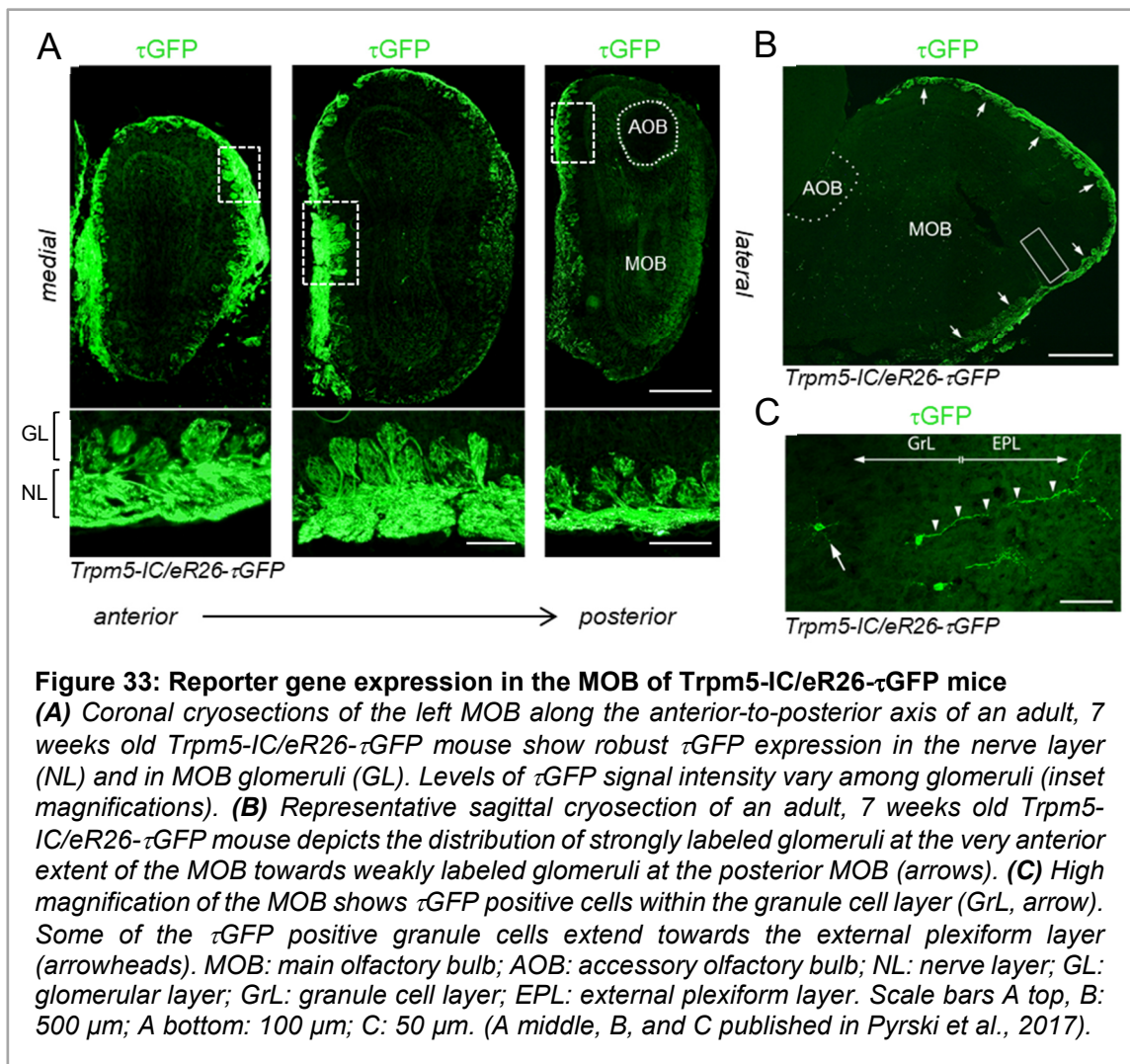
The third type of  $\tau$ GFP positive MV cells exhibits a club-shaped morphology, with somata residing next to sustentacular cell (SUS) somata in the most apical layer of the MOE. Furthermore, club-shaped MV cells possess one single basal process that traverses the MOE towards the basal lamina (Figure 32B,C).



Besides OSNs and MV cells, a third group of cells, the Bowman gland cells exhibited a strong  $\tau$ GFP signal (Figure 32A). To analyze the proportion of  $\tau$ GFP expression attributed to the different cell types, I quantified different  $\tau$ GFP cells within the MOE. For this analysis, cells were manually counted at endoturbinates I and II of two *Trpm5-IC/eR26- $\tau$ GFP* reporter mice. This analysis showed that out of a total of 1242  $\tau$ GFP positive cells, 85% were OSNs (Figure 32D). Type A and B MV cells comprised a total share of 7% of  $\tau$ GFP positive cells, whereas 15% were attributed to the club-shaped, type-C MV cells. Bowman gland cells described only 1% of the total proportion of  $\tau$ GFP positive cells in the MOE.

### 4.2.3 Axonal projections of $\tau$ GFP OSNs to the MOB

The first relay station of OSNs in the brain is the MOB. Here in regions of dense neuropil, known as glomeruli, OSNs make synaptic contact to second order neurons, the mitral and tufted cells (Mombaerts *et al.*, 1996). The *Trpm5-IC/eR26- $\tau$ GFP* mouse enables tracking of OSN axonal projections to the MOB through the microtubule-associated protein  $\tau$  in the  $\tau$ GFP. To address the projection pattern of  $\tau$ GFP labeled OSNs, I analyzed  $\tau$ GFP expression in MOB cryosections of adult, 7 weeks old *Trpm5-IC/eR26- $\tau$ GFP* mice (Figure 33).



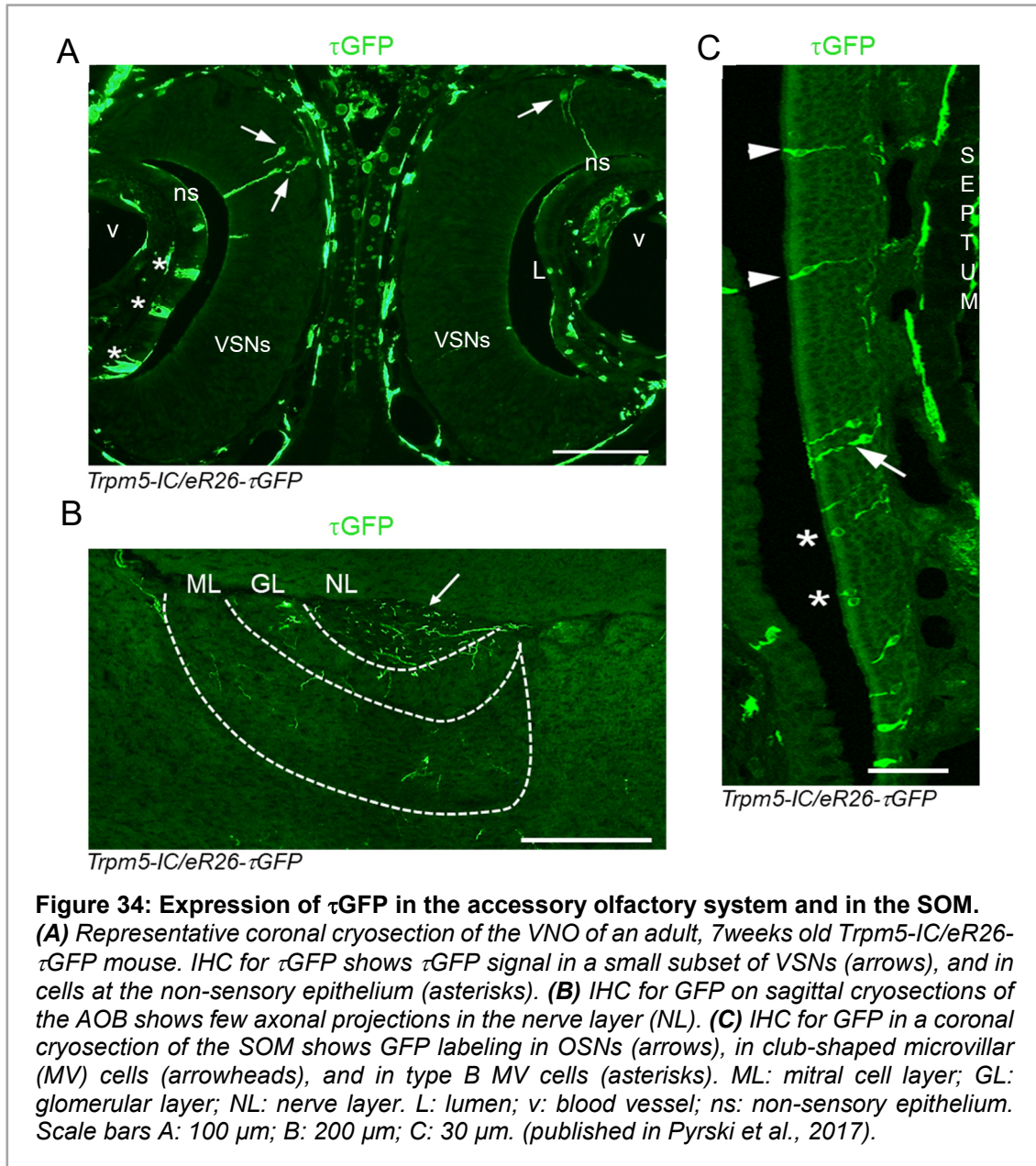
IHC for GFP showed that the level of innervation by  $\tau$ GFP OSNs differs among glomeruli along the anterior-to-posterior axis of the MOB (Figure 33A). This observation is in line with the patchy distribution of  $\tau$ GFP positive OSNs in the MOE. In detail, the nerve layer and glomeruli of the dorso-lateral areas of the anterior MOB exhibit the highest levels of  $\tau$ GFP fluorescence, whereas glomeruli residing at the posterior MOB showed lower

$\tau$ GFP levels (Figure 33A,B, arrows). Thus, virtually all MOB glomeruli are innervated by  $\tau$ GFP positive OSNs, solely differing in the level of innervation. Occasionally,  $\tau$ GFP labeling was also evident in neurons of the granule cell layer (Figure 33C).  $\tau$ GFP positive granule cells exhibited long processes, reaching towards the external plexiform layer (Figure 33C, arrowheads).

#### **4.2.4 $\tau$ GFP expression in the accessory olfactory system and in the septal organ of Masera**

To analyze  $\tau$ GFP expression in the accessory olfactory system, I performed IHC for  $\tau$ GFP on coronal cryosections of the VNO and on sagittal cryosections of the AOB of adult, 7 weeks old *Trpm5-IC/eR26- $\tau$ GFP* mice (Figure 34A,B). This experiment showed that in contrast to the MOE, only few VSNs (Figure 34A, arrows) and few cells of the non-sensory epithelium (Figure 34A, asterisks) express GFP. Approximately 50 VSNs of a total of 100000 to 200000 VSNs contained in the whole VNO (Wilson and Raisman, 1980) were GFP positive. This is consistent with the results obtained in the AOB, the first relay station of VSNs in the brain (Figure 34B), where only few  $\tau$ GFP labeled fibers were detected in the nerve layer (Figure 34B, arrow).

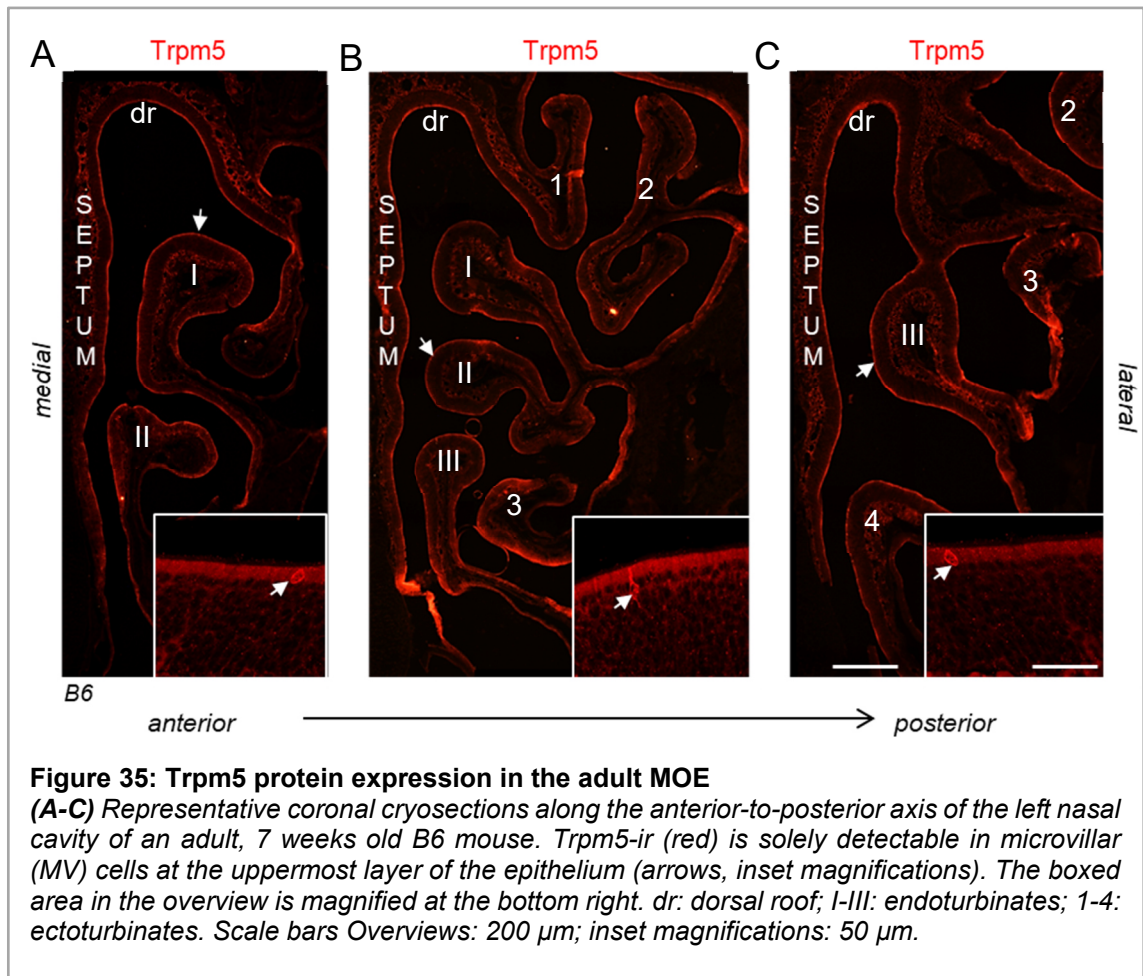
IHC analysis of reporter gene expression in the SOM of adult, 7 weeks old *Trpm5-IC/eR26- $\tau$ GFP* mice revealed a distribution of  $\tau$ GFP-ir cells that was very similar to the findings in the MOE.  $\tau$ GFP was expressed in a subset of OSNs and in different types of MV cells (Figure 34C). This result is consistent with the concept that the SOM is a functional but separated part of the MOE and comprises the same subset of cell types (Ma *et al.*, 2003).



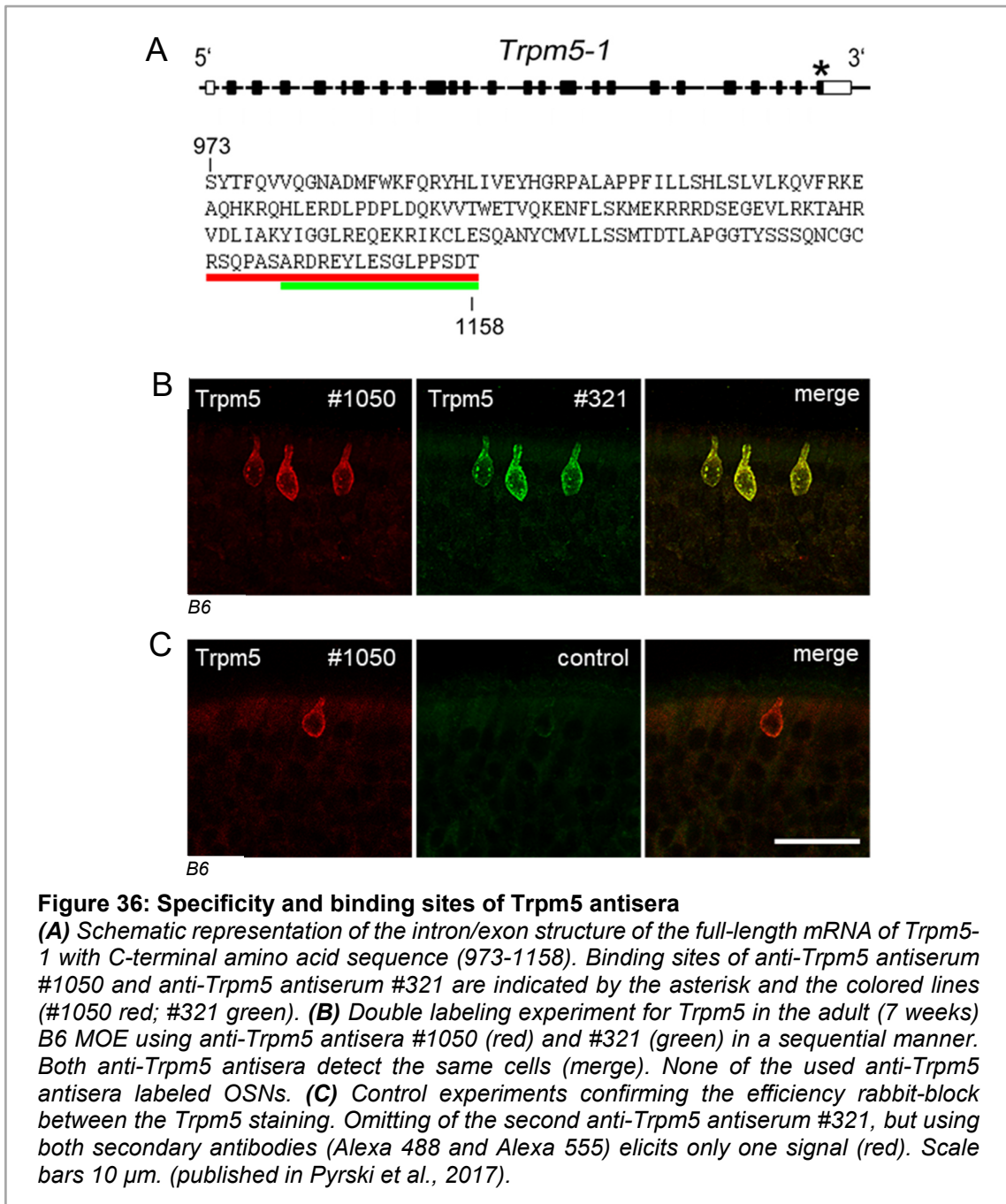
#### 4.2.5 Trpm5 protein expression in the adult MOE

To correlate Trpm5 protein expression with the expression of  $\tau$ GFP, I performed double-labeling IHC for Trpm5 and  $\tau$ GFP on coronal cryosections of the MOE of Trpm5-IC/eR26- $\tau$ GFP mice (Figure 35). I employed a polyclonal anti-Trpm5 antiserum (#1050), directed against the C-terminal part of the Trpm5 protein. This antiserum has been previously validated on taste receptor cells of the tongue and on chemosensory cells of the gastrointestinal tract (Kusumakshi et al., 2015). Coronal cryosections of B6 mice were analyzed for Trpm5-ir along the anterior-to-posterior axis (Figure 35).

Surprisingly, Trpm5-ir was different from the previously observed  $\tau$ GFP expression. In contrast to the multiple different cell types exhibiting  $\tau$ GFP expression, only a single cell type showed Trpm5 protein expression. Based on their morphology and localization in the MOE, Trpm5 positive cells likely represent MV cells (Figure 35, arrows). A previous study showed that these cells express villin, a typical marker for MV cells, and that they are devoid of OMP, a marker for mature OSNs (Pyrski *et al.*, 2017).



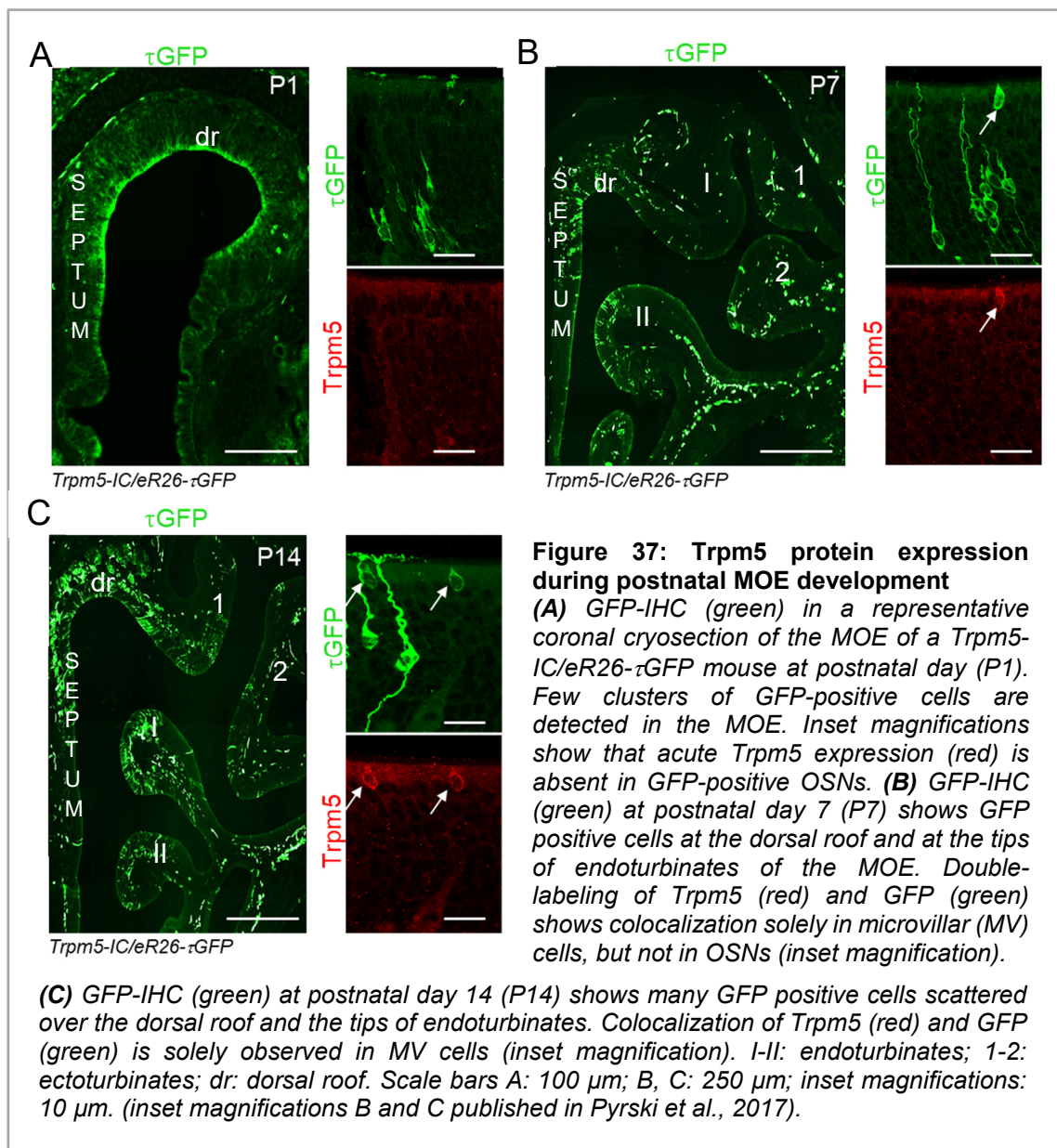
To verify these results, I performed control experiments using a second anti Trpm5 antiserum (#321; Kaske *et al.*, 2007) (Figure 36). Anti-Trpm5 #321 antiserum is directed against the C-terminal amino acid sequence ARDREYLESGLPPSDT (Kaske *et al.*, 2007), and overlaps with the last third of the amino acid sequence detected by serum #1050 (Figure 36A). IHC experiments using the anti-Trpm5 antiserum #321 yielded the same result, with Trpm5-ir exclusively present in MV cells (Figure 36B). Furthermore, double labeling experiments using antiserum #1050 and #321 revealed that both antisera labeled the same MV cells (Figure 36B).



Control experiments omitting the second anti-*Trpm5* antiserum, to rule out cross reactivity of the secondary antibodies, were devoid of any signal (Figure 36C). Thus, the results show that *Trpm5* protein is absent in adult OSNs and that the expression is confined to MV.

#### 4.2.6 Trpm5 protein in the postnatal MOE is not expressed in OSNs

As demonstrated above, analysis of Trpm5-IC/eR26- $\tau$ GFP reporter mice showed that  $\tau$ GFP is expressed in OSNs while the Trpm5 protein is absent. This result indicates that at some point during MOE development, OSNs indeed have expressed Trpm5. To address the question whether Trpm5 expression in OSNs occurs during MOE development, I analyzed coronal cryosections of the MOE of Trpm5-IC/eR26- $\tau$ GFP mice at different postnatal ages via Trpm5-IHC. MOE sections derived from mice at postnatal day 1 (P1), P7, and P14 (Figure 37). At P1, few  $\tau$ GFP positive OSNs were present in the MOE (Figure 37A). At P7, the number of  $\tau$ GFP positive OSNs and MV cells increased, mainly localized to the dorsal roof and the tips of the endoturbinates (Figure 37B).



At P14,  $\tau$ GFP positive OSNs and MV cells were scattered throughout the MOE, except for the most ventral aspects of the MOE and the rear ends of the endo- and ectoturbinates (Figure 37D). In contrast, Trpm5-ir was solely detected in MV cells, emerging at around the first postnatal week, but not in OSNs (Figure 37, magnifications, arrows).

Thus, these results further support the previous finding that Trpm5 protein expression is taking place exclusively in MV cells. No evidence for Trpm5 protein was found in OSNs, neither during the first 2 weeks of postnatal development, nor in adult mice (see 4.2.5).

#### **4.2.7 Trpm5 protein is transiently expressed in a subpopulation of embryonic OSNs**

The results obtained so far demonstrated that postnatally, OSNs are devoid of the Trpm5 protein. However,  $\tau$ GFP expression in OSNs from Trpm5-IC/eR26- $\tau$ GFP mice indicates the presence of Trpm5 at an even earlier stage of MOE development. Therefore, I performed Trpm5-IHC analyses on coronal MOE cryosections deriving from B6 mice at different prenatal stages, at embryonic day 15 (E15), E17, E18, and E19 (Figure 38). Robust Trpm5-ir was visible at E18 in a distinct subpopulation of OSNs distributed throughout the whole depth of the MOE (Figure 38A). Antibody specificity was confirmed by Trpm5-IHC on coronal MOE cryosections of age-matched, E18-Trpm5<sup>-/-</sup> embryos, that were devoid of any Trpm5 signal (Figure 38B).

Double-labeling IHC for Trpm5 and the maturity marker OMP showed that approximately 85% of Trpm5-positive OSNs coexpress OMP (Figure 38C). Additional double-labeling IHC for Trpm5 and the growth associated protein Gap43, a marker for immaturity, showed that only a subset of the Trpm5-positive OSNs express Gap43 (Figure 38D). Thus, these experiments demonstrate that Trpm5 positive OSNs are early mature neurons.

Furthermore, quantification of the number of Trpm5-positive OSNs at the different prenatal age stages revealed that Trpm5 protein expression exhibits transient characteristics and is confined to a narrowly-timed window around E18 (Figure 38E). Cell numbers of Trpm5 positive OSNs peak at E18, with on average 900 OSNs per MOE (Figure 38E). In contrast, only few cells are positive for Trpm5 at E17 and E19. The early postnatal age P1 shows essentially no Trpm5-positive OSNs (Figure 38E).

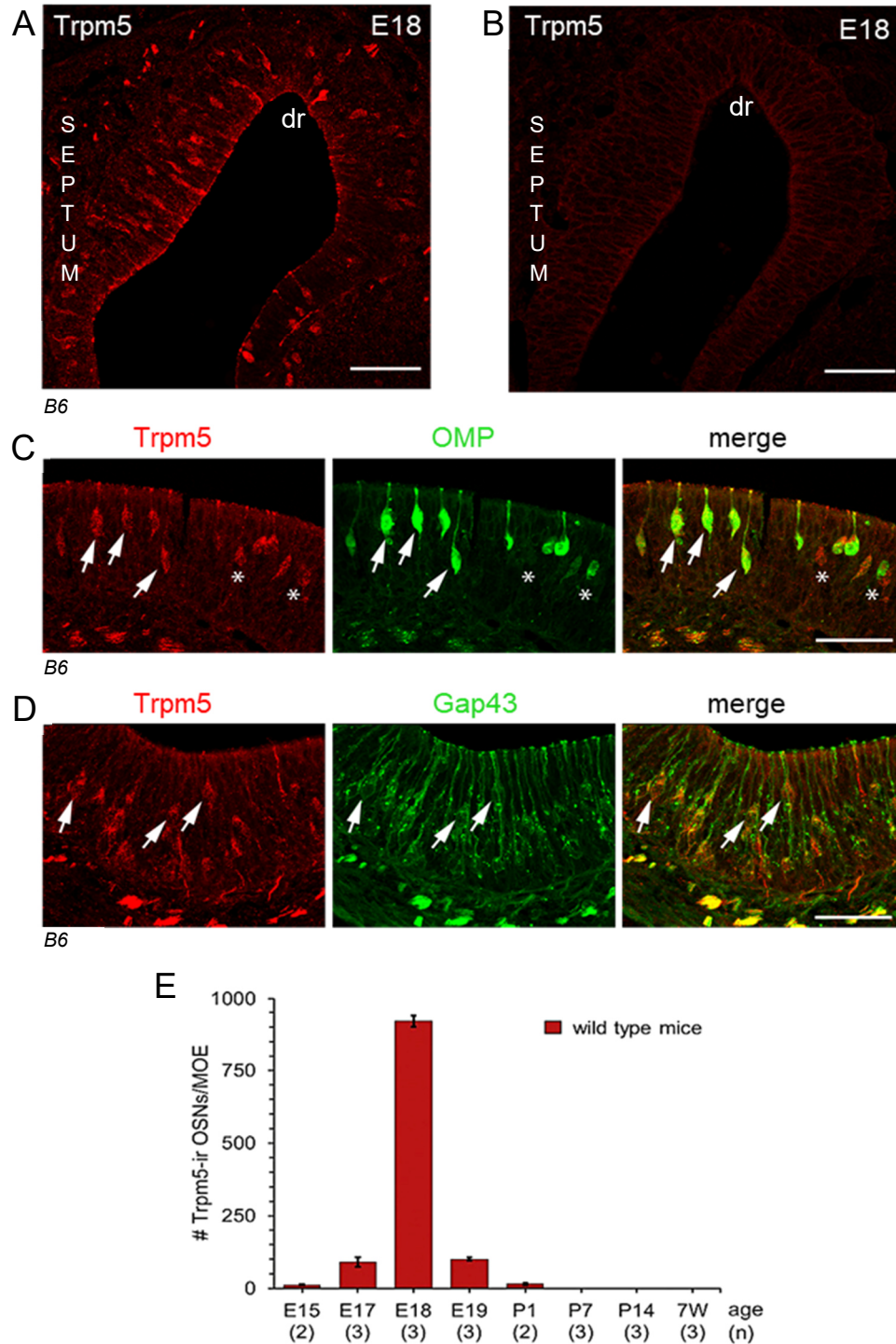
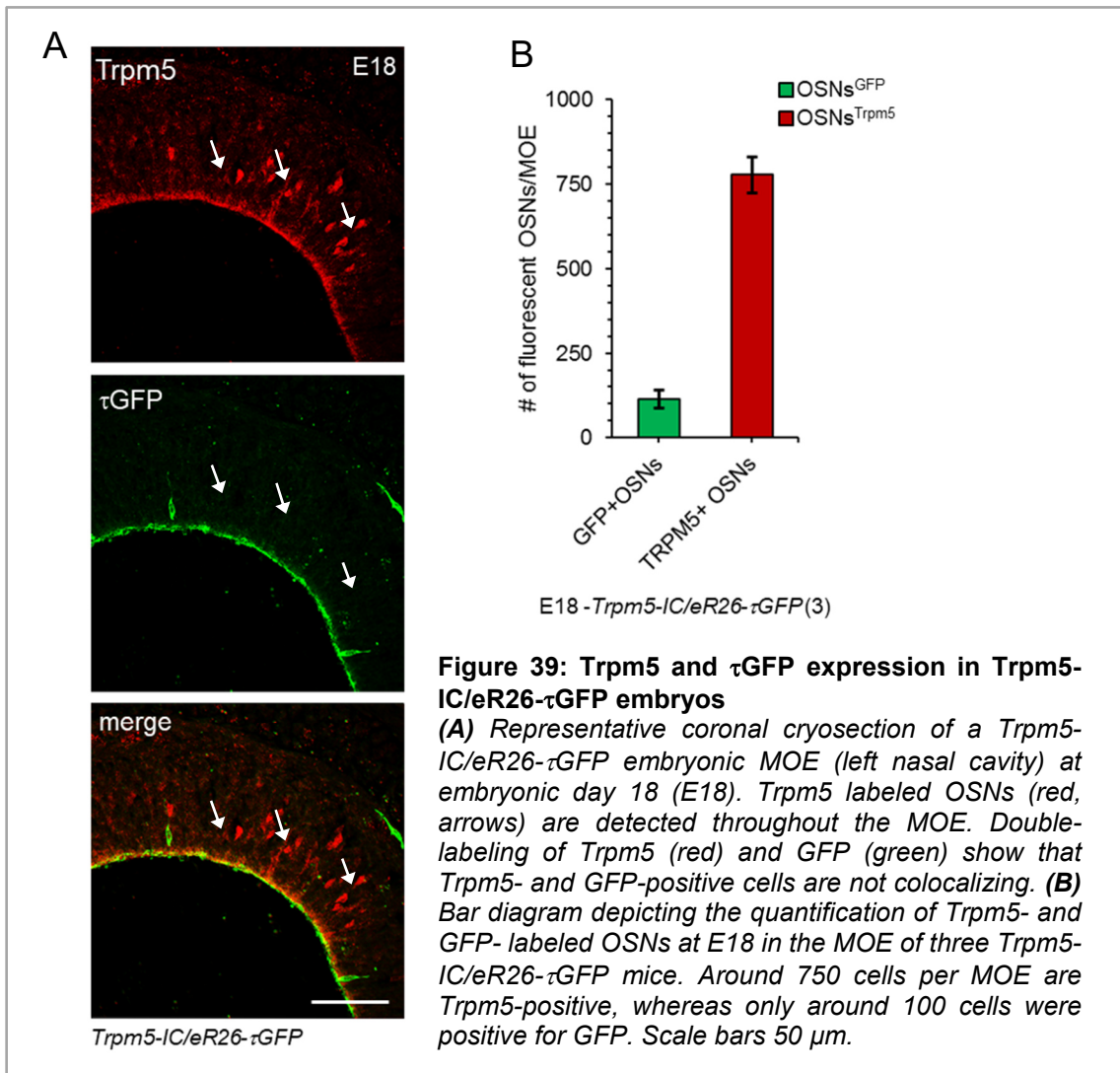


**Figure 38: Trpm5 protein is transiently expressed in embryonic OSNs**

(A) Representative coronal cryosection of a B6 MOE (left nasal cavity) at embryonic day 18 (E18). IHC for Trpm5 reveals Trpm5-positive OSNs scattered throughout the MOE. (B) IHC for Trpm5 in age-matched Trpm5<sup>-/-</sup> embryos confirmed the specificity of the staining by the lack of any Trpm5-ir. (C) Double-labeling IHC for Trpm5 (red) and OMP (green) identifies the majority of Trpm5-positive cells as early mature OSNs (arrows). Only a small fraction of Trpm5-ir OSNs is OMP-negative (asterisks). (D) Double-labeling for Trpm5 (red) and Gap43 (green) shows that few Trpm5-positive OSNs are immature (arrows). (E) Bar diagram depicting the quantification of Trpm5 labeled OSNs at different developmental ages around birth. At E18 the number of Trpm5-positive cells transiently peaks with about 900 cells per MOE. After birth, (P1 to P7) number of Trpm5 labeled OSNs decreases towards zero. dr: dorsal roof. Scale bars A, B: 50  $\mu$ ; C, D: 20  $\mu$ m. (published in Pyrski et al., 2017).

Comparing the cell numbers in B6 animals during late embryonic stages with age-matched *Trpm5*-IC/eR26- $\tau$ GFP mice at E18, a similar number of *Trpm5*-ir OSNs was observed, with an average of 750 OSNs per MOE (Figure 39). In contrast, no coexpression of  $\tau$ GFP was observed in these cells (Figure 39A). Quantification of  $\tau$ GFP positive OSNs in three different *Trpm5*-IC/eR26- $\tau$ GFP embryos at E18 resulted in an average of only 100 OSNs per MOE (Figure 39B).



Taken together, the *Trpm5* protein is expressed in a distinct subset of OSNs during a short period of embryonic MOE development. The acute expression of *Trpm5* does not correlate with the expression of  $\tau$ GFP.

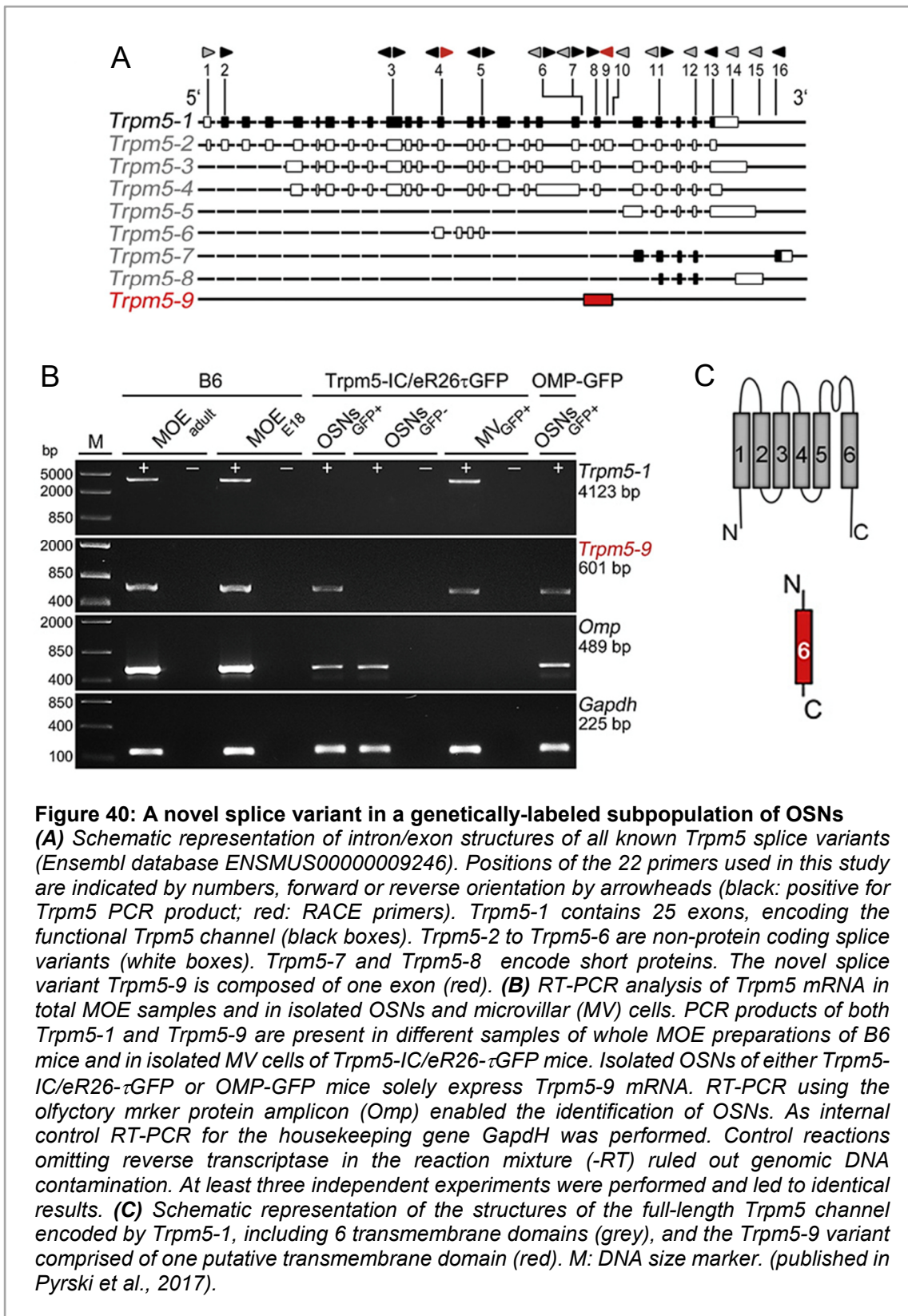
#### 4.2.8 *Trpm5-9*, a novel splice variant in genetically-labeled adult OSNs

As anti-*Trpm5* antibodies detect *Trpm5* protein expression in embryonic, but not in adult OSNs, it is conceivable that a specific adults-only splice variant exists, that is not recognized by any of the antibodies employed in this study.

To address this possibility, I analyzed the sequences of all known *Trpm5* splice variants, annotated in the ensemble database ([www.ensembl.org](http://www.ensembl.org)). Eight *Trpm5* splice variants are described (ENSMUSG00000009246; Figure 40A). The functional *Trpm5* channel is encoded by the 4123 bp long splice variant *Trpm5-1*, that contains 25 exons, of which 24 encode the 1158 amino acid long protein (UniProt: Q9JJH7, RefSeq: NM\_020277). *Trpm5-2* is a C-terminally truncated variant that is annotated to undergo nonsense-mediated decay (UniProt: Q9JJH7-3). *Trpm5-3* to *Trpm5-6* are non-protein coding splice variants, as both contain retained introns due to incomplete splicing. *Trpm5-7* and *Trpm5-8* encode short proteins, however, they lack the pore-region and transmembrane domains.

To assess whether the 8 splice variants are present in the MOE, I analyzed mRNA expression of the 8 annotated *Trpm5* splice variants via reverse transcriptase polymerase chain reaction (RT-PCR, Figure 40B). MOE cDNA derived from adult, 7 weeks old B6 mice and from B6 embryos at E18. For the analysis, I employed 22 different primers and a total of 25 primer combinations encompassing various regions of the 8 *Trpm5* splice variants (Table 4, Figure 40A).

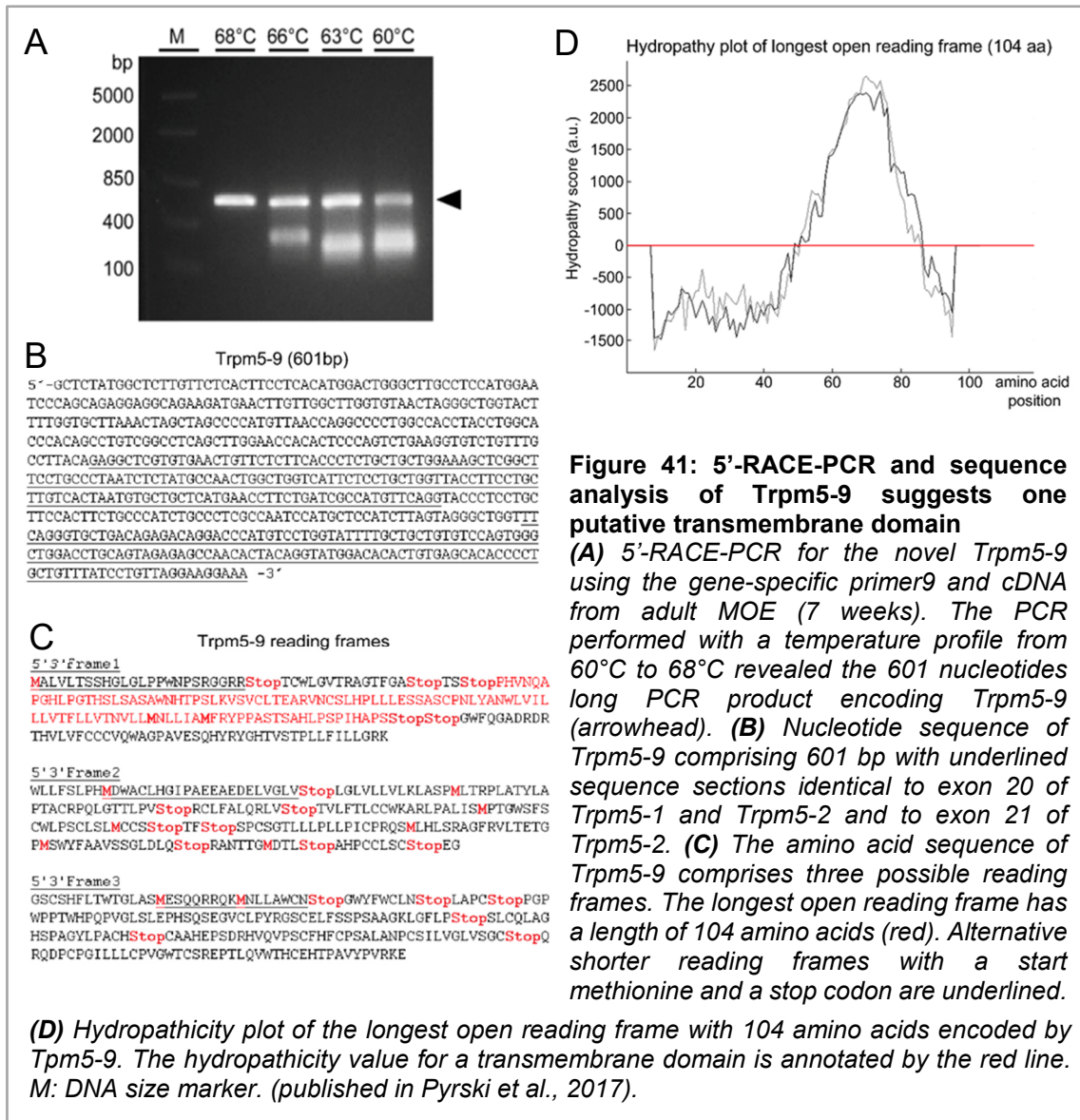
The results show that low amounts of two different *Trpm5* products with the size of 4123 bp and 601 bp were present in both adult and embryonic total MOE samples (Figure 40B). Sequence analysis revealed that the 4123 bp PCR product corresponds to *Trpm5-1*, which is annotated to encode the functional *Trpm5* channel. Surprisingly, the smaller PCR product with a length of 601 bp has not yet been described, therefore it represents a novel olfactory *Trpm5* splice variant, denoted as *Trpm5-9*.



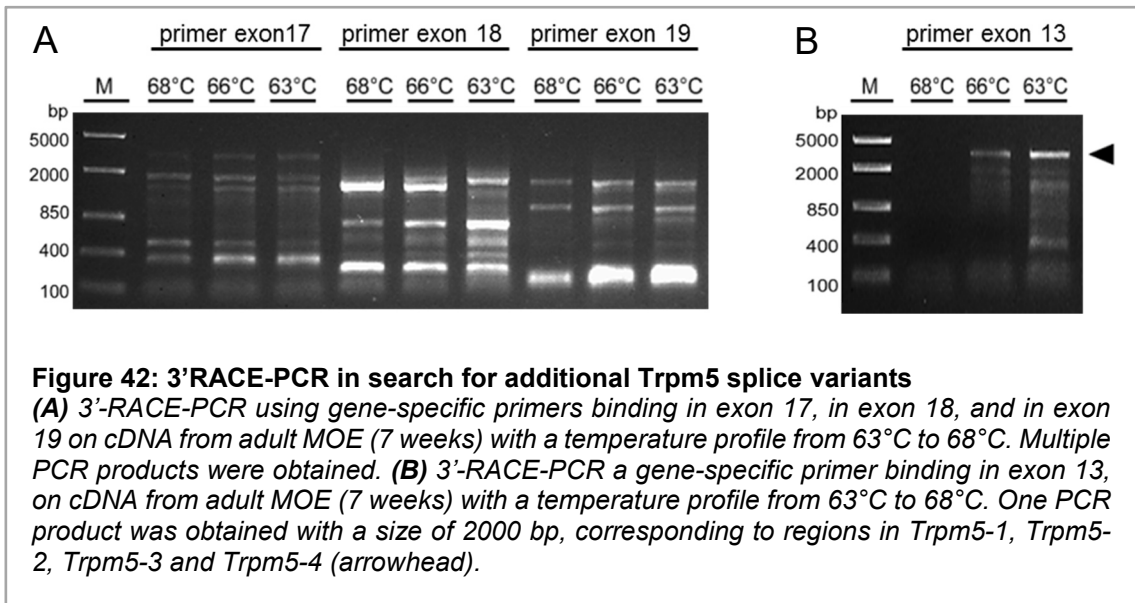
To further dissect which MOE cell types express *Trpm5-1* and *Trpm5-9*, I conducted RT-PCR experiments on cDNA from fluorescently-labeled OSNs and MV cells, manually collected from adult, 7 weeks old *Trpm5-1C/eR26- $\tau$ GFP* mice or OSNs from adult, 7 weeks old OMP-GFP mice (Figure 40B). These experiments revealed that the mRNAs encoding both splice variants, *Trpm5-1* and *Trpm5-9* are expressed in  $\tau$ GFP positive MV cells. In contrast,  $\tau$ GFP positive OSNs express mRNA encoding solely the new splice variant *Trpm5-9*. As expected, the negative control,  $\tau$ GFP-negative OSNs were devoid of *Trpm5-9* and *Trpm5-1*. As positive control for OSN identity, I analyzed isolated GFP-positive OSNs deriving from OMP-GFP mice and confirmed the lack of *Trpm5-1*, but presence of *Trpm5-9* in mature OSNs (Figure 40B).

Sequence analysis of the newly obtained *Trpm5-9* fragment revealed that every possible reading frame contains a stop codon, thereby representing the C-terminal end of all putative proteins that might be encoded by *Trpm5-9* (Figure 41C). In contrast, the N-terminal region was yet to be examined. To determine the N-terminal region of *Trpm5-9*, I performed a 5'-RACE-PCR. With increasing temperature, these experiments yielded one single specific product with a size of 601 nucleotides (Figure 41A), indicating that *Trpm5-9* consists of one single exon. Comparison of the newly identified *Trpm5-9* to the 8 known *Trpm5* splice variants showed that *Trpm5-9* differs from all other splice variants. The nucleotides 237 to 395 are identical to exon 20 of *Trpm5-1* and the nucleotides 460 to 601 are identical to exon 21 of *Trpm5-2*. Whereas nucleotides 1 to 236, and 396 to 459 correspond to the intron sequences 19/20 and 20/21 of the *Trpm5* gene (Figure 40A). Analysis of *Trpm5-9* for potential open reading frames showed that *Trpm5-9* possesses an open reading frame with a maximum length of 104 amino acids (Figure 41C). Yet, this reading frame lacks a start methionine and the sequence encoding the channel pore (Figure 41B,C). To assess a possible model for the transmembrane topology of this previously unknown splice variant, I used the software TMpred and generated a hydropathy plot. This indicated that *Trpm5-9* exhibits characteristics of a single transmembrane domain (Figure 41C), corresponding to parts of transmembrane domain 6 of *Trpm5-1* (Figure 40C).

Altogether, this protein clearly does not encode a functional channel. Furthermore, the *Trpm5-9* sequence does not contain exon 26, encoding the epitope that is recognized by the antibodies used in this study.



Another explanation for the lack of Trpm5-ir in adult OSNs could be the existence of additional splice variants that, similar to Trpm5-9, lack the C-terminal antibody binding sequence (Figure 36A). Therefore, in search for alternative C-terminal splicing events, a 3'-RACE-PCR on cDNA obtained from total MOE of adult B6 mice was performed. A gene specific primer that binds in exon 13, yielded a Trpm5 RACE product of 2000 bp, corresponding to Trpm5-1, Trpm5-2, Trpm5-3 and Trpm5-4 (Figure 42B). These four variants are the only known representatives containing all necessary domains that are needed to encode a functional Trpm5 channel. Three other primers, binding to exon 17, exon 18, and exon 19 resulted in multiple RACE products (Figure 42A). However, sequence analysis revealed that none of the products encoded a Trpm5 variant undergoing alternative C-terminal splicing.



Taken together, the experiments revealed the existence of the newly identified splice variant *Trpm5-9* that is present in a subset of adult OSNs and in  $\tau$ GFP positive MV cells. The presence of *Trpm5-9* explains the activation of the *Trpm5* promoter and thereby expression of Cre recombinase, resulting in  $\tau$ GFP-ir in OSNs of *Trpm5-IC/eR26- $\tau$ GFP* reporter mice. In contrast, mRNA encoding the functional *Trpm5* channel, *Trpm5-1* was exclusively detected in total MOE extracts and in  $\tau$ GFP positive MV cells, thus indicating that *Trpm5-1*, detected in total MOE extracts, is associated with MV cells but not with OSNs.

## 5 Discussion

Transient receptor potential channels Trpm4 and Trpm5 are described to share key properties like voltage-sensitivity, selectivity to monovalent cations, and activation by increased intracellular  $\text{Ca}^{2+}$  (Nilius and Owsianik, 2011). Furthermore, Trpm4 and Trpm5 share about 40% amino acid sequence homology (Nilius and Owsianik, 2011). To define the expression of both Trpm4 and Trpm5, and to highlight similarities or differences of these channels in the two major olfactory systems, the MOE and the VNO, I employed RT-PCR, qRT-PCR, immunohistochemistry, and surgical gonadectomy combined with hormone supplementation.

My results provide morphological and functional evidence that in spite of their similar biophysical properties Trpm4 and Trpm5 play different roles in the major olfactory systems. (1) Both Trpm4 and Trpm5 are expressed in different olfactory cell types. (2) Both Trpm channels exhibit distinct expression patterns during development. (3) Trpm4 but not Trpm5 shows sexually dimorphic expression in the vomeronasal organ, and is (4) regulated by gonadal hormones.

### 5.1 Trpm4 protein is transiently expressed during postnatal MOE development

This study provides the first identification of Trpm4 expression in the main olfactory system. I could show that Trpm4 in the main olfactory system is specifically expressed in OSNs of the MOE using RT-PCR, immunohistochemistry, and by analyzing the novel Trpm4 reporter mouse line Trpm4-IC/ $\tau$ GFP. I found that Trpm4 is transiently expressed in mature OMP-positive OSNs of juvenile mice. Robust immuno-labeling of OSN somata, dendrites, and dendritic knobs started at P7, peaked at around P14, declined towards weaning at P21, and was not detectable in the adult MOE of both male and female mice. All Trpm4-ir OSNs also colocalized with  $\tau$ GFP in the Trpm4-IC/ $\tau$ GFP mice. However,  $\tau$ GFP labeling was still present in OSNs of adult Trpm4-IC/ $\tau$ GFP mice, due to the genetic strategy employed in this reporter mouse line. Once Trpm4-dependent Cre-recombinase has activated GFP, its expression is maintained over the entire 90-days lifetime of OSNs (Caggiano et al., 1994; Farbman, 1990). These results show that the novel reporter mouse line Trpm4-IC/ $\tau$ GFP represents a suitable tool to visualize Trpm4 expression in OSNs during prepubertal ages. Moreover, Trpm4 appears to play an important role in the MOE during pubertal development but is not required in adult, sexually mature mice.

Although olfactory functions are already present at birth, completion of development of this system takes place postnatally. Immature patterns of neuronal connectivity are established in an exuberant manner and later on transformed into mature patterns by trimming down excessive and misdirected connections. This activity-dependent process is termed axon pruning (Zou *et al.*, 2004; Luo and O'Leary, 2005; Low and Cheng, 2006; Marcucci *et al.*, 2011; Hyman and Yuan, 2012). The number of exuberant projections peaks around P8 and decreases towards P20 (Zou *et al.*, 2004; Marcucci *et al.*, 2011). As the expression of Trpm4 peaks between P7 and P14, is it possible that Trpm4 might play a role in axon outgrowth and synapse formation of OSNs. Axonal projections and synapses are strengthened and refined during the early postnatal development. The time point of down-regulation of Trpm4 protein expression in OSNs between P14 and P21 coincides with the decrease of exuberant projections and synapses (Zou *et al.*, 2004; Marcucci *et al.*, 2011).

Furthermore, the down-regulation of Trpm4 protein in OSNs correlates with the time of weaning at about P21. In nature, weaned offspring eventually change their entire environment and become independent of their mother (Henning, 1981). During this time, the pups' diet shifts from milk to environmental foods. Here, the food-seeking behavior is strongly dependent on olfaction (Murofushi *et al.*, 2018). One possible hypothesis for Trpm4 protein expression in OSNs before weaning might be the need for Trpm4 function in olfactory processes during the suckling period. However, once the offspring begin to eat solid foods, Trpm4 is no longer needed and is down-regulated.

## **5.2 Trpm4 protein is expressed in sensory neurons of the vomeronasal organ**

My results also show that Trpm4 is expressed in sensory neurons of the vomeronasal organ. In contrast to the MOE, Trpm4 expression in the VNO seems to follow a regular developmental process in both males and females. Trpm4 expression in VSNs starts around the first postnatal week and the number of Trpm4-positive VSNs reaches 100% until adulthood and stays constant throughout life. I detected robust Trpm4-ir in the somata, dendrites and dendritic knobs of OMP-positive, mature VSNs. Thus, Trpm4 in VSNs does not exhibit the transient expression described for OSNs. This indicates its importance in the adult VNO. Moreover, my results further substantiate earlier reports, suggesting the presence of Trpm4-like currents in hamster VSNs (Liman, 2003) and in mouse VSNs (Spehr *et al.*, 2009).

Furthermore, I compared the differential subcellular distribution of Trpc2 and Trpm4 by double-labeling experiments using antibodies specific for Trpc2 and Trpm4 on VNO cryosections and on isolated VSNs. The main compartment for vomeronasal signal transduction, the microvilli, displayed a strong Trpc2 expression and were devoid of Trpm4-ir. With Trpm4 protein being coexpressed with Trpc2 in VSNs, these results are indicative for Trpm4 being responsible for the reported residual VSN activation in Trpc2 knockout mice by other studies (Kelliher *et al.*, 2006, Yang and Delay, 2010; Kim *et al.*, 2011; Yu, 2015). However, the absence of Trpm4 protein in VSNs microvilli implicates that this channel is unlikely to participate in the primary signal transduction machinery. In addition, the localization of Trpm4 in close proximity to the the major cellular Ca<sup>2+</sup> stores, the endoplasmic reticulum (Zufall, Leinders-Zufall and Greer, 2000) and mitochondria (Fluegge *et al.*, 2012) in the dendrite indicates that Trpm4 could play a role in the modulation of VSN activity, for example as a downstream amplifier in the processing of specific vomeronasal stimuli by influencing intracellular Ca<sup>2+</sup> dynamics (Morhardt *et al.*, 2018). Furthermore, Trpm4 may be involved in general vomeronasal homeostasis.

### **5.3 Trpm4 expression in VSNs is sexually dimorphic and estrous cycle dependent**

While vomeronasal Trpm4 expression during the first 3 postnatal weeks did not exhibit any obvious sex-specific differences, in adult females approximately 50% of VNOs were devoid of any Trpm4-ir. In contrast, VSNs from various analyzed adult males exhibited equally abundant Trpm4-ir without any obvious differences in Trpm4 expression between individual animals. Furthermore, employing IHC and qRT-PCR for Trpm4, I could demonstrate that female vomeronasal Trpm4 expression is tightly linked to the murine estrous cycle that is characterized by drastic and recurrent hormonal changes over a time-period of 4 to 5 days (Butcher *et al.*, 1974, Sisk *et al.*, 2001). I observed robust Trpm4-ir and 2-fold increased mRNA expression levels during receptive periods around ovulation (proestrus and estrus) in comparison to non-receptive periods (metestrus and diestrus) showing weak Trpm4-ir in VSNs.

This result is in line with several studies that provide evidence for a direct influence of female cyclicity on gene expression in cells of various organs, for example in gonadotropes in the anterior pituitary gland (Qiao *et al.*, 2016) and in cells of the human and murine endometrium (DeClercq *et al.*, 2015; DeClercq *et al.*, 2017; Persoons *et al.*, 2018). Most intriguingly, Trpm4 is also expressed in human and murine endometrium,

and its expression level follows fluctuations of ovarian hormones during the estrous cycle (DeClercq *et al.*, 2015; DeClercq *et al.*, 2017; Persoons *et al.*, 2018). However, contrasting my data, *Trpm4* mRNA levels are slightly upregulated during diestrus in the endometrium (DeClercq *et al.*, 2017). In human endometrium, qRT-PCR analyses of *Trpm4* mRNA demonstrated an upregulated relative *Trpm4* expression during the follicular and early luteal phase (corresponding to murine estrus and diestrus; Persoons *et al.*, 2018). Similar changes in expression levels are reported for other members of the Trp-channel family, like *Trpm3*, *Trpv6*, and *Trpc1* (DeClercq *et al.*, 2015; DeClercq *et al.*, 2017; Persoons *et al.*, 2018).

Alternatively, *Trpm4* may undergo cycle-dependent posttranslational modifications such as phosphorylation, covalent binding of chemicals, and N-linked glycosylation. These modifications can affect and modulate ion channel biophysical properties, gating, subcellular targeting (Voolstra and Huber, 2014), and may even affect the immune-detection of *Trpm4* by epitope masking. Several types of posttranslational modifications have been reported for different members of the Trp channel family, including *Trpm4* (Voolstra and Huber, 2014). In detail, Woo *et al.*, have shown in 2013, that *Trpm4* undergoes N-linked glycosylation at the pore-forming loop. This posttranslational modification is suggested to play an important role in the stabilization of *Trpm4* membrane expression, as the disruption of the N-linked glycosylation results in a faster disappearance of the channel from the plasma membrane (Woo *et al.*, 2013). Whether the estrous cycle-regulated loss of *Trpm4* expression in VSNs might be attributed to posttranslational modifications has yet to be examined.

Several studies have reported that the estrous cycle and changes in sex-steroid hormone levels can directly influence olfactory function, resulting in different sexual output behaviors (Xiao *et al.*, 2004; Moncho-Bogani *et al.*, 2002; Moncho-Bogani *et al.*, 2004, Dey *et al.*, 2015; McCarthy *et al.*, 2018). In 2015, Dey *et al.*, have shown that subpopulations of VSNs of non-receptive females at diestrus are even rendered “blind” towards components of male urine, contrasting to females in estrus that exhibit attractive behaviors towards male urine.

Each estrous cycle stage is characterized by distinct hormonal blood serum concentration levels. In adult, cycling females, the ovarian hormones 17 $\beta$ -estradiol (E2) and progesterone (P4) are secreted at basal levels throughout the cycle. E2 transiently surges during late proestrus, whereas P4 displays a first peak during diestrus (Butcher *et al.*, 1974; Fata *et al.*, 2001; Sisk *et al.*, 2001), and a second peak around the time of estrus (Walmer *et al.*, 1992). Comparing *Trpm4* expression in VSNs throughout the estrous cycle, I propose that *Trpm4* expression is not only correlated to the estrous cycle,

but is also directly influenced by variations in blood serum level concentrations of ovarian hormones.

Interestingly, my results also demonstrate that Trpc2 expression in VSNs does not correlate with the female estrous cycle. By IHC analysis of acute Trpc2 expression in VSNs during the four different stages of the estrous cycle, I could show that vomeronasal Trpc2 remains constant throughout all stages. This result is consistent with the central doctrine of Trpc2 as the main channel in the vomeronasal signal transduction cascade (Liman *et al.*, 1999; Menco *et al.*, 2001; Leypold *et al.*, 2002; Stowers *et al.*, 2002; Lucas *et al.*, 2003; Zufall *et al.*, 2005). In order to fulfil its function, Trpc2 has to be expressed equally at every estrous cycle stage. Thus, with the hypothesis of Trpm4 being a downstream amplifier in the vomeronasal signal transduction, changes in expression levels following different states of female receptivity are reasonable.

#### **5.4 Trpm4 protein expression in VSNs is down-regulated during pregnancy**

In addition to the analysis of Trpm4 expression in normally-cycling adult female mice, I examined Trpm4 expression during pregnancy, one naturally occurring event resulting in estrous cycle arrest. Females during a late stage of pregnancy (GD19) were devoid of Trpm4-ir in VSNs.

My results suggest that Trpm4 expression is down-regulated in the female VNO during non-receptive conditions such as pregnancy or the post-ovulatory phases of the estrous cycle. These results are in line with studies showing non-receptive, and elevated aggressive behavior towards males during late pregnancy (Noirot *et al.*, 1975; D'Amato *et al.*, 2006; Martin-Sánchez *et al.*, 2015). Pregnant females exhibit an inverse relationship in serum level concentrations of P4 and E2 (Norwitz *et al.*, 2001). Beginning from the first half of pregnancy, circulating P4 levels are high and important for the maintenance of pregnancy (Lonstein *et al.*, 2015), whereas at term, release of P4 from the ovaries is terminated to enable the initiation of parturition. In contrast, circulating serum E2 levels rise during the second half of pregnancy until the day of parturition with a gestation period of approximately 21 days in mice (Lonstein *et al.*, 2015). Both, the decline in P4 and the rise in E2 levels are necessary to prepare for the transition from gestation to lactation, but also to stimulate receptive behaviors (Siegel, 1986; Lonstein *et al.*, 2015).

## 5.5 Trpm4 protein expression in VSNs depends on gonadal hormones

My study showed that a disruption of the main source of sex-steroid hormone production in females by OVX, and in males by ORX resulted in abolished vomeronasal Trpm4 expression, substantiating the proposed crucial role of gonadal hormones in Trpm4 regulation. Output behavior analyses on OVX mice, performed by others (Moncho-Bogani *et al.*, 2004, McCarthy *et al.*, 2018) have furthermore shown that OVX also results in diminished preference behavior of female mice towards male urine.

Additionally, I analyzed Trpm4 expression in VSNs of senescent females and revealed that sexual senescence diminished, but not completely abolished Trpm4 expression in VSNs. The female transition towards reproductive senescence is mainly driven by the neuroendocrine system resulting in diminished GnRH output to the pituitary gland while ovaries of aged female mice still being able to exert moderate amounts of gonadal hormones and contain viable follicles (Brinton, 2012; Koebele and Bimonte-Nelson, 2016). In detail, reproductive senescence is described by a sequence of events, starting by cyclic disturbances and cycle cessation with a subsequent persistent vaginal cornification (PVC), characterized by moderate levels of  $17\beta$ -estradiol (Brinton, 2012; Koebele and Bimonte-Nelson, 2016). With progressing age, PVC is replaced by either spontaneous pseudo pregnancy with elevated progesterone (Brinton, 2012; Koebele and Bimonte-Nelson, 2016) or a persistent anaestrus state, characterized by low plasma estradiol and progesterone levels (Brinton, 2012; Koebele and Bimonte-Nelson, 2016). As the female reproductive senescence is mainly characterized by malfunction in regulation of the neuroendocrine system and not by ovarian failure, the current results suggest a major role of ovarian hormones in vomeronasal Trpm4 regulation.

Moreover, I was able to identify the hormones regulating Trpm4 expression in VSNs. I could rescue the OVX phenotype in VSNs by systemic treatment with E2. In contrast, progesterone administration rather counteracted the effect of E2. Other studies have shown that in other systems sex-steroid hormones also have a severe impact on the regulation of Trp-channel expression. In human endometrium and in hESCs, administration of estrogen resulted in an increase in Trpm2 expression (Hiroi *et al.*, 2013). In the murine endometrium, mRNA expression of *Trpv2*, *Trpv6*, *Trpc4* and *Trpm4* increased after E2 administration, and was reduced 2 days upon progesterone treatment (DeClercq *et al.*, 2017). Furthermore, other studies conducting behavioral analyses on OVX females reported that the females' attractive behavior towards male urine can be restored by administration of sex-steroid hormones (Moncho-Bogani *et al.*, 2004, McCarthy *et al.*, 2018).

Comparing the results obtained from systemic hormone treatments in females with males, this study revealed that ORX induced loss of vomeronasal Trpm4 expression could not be restored by systemic T4 treatment. Application of E2 however, induced and increased Trpm4 expression upon ORX. This result was rather surprising as testosterone, but not estrogen is described as the predominant hormone in males. But it is also reported that estrogen functions in regulatory mechanisms in the male reproductive tract (Hess 2003), therefore it is possible that E2 also participates in male vomeronasal Trpm4 regulation.

### **5.6 Trpm4 protein expression in VSNs depends on endogenous E2 production**

To substantiate the fundamental role of 17 $\beta$ -estradiol on the regulation of vomeronasal Trpm4 expression, I treated ovary- and testes-intact mice systemically with the synthetic steroid exemestane (EXE), an inhibitor that irreversibly binds to the enzyme aromatase (Di Salle *et al.*, 1992). Endogenous synthesis of 17 $\beta$ -estradiol is accomplished by the estrogen-synthetizing enzyme aromatase (Santen *et al.*, 2009). Five days of EXE administration resulted in estrous cycle arrest and decreased or abolished Trpm4 expression in VSNs of both female and male mice. These results are in line with Mirsky *et al.*, 2011, that reported estrous cycle arrest in female rats upon EXE treatment.

Taken together, Trpm4 appears to play primarily a neuronal role in the olfactory system. This is in line with Trpm4 expression in neurons of the other olfactory organs, the SOM and GG. In the MOE, Trpm4 is only transiently expressed during development and in the VNO it is likely to play an important role with its regulation by gonadal hormones. My study shows that not only the external administration of E2 to castrated males and females but also endogenous 17 $\beta$ -estradiol, produced by aromatase in intact females and males, is crucial for vomeronasal Trpm4 expression. In contrast, P4 administration has a dampening effect on E2 activated upregulation of Trpm4 expression in females, and restoration of Trpm4 expression in male VSNs cannot be induced by T4. Thus, 17 $\beta$ -estradiol plays a fundamental role in the up-regulation of Trpm4 expression in VSNs.

## 5.7 Trpm5 protein is exclusively expressed in MV cells of the adult MOE

In the second chapter of this thesis, I conducted a detailed analysis of the expression of Trpm5 in the murine olfactory system. I could show that in contrast to Trpm4, Trpm5 expression is absent in OSNs during all stages of postnatal MOE development and during adulthood in both males and females (see 4.2.6). Moreover, using two independent and validated anti-Trpm5 antisera and by RT-PCR, I could show that in the adult MOE, protein and mRNA expression of the classical Trpm5 channel is confined to MV cells. This result is in line with other reports that have provided evidence for *Trpm5* mRNA (Pyrski *et al.*, 2017; Yamaguchi *et al.*, 2014) and Trpm5 protein expression (Kusumakshi *et al.*, 2015) exclusively in MV cells. Furthermore, Trpm5 expressing MV cells are proposed to play important roles in the detection of harmful stimuli (Lin *et al.*, 2008b; Ogura *et al.*, 2011) and in the maintenance of olfactory function by cholinergic modulation (Hansen and Finger, 2008; Lemons *et al.*, 2017). No Trpm5 expression in OSNs was reported in these studies.

However, this result is in contrast to earlier studies performed in Trpm5-GFP transgenic mice that propose the presence of Trpm5 in cilia of adult OSNs (Lin *et al.*, 2007) and recorded a Ca<sup>2+</sup>-activated cation channel in the cilia of a subset of OSNs upon stimulation with the putative pheromone 2,5-dimethylpyrazine and the semiochemical (methylthio)methanethiol (MTMT). These studies suggest a function of Trpm5 expressing OSNs in the coding of pheromonal information. However, it was not yet proven that this channel activity is attributed to the function of the classical Trpm5 channel (Oshimoto *et al.*, 2013; Lopez *et al.*, 2014).

By contrast, Pyrski *et al.*, have shown via Ca<sup>2+</sup> imaging in OSNs of the Trpm5-GCaMP3 reporter mice, that these neurons exhibit only classical odor detection properties, responding to a general odor ligand mix. Solely a small subset of Trpm5-GCaMP3 positive cells was also able to detect predator urine (Pyrski *et al.*, 2017).

In addition, I performed double labeling experiments for Trpm5 and  $\tau$ GFP in Trpm5-IC/eR26- $\tau$ GFP mice, in which  $\tau$ GFP expression is dependent on Trpm5-promoter activity. These experiments confirmed that Trpm5 protein expression is confined to MV cells, whereas  $\tau$ GFP expression is present not only in different types of MV cells but also in OSNs. Similar to the Trpm4-IC/ $\tau$ GFP reporter mouse line, following the initial Trpm5-dependent activation of Cre-recombinase,  $\tau$ GFP expression in the Trpm5-IC/eR26- $\tau$ GFP mouse line is maintained over the entire 90-day lifespan of OSNs (Caggiano *et al.*, 1994; Farbman, 1990), even though the actual Trpm5 protein expression has already been down-regulated at one point of time.

## 5.8 Trpm5 protein is transiently expressed in a subset of embryonic OSNs

Trpm5 protein is absent in OSNs of the adult MOE, however, using IHC for Trpm5 on embryonic MOE cryosections at late embryonic stages E15, E17, E18, and E19, I could show that Trpm5 protein is expressed in a subset of OSNs during a very narrow timed period, with a peak at embryonic day 18 (E18) (see 4.2.7). This result coincides with and explains the GFP expression detected in OSNs of adult Trpm5-IC/eR26- $\tau$ GFP mice. At E18, I detected Trpm5-ir in dendrites, somata and axons of OMP- and Gap43-positive, early-mature OSNs. After E18, Trpm5 protein expression in OSNs then sharply declines to non-detectable levels after birth. This finding is in line with a previous study, which described a similar transient expression of Trpm5, with a peak of expression around E18 in dorsal root ganglia during embryonic development (StAAF *et al.*, 2010). Although the physiological role of this result is still unknown, the transient expression of Trpm5 in embryonic OSNs coincides with several critical periods of MOE development during late prenatal life (Gesteland *et al.*, 1982; Farbman, 1986; Maier *et al.*, 1999; Voyron *et al.*, 1999, Cowan and Roskams, 2002).

My data indicate that Trpm5 plays a fundamental role in developmental processes during embryogenesis. Coexpression of Gap43 in Trpm5 positive embryonic OSNs is indicative for a function in axonal outgrowth, as Gap43 is described to be critical in the process of axon path-finding (Maier *et al.*, 1999). Several studies have reported that prenatally, around embryonic days E18 and E19, first synaptic connections of olfactory receptor cell axons are established in the OB (Farbman 1986, Farbman and Menco 1986). During this time, Trpm5-positive OSNs might function as guidance neurons to set axonal pathways towards glomeruli of the MOB for upcoming OSN generations. After having fulfilled this task, Trpm5-positive OSNs may undergo apoptosis. This process would nicely describe the sharp decline in Trpm5-ir after E18. Apoptosis is reported to play a crucial role in fine-tuning the number of cells in the central nervous system (CNS) during the entire lifespan of an animal (Buss *et al.*, 2006; Dekkers *et al.*, 2013). Massive prenatal apoptotic OSN cell death is reported at E12 and E16, however, lower levels of apoptosis are also observed around E19 (Voyron *et al.*, 1999, Cowan and Roskams, 2002). The Trpm5 positive OSN population could represent one of the last generations of guidance neurons affected and regulated by prenatal apoptosis.

Furthermore, the transient expression of Trpm5 in embryonic OSNs could indicate that these cells function in recognition of specific molecular cues, that are either crucial for late embryonic development or play an important role in preparing the embryo for parturition. Gesteland *et al.*, have already shown in 1982 that in rat embryos at E19, many OSNs are described to become specifically receptive to odorants, and is was

possible to measure olfactory activity by electro-olfactograms (Gesteland *et al.*, 1982). Even more studies demonstrated embryonic olfactory function *in utero* (Pedersen *et al.*, 1983; Schaal and Orgeur, 1992). In 2013, Lam and Mombaerts reported OSNs activity in mouse embryos beginning at E16.5 in response to cognate odorous ligands for the OR genes S1 or MOR23 using patch-clamp recordings. Furthermore, a recent study showed that in addition to OR expression, OSN-activity is crucial for olfactory circuit formation in the olfactory bulb (Nakashima *et al.*, 2019).

Moreover, the amniotic fluid is described as a source of possible olfactory cues for the embryo (Schaal and Orgeur, 1992) and that maternal gestational diet can influence olfactory function in the offspring (Hepper, 1988). Here, dams were fed with garlic during gestation, resulting in the offspring's preference for garlic after birth (Hepper, 1988). More recent studies have shown that the amniotic fluid of pregnant mothers contains specific nutrients, growth factors and hormones (Underwood *et al.*, 2005) that could be recognized by the embryonic MOE. Further supporting evidence is provided by Logan *et al.*, 2012, reporting that the amniotic fluid contains suckling-promoting olfactory ligands. Here, calcium-imaging experiments have shown that presentation of different fractions of the amniotic fluid elicited responses in dissociated embryonic OSNs during late embryogenesis (E17.5 and later). Taken together, specific cell differentiation, axonal outgrowth, synapse formation, and the preparation of the embryo for birth take place during late prenatal ages. Trpm5 might act as an amplifier in a subset of OSNs that detect specific olfactory cues in the amniotic fluid during this critical period.

Additionally, I performed double labeling experiments for Trpm5 and  $\tau$ GFP in MOE sections in embryonic Trpm5-IC/eR26- $\tau$ GFP mice. These experiments revealed that the Trpm5-dependent reporter gene expression during embryogenesis is rather complex. In contrast to the robust Trpm5 protein expression in embryonic OSNs at E18,  $\tau$ GFP at E18 was weak or even absent in OSNs. Cell counts within a whole embryonic MOE showed on average only 100  $\tau$ GFP OSNs compared to about 900 Trpm5-positive OSNs per MOE. However, numbers of  $\tau$ GFP-positive OSNs at later stages clearly increased.

This discrepancy is likely explained by the composition of the genetic construct in the Trpm5-IC/eR26- $\tau$ GFP mice. It is well known that bicistronic genetic constructs with an introduced IRES-site occasionally lead to lower levels of protein translation from the downstream gene (Hellen and Sarnow, 2001; Licursi *et al.*, 2011). Thus, it is conceivable that expression of the downstream gene encoding Cre-recombinase is insufficient at this early stage. Second, the properties of the genetic strategy of this mouse line leads to a temporarily delayed reporter gene expression, since  $\tau$ GFP is only activated after the Cre-

recombinase-mediated excision of the floxed stop codon preceding the coding region of  $\tau$ GFP. In addition, the time frame of *Trpm5* expression in embryonic OSNs is very narrow with about 2 days. Thus, in combination, these effects may contribute to the lack of  $\tau$ GFP in *Trpm5*-positive OSNs at E18.

## 5.9 A novel *Trpm5* splice variant exists in OSNs of the adult MOE

This study provides the first evidence for the presence of two distinct *Trpm5* splice variants in the MOE, *Trpm5-1*, which encodes the classical *Trpm5* channel described in taste receptor cells (Pérez *et al.*, 2002), and the prior to this study unknown splice variant *Trpm5-9* (see 4.2.8).

Conducting RT-PCR on adult and embryonic MOE, and on fluorescently-labeled OSNs and MV cells of adult *Trpm5-IC/eR26- $\tau$ GFP* mice, I could demonstrate that *Trpm5-1* is exclusively present in MV cells, whereas the novel splice-variant *Trpm5-9* is expressed in both cell types. This further supports my results on *Trpm5* protein expression in the MOE, where I detected *Trpm5-ir* solely in MV cells and not in OSNs. This result is also in line with previous studies that have provided evidence for *Trpm5* mRNA expression in MV cells, but not in any subpopulations of OSNs in adult mice using *in situ* hybridization analyses (Yamaguchi *et al.*, 2014; Pyrski *et al.*, 2017). Moreover, the presence of *Trpm5-9* in OSNs may also explain  $\tau$ GFP expression in OSNs, despite the absence of the functional *Trpm5* channel. By sequence analyses, I could show that *Trpm5-9* is unlikely to encode a functional channel, but it could have a modulatory function on the classical *Trpm5*-channel, as it has been reported for shorter splice variants of other members of the Trp channel family (Vasquez and Valverde, 2006). For example, Schaefer *et al.*, have shown in 2002 that the *Trpc4 $\alpha$*  isoform is a dominant negative modulator of *Trpc4 $\beta$* . A similar dominant negative modulatory effect was also reported for *Trpv1b* (Wang *et al.*, 2004), *smTrpc2* (Chu *et al.*, 2005), and *Trpm2-S* (Miller, 2006).

The results of this study indicate that no other splice variants than *Trpm5-1* and *Trpm5-9* are present in the MOE. This is in line with existing data sets, obtained by others. Deep sequencing RNA analyses of whole MOE samples for example, show that the amount of *Trpm5* mRNA is 35- to 80-fold lower in comparison with mRNA levels of members of the olfactory signal transduction like the ion channels *Cnga2* and *Ano2*, thereby arguing against a fundamental role of *Trpm5* in the MOE (Ibarra-Soria *et al.*, 2014; Saraiva *et al.*, 2015). Going deeper from whole MOE analyses to single-cell RNA deep sequencing, Saraiva *et al.*, have shown in 2015 that out of 30 analyzed mature OSNs 29 were devoid

of *Trpm5* mRNA. Solely 1 OSN expressed *Trpm5* mRNA at very low levels, which in turn, could be attributed to the presence of *Trpm5-9*.

Taken together, with the exception of embryonic OSNs, my results demonstrate that *Trpm5* plays a role in MV cells of the adult MOE but not in OSNs as has been debated earlier.

## 5.10 Outlook

In summary, this study provides new insights into the role of two members of the melastatin subfamily of Trp-channels, Trpm4 and Trpm5 in the murine olfactory system.

Regarding Trpm5 expression in the olfactory system, I could show that (1) acute protein expression of Trpm5 is confined to MV cells in the adult MOE, (2) adult OSNs express a so far unknown, presumably non-functional Trpm5 splice variant, and are devoid of mRNA encoding the classical Trpm5 channel, and (3) a subset of early mature OSNs expresses the classical Trpm5 channel protein in a transient manner during late embryogenesis. Thus, the data indicate a specific function of Trpm5 *in utero* during a narrow time window in development.

Regarding the functional role of Trpm4 in the olfactory system, I could show that (1) Trpm4 in OSNs is transiently expressed during postnatal ages, and is absent in the adult MOE. Furthermore, this study revealed (2) that Trpm4 is expressed as a second major Trp-channel in VSNs, besides Trpc2, and that Trpm4 expression is absent in VSN microvilli, suggesting that Trpm4 is not involved in the primary signal transduction pathway in these cells. Most exciting, I found that (3) vomeronasal Trpm4 is expressed in a gender-specific, estrous cycle-regulated manner, and is dependent on the sex-steroid hormone  $17\beta$ -estradiol. This strongly indicates a yet undescribed potential role of Trpm4 in gender-specific social and sexual behaviors.

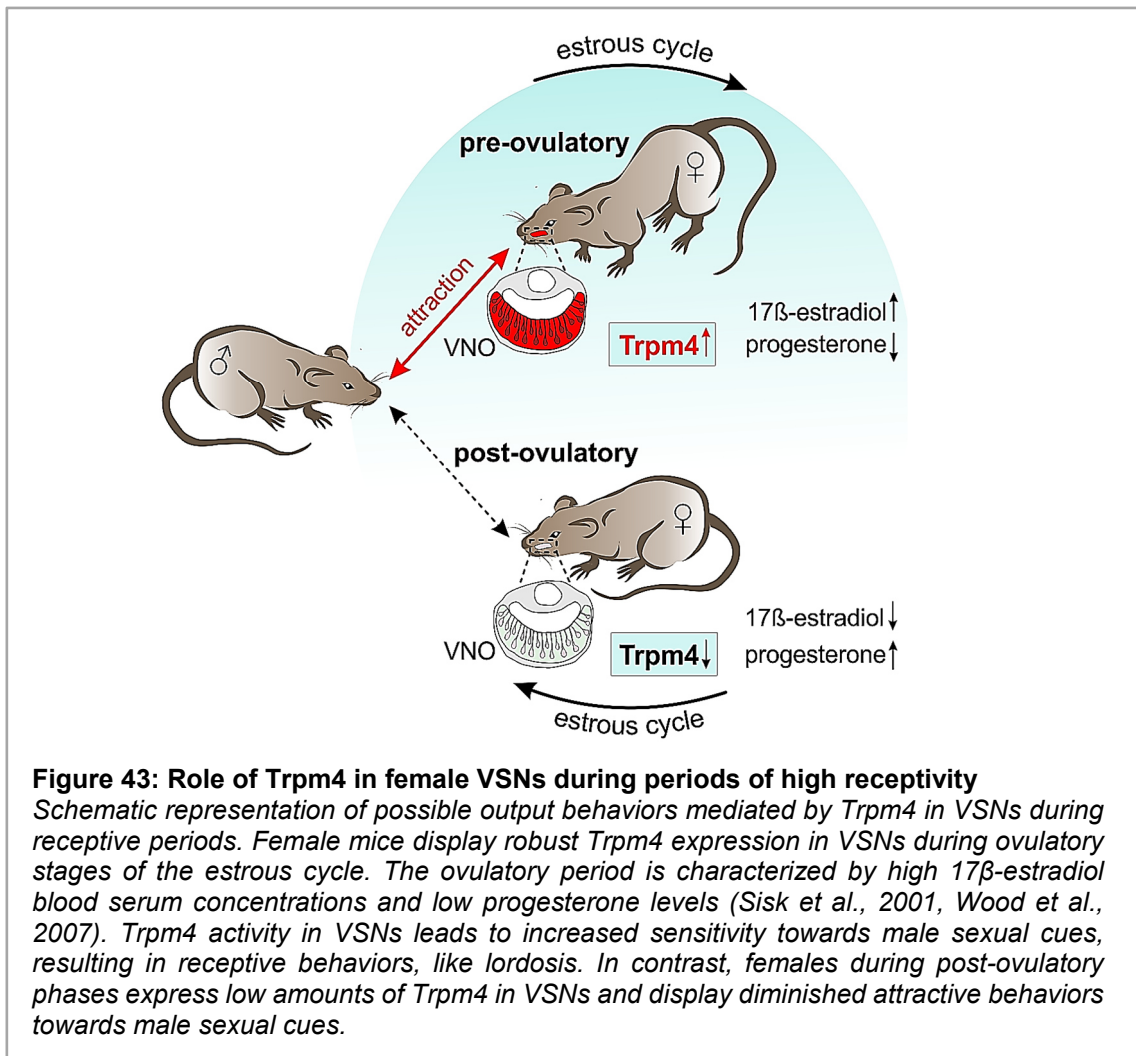
To assess the function of Trpm5 in the olfactory system during embryogenesis, further experiments are required. As previously mentioned, this study suggests that Trpm5 positive OSNs may function as guidance neurons during the process of axonal pathfinding. To test this hypothesis, the first experiment would be a systematic analysis of the anatomy and innervation pattern of the olfactory bulb in Trpm5 knockout mice. If Trpm5 function is necessary during this critical time-period, Trpm5 knockout mice would display alterations in glomerular innervation, compared to Trpm5-intact wild-type mice. Analyses of important components of the axon pathfinding machinery by other groups have revealed that for example deletion of endogenous glycan synthesis, which is described to play an important role in this process (Lipscomb *et al.*, 2003) resulted in axon guidance errors with knockout mice exhibiting a severe disorganization of olfactory bulb innervation (Henion *et al.*, 2005). Similar observations were made in mice lacking specific ORs (P2, Wang *et al.*, 1998), with a complete failure of axonal innervation of glomeruli, and in *Cnga2* knockout mice, with a mild glomerular targeting phenotype (Brunet *et al.*, 1996, Schwarting and Henion, 2012).

Given that massive apoptosis following embryonic axonal outgrowth occurs among OSNs between embryonic ages E12 to E19 (Voyron *et al.*, 1999, Cowan and Roskams, 2002), the next set of experiments such as caspase assays would address the question whether excess apoptosis during this period accounts for the loss of Trpm5 positive OSNs during late embryogenesis. Colocalization of Trpm5-ir and caspase activity in MOE sections at E18 would reveal the amount of apoptotic cell death events in Trpm5-positive OSNs. If the disappearance of Trpm5 positive embryonic OSNs can be correlated to the massive apoptotic events during late embryogenesis, this finding would further indicate a role of Trpm5-positive OSNs as axonal guidance neurons.

To address the postulated guidance role of Trpm5-positive embryonic OSNs, lesioning of the adult MOE by intranasal administration of Triton-X could be performed as described by Bolz *et al.*, 2017. Triton-X induces massive degeneration of the MOE and its subsequent regeneration, due to the activity of mitotic active stem cells at the basal membrane (Verhaagen *et al.*, 1990). Here, the embryonic conditions would be mimicked by the regeneration process as all connectivity to the OB is abolished and needs to be re-established. With Trpm5 playing a fundamental role in OSN development, acute Trpm5 expression should be re-activated during regeneration of the ablated tissue, and adult regenerating olfactory tissue would show presence of Trpm5-ir in OSNs comparable to embryonic MOE. This result would support the hypothesis that Trpm5 in OSNs plays a role during MOE development.

Furthermore, this study suggests a second possible function of embryonic Trpm5 positive OSNs. Trpm5 might act as an amplifier in a subset of embryonic OSNs that detect specific olfactory cues in the amniotic fluid during late pregnancy. To measure the activity of Trpm5-positive embryonic OSNs towards olfactory cues, the novel *en-face* Ca<sup>2+</sup>-imaging on whole-mount MOE preparations of embryonic MOE, as described in Pyski *et al.*, 2017, could be employed. Here, embryonic Trpm5 positive cells would be perfused with amniotic fluid or with different fractions of the amniotic fluid, and their activity would be measured. Following Ca<sup>2+</sup>-imaging, a post-hoc IHC for Trpm5 would be performed, in order to visualize Trpm5-positive OSNs. Furthermore, to assess the specificity of Trpm5 positive OSNs towards specific stimuli, control experiments on MOE tissue obtained from Trpm5<sup>-/-</sup> embryos would be performed.

Furthermore, I hypothesize that Trpm4 might function as a key element in the modulation of VSN sensitivity towards sexual cues during highly receptive periods (Figure 43). To test this hypothesis, different output behavior analyses have to be performed.



First, similar to Xiao et al., 2004; Moncho-Bogani et al., 2002; Moncho-Bogani et al., 2004, Dey et al., 2015; and McCarthy et al., 2018, responses towards male urine would be compared between pre- and post-ovulatory female wild-type mice. Second, the same experiment would be performed comparing ovulatory wild-type female mice with ovulatory Trpm4<sup>-/-</sup> female mice. If Trpm4 plays a role in VNO activation towards sexual cues, as I proposed earlier, Trpm4 deficient females would display little or no interest in male urine in comparison to Trpm4-intact females.

---

Additionally, stimulation of Trpm4-intact females by ESP1, the sex-specific exocrine gland-secreted peptide 1, which is reported to potentiate lordosis behavior (Haga *et al.*, 2010) would result in the display of sexual receptivity. In contrast, Trpm4 knockout females would show diminished receptivity upon presentation of ESP1.

Other than that, the subcellular localization and the biophysical properties of Trpm4 may also indicate a modulatory function by amplifying and/or strengthening vomeronasal responses. This could be tested on Trpm4 knockout females by presentation of different concentrations of pheromonal cues, for example male urine. Knockouts would likely show a decreased sensitivity, thus display an elevated detection threshold compared to wild-type females. This would support an amplifying function of Trpm4 in vomeronasal signal transduction.

And finally, as Trpm4 is constitutively expressed in male VSNs, analyses of male aggressive behaviors could shed light on the function of Trpm4 in the male VNO. Here, I would employ the resident-intruder paradigm that is reported as standardized test for aggressive behaviors in male mice (Koolhaas *et al.*, 2013). I hypothesize, that lack of Trpm4 expression in VSNs of Trpm4 knockout males would result in diminished aggressive behaviors in these mice, compared to wild-type males. Other studies have shown that deletion of the key channel of vomeronasal signal transduction, Trpc2 leads to significantly reduced male aggression towards intruders (Leypold *et al.*, 2002; Stowers *et al.*, 2002; Chamero *et al.*, 2007, Kimchi *et al.*, 2007).

However, as my study indicates a rather downstream function of Trpm4 in the vomeronasal signal transduction, vomeronasal Trpm4 ablation would result in rather mild behavioral phenotypes compared to a deletion of Trpc2.

---

## 6 References

- Banik, D.D., Martin, L.E., Freichel, M., Torregrossa, A.M., Medler, K.F. (2018). TRPM4 and TRPM5 are both required for normal signaling in taste receptor cells. *Proc Natl Acad Sci USA* 115:772-781.
- Baxter, B.D., Larson, E., Ramakrishnan, V., Jones, K., Feinstein, P., Mainland, J.D., Restrepo, D. (2019). Higher Level Of Expression Of Transcripts Involved In Inflammation And Immunity In Trpm5-Gfp Olfactory Sensory Neurons. 41st Annual Meeting of the Association for Chemoreception Sciences (AChems), Bonita Springs, FL.
- Bezencon, C., le Coutre, J., Damak, S. (2007). Taste-signaling proteins are coexpressed in solitary intestinal epithelial cells. *Chem. Senses* 32:41-49.
- Bleymehl, K., Pérez-Gómez, A., Omura, M., Moreno-Pérez, A., Macías, D., Bai, Z., Johnson, R.S., Leinders-Zufall, T., Zufall, F., Mombaerts, P. (2016). A Sensor for Low Environmental Oxygen in the Mouse Main Olfactory Epithelium. *Neuron* 92:1196-1203.
- Bolz, F., Kasper, S., Bufe, B., Zufall, F., Pyrski, M. (2017). Organization and plasticity of sodium channel expression in the mouse olfactory and vomeronasal epithelia. *Fron Neuroanat* 11:28.
- Brann, J.H., Dennis, J.C., Morrison, E.E., Fadool, D.A. (2002). Type-specific inositol 1,4,5-trisphosphate receptor localization in the vomeronasal organ and its interaction with a transient receptor potential channel, TRPC2. *J. Neurochem.* 83:1452-1460.
- Brennan, P.A., Zufall, F. (2006). Pheromonal communication in vertebrates. *Nature* 444:308-315.
- Brinton, R.D. (2012). Minireview: Translational Animal Models of Human Menopause: Challenges and Emerging Opportunities. *Endocrinology* 153:3571-3578.
- Brixel, L.R., Monteilh-Zoller, M.K., Ingenbrandt, C.S., Fleig, A., Penner, R., Enklaar, T., Zabel, B.U., Prawitt, D. (2010). TRPM5 regulates glucose-stimulated insulin secretion. *Pflügers Arch.* 460:69-76.
- Bruce, H.M. (1959). An exteroceptive block to pregnancy in the mouse. *Nature* 184:105.

- 
- Bruce, H.M. (1969). Pheromones and behavior in mice. *Acta Neurol Psychiatr Belg* 69:529-538.
- Brunet, L.J., Gold, G.H., Ngai, J. (1996). General anosmia caused by a targeted disruption of the mouse olfactory cyclic nucleotide-gated cation channel. *Neuron*. 4:681-693.
- Bufe, B., Schumann, T., Zufall, F. (2012). Formyl peptide receptors from immune and vomeronasal system exhibit distinct agonist properties. *J. Biol. Chem.* 287:33644-33655.
- Buss, R.R., Sun, W., Oppenheim, R.W. (2006). Adaptive roles of programmed cell death during nervous system development. *Ann Rev Neurosci* 29:1-35.
- Butcher, R.L., Collins, W.E., Fugo, N.W. (1974). Plasma concentration of LH, FSH, prolactin, progesterone and estradiol-17beta throughout the 4-day estrous cycle of the rat. *Endocrinology* 94:1704-1708.
- Buck, L, Axel, R. (1991). A novel multigene family may encode odorant receptors: a molecular basis for odor recognition. *Cell* 65:175-187.
- Bustin, S.A., Benes, V., Garson, J.A., Hellems, J., Huggett, J., Kubista, M., Mueller, R., Nolan, T., Pfaffl, M.W., Shipley, G.L., Vandesompele, J., Wittwer, C.T. (2009). The MIQE guidelines: minimum information for publication of quantitative real-time PCR experiments. *Clin Chem* 55:611-622.
- Byers, S.L., Wiles, M.V., Dunn, S.L., Taft, R.A. (2012). Mouse estrous cycle identification tool and images. *PloS one* 7: e35538.
- Caggiano, M., Kauer, J.S., Hunter, D.D. (1994). Globose basal cells are neuronal progenitors in the olfactory epithelium: a lineage analysis using a replication-incompetent retrovirus. *Neuron* 13:339-352.
- Caligioni, C.S. (2009). Assessing reproductive status/stages in mice. *Curr Protoc Neurosci Appendix 4: Appendix 4I*.
- Chamero, P., Marton, T.F., Logan, D.W., Flanagan, K., Cruz, J.R., Saghatelian, A., et al. (2007). Identification of protein pheromones that promote aggressive behavior. *Nature* 450:899-902.
- Chamero, P., Katsoulidou, V., Hendrix, P., Bufe, B., Roberts, R., Matsunami, H., et al. (2011). G protein G(alpha)o is essential for vomeronasal function and aggressive behavior in mice. *Proc Natl Acad Sci USA* 108:12898–12903.

- Chamero, P., Leinders-Zufall, T., Zufall, F. (2012). From genes to social communication: molecular sensing by the vomeronasal organ. *Trends Neurosci.* 35:597-606.
- Chamero P., Weiss J., Alonso M.T., Rodríguez-Prados M., Hisatsune C., Mikoshiba K., Leinders-Zufall T., F. Zufall. (2017). Type 3 inositol 1,4,5-trisphosphate receptor is dispensable for sensory activation of the mammalian vomeronasal organ. *Sci. Rep.* 7:10260.
- Chu, X., Tong, Q., Wozney, J., et al. (2005). Identification of an N-terminal TRPC2 splice variant which inhibits calcium influx. *Cell Calcium* 37:173-182.
- Clapham, D.E. (2003). TRP channels as cellular sensors. *Nature* 426:517-524.
- Clapp, T.R., Medler, K.F., Damak, S., Margolskee, R.F., Kinnamon, S.C. (2006). Mouse taste cells with G protein-coupled taste receptors lack voltage-gated calcium channels and SNAP-25. *BMC Biol.* 4:7.
- Colsoul, B., Schraenen, A., Lemaire, K., Quintens, R., Van Lommel, L., Segal, A., Owsianik, G., Talavera, K., Voets, T., Margolskee, R.F., Kokrashvili, Z., Gilon, P., Nilius, B., Schuit, F.C., Vennekens, R. (2010). Loss of high-frequency glucose-induced Ca<sup>2+</sup> oscillations in pancreatic islets correlates with impaired glucose tolerance in *Trpm5*<sup>-/-</sup> mice. *Proc. Natl. Acad. Sci. USA* 107:5208-5213.
- Cowan, C.M., Roskams, A.J. (2002). Apoptosis in the mature and developing olfactory neuroepithelium. *Microsc. Res. Tech.* 58:204-215.
- Damak, S., Rong, M., Yasumatsu, K., Kokrashvili, Z., Perez, C.A., Shigemura, N., Yoshida, R., Mosinger, B., Jr., Glendinning, J.I., Ninomiya, Y., Margolskee, R.F. (2006). *Trpm5* null mice respond to bitter, sweet, and umami compounds. *Chem. Senses* 31:253-264.
- Damann, N., Voets, T., Nilius, B. (2008). TRPs in our senses. *Curr Biol* 18:880-889.
- D'Amato, Rizzi, R., Moles, A. (2006). Aggression and anxiety in pregnant mice are modulated by offspring characteristics. *Animal Behavior* 72:773-780.
- De Clercq, K., Held, K., Van Bree, R., Meuleman, C., Peeraer, K., Tomassetti, C., Voets, T., D'Hooghe, T., Vriens, J. (2015). Functional expression of transient receptor potential channels in human endometrial stromal cells during the luteal phase of the menstrual cycle. *Hum Reprod* 30:1421-1436.

- De Clercq, K., Van den Eynde, C., Hennes, A., Van Bree, R., Voets, T., Vriens, J. (2017). The functional expression of transient receptor potential channels in the mouse endometrium. *Hum Reprod* 32:615-630.
- Dekkers, M.P.J., Nikolettou, V., Barde, Y.A. (2013). Death of developing neurons: New insights and implications for connectivity. *J Cell Biol* 203:385-393.
- Dewan, A., Pacifico, R., Zhan, R., Rinberg, D., Bozza, T. (2013). Nonredundant coding of aversive odours in the main olfactory pathway. *Nature* 497:486-489.
- Dey, S., Chamero, P., Pru, J.K., Chien, M.S., Ibarra-Soria, X., Spencer, K.R., Logan, D.W., Matsunami, H., Peluso, J.J., Stowers, L. (2015). Cyclic regulation of sensory perception by a female hormone alters behavior. *Cell* 161:1334-1344.
- Dietschi, Q., Tuberosa, J., Rösingh, L., Loichot, G., Ruedi, M., Carleton, A., Rodriguez, I. (2017). Evolution of immune chemoreceptors into sensors of the outside world. *Proc Natl Acad Sci USA* 114:7397-7402.
- Di Salle, E., Ornati, G., Giudici, D., Lassus, M., Evans, T.R., Coombes, R.C. (1992). Exemestane (FCE 24304), a new steroidal aromatase inhibitor. *J Steroid Biochem Mol Biol* 43:137-143.
- Dunston, D., Ashby, S., Krosnowski, K., Ogura, T., Lin, W. (2013). An Effective Manual Deboning Method to Prepare Intact Mouse Nasal Tissue with Preserved Anatomical Organization. *Journal of Visualized Experiments* 78:1–7.
- Elsaesser, R., Montani, G., Tirindelli, R., Paysan, J. (2005). Phosphatidylinositol signaling proteins in a novel class of sensory cells in the mammalian olfactory epithelium. *Eur. J. Neurosci.* 21:2692-2700.
- Enklaar, T., Esswein, M., Oswald, M., Hilbert, K., Winterpacht, A., Higgins, M., Zabel, B., Prawitt, D. (2000). Mtr1, a novel biallelically expressed gene in the center of the mouse distal chromosome 7 imprinting cluster, is a member of the Trp gene family. *Genomics* 67:179–187.
- Farbman, A.I. (1990). Olfactory neurogenesis: genetic or environmental controls? *Trends Neurosci* 13:362-365.
- Farbman, A.I., Menco, B.P.M. (1986). Development of olfactory epithelium in the rat. In: Breipohl W (ed) *Ontogeny of olfaction*. Springer, Berlin Heidelberg New York, 45–56.

- 
- Fata, J.E., Chaudhary, V., Khokha, R. (2001). Cellular turnover in the mammary gland is correlated with systemic levels of progesterone and not 17beta-estradiol during the estrous cycle. *Biol. Reprod.* 65:680-688.
- Ferrero, D.M., Lemon, J.K., Fluegge, D., Pashkovski, S.L., Korzan, W.J., Datta, S.R., Spehr, M., Fendt, M., Liberles, S.D. (2011). Detection and avoidance of a carnivore odor by prey. *Proc Natl Acad Sci USA* 108:11235-11240.
- Firestein, S. (2001). How the olfactory system makes sense of scents. *Nature* 413:211-218.
- Fleischer, J., Breer, H., Strotmann, J. (2009). Mammalian olfactory receptors. *Front Cell Neurosci* 3:9.
- Flügge, D.P., Möller, L., Cichy, A., Gorin, M., Weth, A., Veitinger, S., Cainarca, S., Lohmer, S., Corazza, S., Neuhaus, E.M., Baumgartner, W., Spehr, J., Spehr, M. (2012). Mitochondrial Ca<sup>2+</sup> mobilization is a key element in olfactory signaling. *Nature Neuroscience*, 15:754-762.
- Gallagher, S.R., Desjardins, P.R. (2008). Quantitation of DNA and RNA with Absorption and Fluorescence Spectroscopy. *Current Protocols in Protein Science SUPPL.* 52:1–21.
- Gavrieli, Y., Sherman, Y., Ben-Sasson, S.A. (1992). Identification of programmed cell death in situ via specific labeling of nuclear DNA fragmentation. *J Cell Biol* 119:493-501.
- Gesteland, R.C., Yancey, R.A., Farbman, A.I. (1982). Development of olfactory receptor neuron selectivity in the rat fetus. *Neuroscience* 7:3127-3136.
- Gjerstad, J., Valen, E. C., Trotier, D., Doving, K. (2003). Photolysis of caged inositol 1,4,5-trisphosphate induces action potentials in frog vomeronasal microvillar receptor neurones. *Neuroscience*. 119:193-200.
- Goldman, J.M., Murr, A.S., Cooper, R.L. (2007). The rodent estrous cycle: characterization of vaginal cytology and its utility in toxicological studies. *Birth Defects Res B Dev Reprod Toxicol* 80:84-97.
- Grueneberg, H. (1973). A ganglion probably belonging to the N. terminalis system in the nasal mucosa of the mouse. *Z Anat Entwicklungsgesch.* 140:39-52.

- 
- Haga, S., Hattori, T., Sato, T., Sato, K., Matsuda, S., Kobayakawa, R., et al. (2010). The male mouse pheromone ESP1 enhances female sexual receptive behavior through a specific vomeronasal receptor. *Nature* 466:118-122.
- Hansen, A., Finger, T.E. (2008). Is TrpM5 a reliable marker for chemosensory cells? Multiple types of microvillous cells in the main olfactory epithelium of mice. *BMC Neurosci.* 9:115.
- Hantute-Ghesquier, A., Haustrate, A., Prevarskaya, N., Lehenkyi, V. (2018). TRPM Family Channels in Cancer. *Pharmaceuticals (Basel)* 11.
- Hegg, C.C., Jia, C., Chick, W.S., Restrepo, D., Hansen, A. (2010). Microvillous cells expressing IP3 receptor type 3 in the olfactory epithelium of mice. *Eur. J. Neurosci.* 32:1632-1645.
- Hellen, C., Sarnow, P. (2001). Internal ribosome entry sites in eukaryotic mRNA molecules. *Genes Dev* 15:1593-1612.
- Henning, S.J. (1981). Postnatal development: coordination of feeding, digestion, and metabolism. *Am. J. Physiol.* 241:199-214.
- Henion, T.R., Raitcheva, D., Grosholz, R., Biellmann, F., Skarnes, W.C., Hennet, T., Schwarting, G.A. (2005).  $\beta$ 1,3-N-Acetylglucosaminyltransferase 1 Glycosylation Is Required for Axon Pathfinding by Olfactory Sensory Neurons. *J Neurosci* 25:1894-1903.
- Hepper, P.G. (1988). Adaptive fetal learning: Prenatal exposure to garlic affects postnatal preferences. *Animal Behavior* 35:1343-1346.
- Hiroi, H.; Momoeda, M., Watanabe, T., Ito, M., Ikeda, K., Tsutsumi, R.; Hosokawa, Y., Koizumi, M., Zenri, F., Muramatsu, M., (2013). Expression and regulation of transient receptor potential cation channel, subfamily M, member 2 (TRPM2) in human endometrium. *Mol. Cell Endocrinol.* 365:146–152.
- Hofmann, T., Chubanov, V., Gudermann, T., Montell, C. (2003). TRPM5 is a voltage modulated and Ca<sup>2+</sup>-activated monovalent selective cation channel. *Curr. Biol.* 13:1153-1158.
- Hyman, B.T., Yuan, J. (2012). Apoptotic and non-apoptotic roles of caspases in neuronal physiology and pathophysiology. *Nat. Rev. Neurosci.* 13:395-406.
- Ibarra-Soria, X., Levitin, M.O., Saraiva, L.R., Logan, D.W. (2014). The olfactory transcriptomes of mice. *PLoS Genet.* 10:e1004593.

- Ishii, T., Hirota, J., Mombaerts, P. (2003). Combinatorial coexpression of neural and immune multigene families in mouse vomeronasal sensory neurons. *Curr. Biol.* 13:394-400.
- Johnson, M.A., Tsai, L., Roy, D.S., Valenzuela, D.H., Mosley, C., Magklara, A., Lomvardas, S., Liberles, S.D., Barnea, G. (2012). Neurons expressing trace amine-associated receptors project to discrete glomeruli and constitute an olfactory subsystem. *Proc Natl Acad Sci USA* 109:13410-13415.
- Kaske, S., Krasteva, G., König, P., Kummer, W., Hofmann, T., Gudermann, T., Chubanov, V. (2007). TRPM5, a taste-signaling transient receptor potential ion-channel, is a ubiquitous signaling component in chemosensory cells. *BMC Neurosci.* 8:49.
- Kelliher, K.R., Spehr, M., Li, X.H., Zufall, F., Leinders-Zufall, T. (2006). Pheromonal recognition memory induced by TRPC2-independent vomeronasal sensing. *Eur J Neurosci.* 23:3385-3390.
- Kim, S., Ma, L., Yu, C.R. (2011). Requirement of calcium-activated chloride channels in the activation of mouse vomeronasal neurons. *Nat Commun* 2:365.
- Kimchi, T., Xu, J., Dulac, C. (2007). A functional circuit underlying male sexual behavior in the female mouse brain. *Nature* 448:1009-1014.
- Koebele, S.V., Bimonte-Nelson, H.A. (2016). Modeling menopause: The utility of rodents in translational behavioral endocrinology research. *Maturitas.* 87:5-17.
- Koike, C., Numata, T., Ueda, H., Mori, Y., Furukawa, T. (2010). TRPM1: a vertebrate TRP channel responsible for retinal ON bipolar function. *Cell Calcium* 48:95-101.
- Kokrashvili, Z., Rodriguez, D., Yevshayeva, V., Zhou, H., Margolskee, R.F., Mosinger, B. (2009). Release of endogenous opioids from duodenal enteroendocrine cells requires Trpm5. *Gastroenterology* 137:598-606.
- Koolhaas, J.M., Coppens, C.M., de Boer, S.F., Buwalda, B., Meerlo, P., Timmermans, P.J.A. (2013). The Resident-intruder Paradigm: A Standardized Test for Aggression, Violence and Social Stress. *J Vis Exp* 77:4367.
- Kusumakshi, S., Voigt, A., Hübner, S., Hermans-Borgmeyer, I., Ortalli, A., Pyrski, M., Dörr, J., Zufall, F., Flockerzi, V., Meyerhof, W. (2015). A binary genetic approach to characterize TRPM5 cells in mice. *Chem. Senses* 40:413-425.

- 
- Lam, R.S., Mombaerts, P. (2013). Odorant responsiveness of embryonic mouse olfactory sensory neurons expressing the odorant receptors S1 or MOR23. *Eur. J. Neurosci.* 38:2210-2217.
- Launay, P., Fleig, A., Perraud, A.L., Scharenberg, A.M., Penner, R., Kinet, J.P. (2002). TRPM4 is a Ca<sup>2+</sup>-activated nonselective cation channel mediating cell membrane depolarization. *Cell* 109:397-407.
- Leinders-Zufall, T., Lane, A.P., Puche, A.C., Ma, W., Novotny, M.V., Shipley, M.T., Zufall, F. (2000). Ultrasensitive pheromone detection by mammalian vomeronasal neurons. *Nature* 405:792-796.
- Leinders-Zufall, T., Ishii, T., Chamero, P., Hendrix, P., Oboti, L., Schmid, A., et al. (2014). A family of nonclassical class I MHC genes contributes to ultrasensitive chemodetection by mouse vomeronasal sensory neurons. *J. Neurosci.* 34:5121-5133.
- Leinders-Zufall, T., Storch, U., Bleymehl, K., Mederos, Y., Schnitzler, M., Frank, J.A., Konrad, D.B., Trauner, D., and Gudermann, T., Zufall, F. (2018). PhoDAGs Enable Optical Control of Diacylglycerol-Sensitive Transient Receptor Potential Channels. *J Biol Chem* 25:215-223.
- Lemons, K., Fu, Z., Aoudé, I., Ogura, T., Sun, J., Chang, J., Mbonu, K., Matsumoto, I., Arakawa, H., Lin, W. (2017). Lack of TRPM5-Expressing Microvillous Cells in Mouse Main Olfactory Epithelium Leads to Impaired Odor-Evoked Responses and Olfactory-Guided Behavior in a Challenging Chemical Environment. *eNeuro* 4.
- Levine, J.E. (2015). Neuroendocrine control of the ovarian cycle of the rat. In Knobil and Neill's *Physiology of Reproduction*, Volume 2, T.M. Plant and A.J. Zeleznik, eds. (Academic Press), 1199-1257.
- Leybold, B.G., Yu, C.R., Leinders-Zufall, T., Kim, M.M., Zufall, F., Axel, R. (2002). Altered sexual and social behaviors in *trp2* mutant mice. *Proc. Natl. Acad. Sci. USA* 99:6376-6381.
- Li, Q., Liberles, S.D. (2015). Aversion and attraction through olfaction. *Curr Biol* 25:120-129.
- Liberles, S.D., Buck, L.B. (2006). A second class of chemosensory receptors in the olfactory epithelium. *Nature* 442:645-650.

- Liberles, S.D., Horowitz, L.F., Kuang, D., Contos, J.J., Wilson, K.L., Siltberg-Liberles, J., Liberles, D.A., Buck, L.B. (2009). Formyl peptide receptors are candidate chemosensory receptors in the vomeronasal organ. *Proc. Natl. Acad. Sci. USA* 106:9842-9847.
- Liberles, S.D. (2014). Mammalian pheromones. *Annual Review of Physiology* 76:151-175.
- Liberles, S.D. (2015). Trace amine-associated receptors: ligands, neural circuits, and behaviors. *Current Opinion in Neurobiology* 34:1-7.
- Licursi, M., Chrisitan, S.L., Pongnonpparat, T., Hirasawa, K. (2011). In vitro and in vivo comparison of viral and cellular internal ribosome entry sites for bicistronic vector expression. *Gene therapy* 18:631-636.
- Liman, E.R. (2003). Regulation by voltage and adenine nucleotides of a Ca<sup>2+</sup>-activated cation channel from hamster vomeronasal sensory neurons. *J. Physiol.* 548:777-787.
- Liman, E.R., Corey, D.P., Dulac, C. (1999). TRP2: a candidate transduction channel for mammalian pheromone sensory signaling. *Proc. Natl. Acad. Sci. USA* 96:5791-5796.
- Liman, E. (2014). TRPM5. In: B. Nilius, V. Flockerzi, (Eds.), *Mammalian Transient Receptor Potential (TRP) Cation Channels*. Springer, Heidelberg, *Handbook of experimental pharmacology*, 489-502.
- Lin, W., Margolskee, R., Donnert, G., Hell, S.W., Restrepo, D. (2007). Olfactory neurons expressing transient receptor potential channel M5 (TRPM5) are involved in sensing semiochemicals. *Proc. Natl. Acad. Sci. USA* 104:2471-2476.
- Lin, W., Ezekwe, E.A., Jr., Zhao, Z., Liman, E.R., Restrepo, D. (2008a). TRPM5-expressing microvillous cells in the main olfactory epithelium. *BMC Neurosci.* 9:114.
- Lin, W., Ogura, T., Margolskee, R.F., Finger, T.E., Restrepo, D. (2008b). TRPM5-expressing solitary chemosensory cells respond to odorous irritants. *J. Neurophysiol.* 99:1451-1460.
- Lipscomb, B.W., Treloar, H.B., Klenoff, J., Greer, C.A. (2003). Cell surface carbohydrates and glomerular targeting of olfactory sensory neuron axons in the mouse. *J Comp Neurol* 467:22-31.

- Loconto, J., Papes, F., Chang, E., Stowers, L., Jones, E.P., Takada, T., et al. (2003). Functional expression of murine V2R pheromone receptors involves selective association with the M10 and M1 families of MHC class Ib molecules. *Cell* 112:607-618.
- Logan, D.W., Brunet, L.J., Webb, W.R., Cutforth, T., Ngai, J., Stowers, L. (2012). Learned recognition of maternal signature odors mediates the first suckling episode in mice. *Curr Biol* 22:1998-2007.
- Lonstein, J.S., Pereira, M., Morrell, J.I., Marler, C.A. (2015). Parenting Behavior. In Knobil and Neill's *Physiology of Reproduction*, Volume 2, P.T. M. and A.J. Zeleznik, eds. (Academic Press), 2371-2437.
- Lopez, F., Delgado, R., Lopez, R., Bacigalupo, J., Restrepo, D. (2014). Transduction for pheromones in the main olfactory epithelium is mediated by the Ca<sup>2+</sup> - activated channel TRPM5. *J. Neurosci.* 34:3268-3278.
- Low, V.F., Mombaerts, P. (2017). Odorant receptor proteins in the mouse main olfactory epithelium and olfactory bulb. *Neuroscience* 344:167-177.
- Low, K.L., Cheng, H.J. (2006). Axon pruning: an essential step underlying the developmental plasticity of neuronal connections. *Philos Trans Soc Lond B Biol Sci* 361:1531-1544.
- Lowe, G., Gold, G.H. (1993). Nonlinear amplification by calcium-dependent chloride channels in olfactory receptor cells. *Nature* 366:283-286.
- Lucas, P., Ukhanov, K., Leinders-Zufall, T., Zufall, F. (2003). A diacylglycerol-gated cation channel in vomeronasal neuron dendrites is impaired in TRPC2 mutant mice: mechanism of pheromone transduction. *Neuron* 40:551-561.
- Luo, L., O'Leary, D.D. (2005). Axon retraction and degeneration in development and disease. *Annu. Rev. Neurosci.* 28:127-156.
- Ma, M., Grosmaître, X., Iwema, C.L., Baker, H., Greer, C.A., Shepherd, G.M. (2003). Olfactory signal transduction in the mouse septal organ. *J Neurosci.* 23:317–324.
- Mathar, I., Jacobs, G., Kecskes, M., Menigoz, A., Philippaert, K., Vennekens, R. (2014). Trpm4. In *Mammalian Transient Receptor Potential (TRP) Cation Channels*, Volume 1, B. Nilus and V. Flockerzi, eds. (Heidelberg: Springer), 461-487.

- Mandiyan, V.S., Coats, J.K., Shah, N.M. (2005). Deficits in sexual and aggressive behaviors in *Cnga2* mutant mice. *Nat Neurosci* 12:1660-1662.
- Marcucci, F., Maier-Balough, E., Zou, D.L., Firestein, S. (2011). Exuberant growth and synapse formation of olfactory sensory neuron axonal arborizations. *J Comp Neurol* 519:3713-3726.
- Martín-Sánchez, A., McLean, L., Beynon, R.J., Hurst, J.L., Ayala, G., Lanuza, E., Martínez-García, F. (2015). From sexual attraction to maternal aggression: when pheromones change their behavioral significance. *Horm Behav* 68:65-76.
- McCarthy, E.A., Naik, A.S., Coyne, A.F., Cherry, J.A., Baum, M.J. (2018). Effect of ovarian hormones and mating experience on the preference of female mice to investigate male urinary pheromones. *Chem. Senses* 43:97-104.
- McClintock, M.K. (1984). Estrous synchrony: modulation of ovarian cycle length by female pheromones. *Physiol Behav* 32:701-705.
- Menco, B.P. (1983). The ultrastructure of olfactory and nasal respiratory epithelium surfaces. In: Reznik G, Stinson SF (eds) *Nasal tumors in animals and man*, vol. 1, anatomy, physiology, and epidemiology. CRC Press Inc, 45–102.
- Miller, B.A. (2006). The role of TRP channels in oxidative stress-induced cell death. *J Membr Biol* 209:31-41.
- Miller, B.A. (2014). *Trpc2*. In: B. Nilius, V. Flockerzi, (Eds.), *Mammalian Transient Receptor Potential (TRP) Cation Channels*. Springer, Heidelberg, *Handbook of experimental pharmacology* 222:53-65.
- Mirsky, M.L., Sivaraman, L., Houle, C., Potter, D.M., Chapin, R.E., Cappon, G.D. (2011). Histologic and cytologic detection of endocrine and reproductive tract effects of exemestane in female rats treated for up to twenty-eight days. *Toxicol Pathol* 39:589-605.
- Mombaerts, P., Wang, F., Dulac, C., Chao, S.K., Nemes, A., Mendelsohn, M., Edmondson, J., Axel, R. (1996). Visualizing an olfactory sensory map. *Cell* 8:675-686.
- Mombaerts, P. (2004). Genes and ligands for odorant, vomeronasal and taste receptors. *Nature Reviews Neuroscience* 5:263–78.

- 
- Mombaerts, P. (2006). Axonal wiring in the mouse olfactory system. *Annual Review of Cell and Developmental Biology* 22:713-737.
- Moncho-Bogani, J., Lanuza, E., Lorente, M.J., Martinez-Garcia, F. (2002). Attractive properties of sexual pheromones in mice: innate or learned? *Physiol Behav.*77:167–176.
- Moncho-Bogani, J., Lanuza, E., Lorente, M.J., Martinez-Garcia, F. (2004). Attraction to male pheromones and sexual behavior show different regulatory mechanisms in female mice. *Physiol Behav* 81:427-434.
- Montell, C., Birnbaumer, L., Flockerzi, V., Bindels, R.J., Bruford, E.A., Caterina, M.J., Clapham, D.E., Harteneck, C., Heller, S., Julius, D., Kojima, I., Mori, Y., Penner, R., Prawitt, D., Scharenberg, A.M., Schultz, G., Shimizu, N., Zhu, M.X. (2002). A unified nomenclature for the superfamily of TRP cation channels. *Mol Cell* 9:229-231.
- Mohrhardt, J., Nagel, M., Fleck, D., Ben-Shaul, Y., Spehr, M. (2018). Signal Detection and Coding in the Accessory Olfactory System. *Chemical senses*, 43:667-695.
- Munger, S.D., Leinders-Zufall, T., Zufall, F. (2009). Subsystem organization of the mammalian sense of smell. *Annu. Rev. Physiol.* 71:115-140.
- Munger, S.D., Leinders-Zufall, T., McDougall, L.M., Cockerham, R.E., Schmid, A., Wandernoth, P., Wennemuth, G., Biel, M., Zufall, F., Kelliher, K.R. (2010). An olfactory subsystem that detects carbon disulfide and mediates food-related social learning. *Current Biology* 20:1438-1444.
- Münch, J., Billig, G., Hübner, C., Leinders-Zufall, T., Zufall, F., Jentsch T. (2018).  $Ca^{2+}$ -activated  $Cl^-$  currents in the murine vomeronasal organ enhance neuronal spiking but are dispensable for male-male aggression. *J Biol Chem* 293:10392-10403.
- Murofushi, W., Mori, K., Murata, K., Yamaguchi, M. (2018). Functional development of olfactory tubercle domains during weaning period in mice. *Sci Rep* 8:13204.
- Nache, V., Wongsamitkul, N., Kusch, J., Zimmer, T., Schwede, F., Benndorf, K. (2016). Deciphering the function of the CNGB1b subunit in olfactory CNG channels. *Sci Rep* 6:29378.

- Nakashima, A., Ihara, N., Shigeta, M., Kiyonari, H., Ikegaya, Y., Takeuchi, H. (2019). Structured spike series specify gene expression patterns for olfactory circuit formation. *Science* 365:46.
- Nelson, P.L., Beck, A., Cheng, H. (2011). Transient receptor proteins illuminated: current views on TRPs and disease. *Veterinary journal* 187:153-64.
- Nilius, B. (2003). Calcium-impermeable monovalent cation channels: a TRP connection? *Br J Pharmacol* 138:5-7.
- Nilius, B., Prenen, J., Droogmans, G., Voets, T., Vennekens, R., Freichel, M., Wissenbach, U., Flockerzi, V. (2003). Voltage dependence of the Ca<sup>2+</sup>-activated cation channel TRPM4. *J Biol Chem* 278:30813-30820.
- Nilius, B., Talavera, K., Owsianik, G., Prenen, J., Droogmans, G., Voets, T. (2005b). Gating of TRP channels: a voltage connection? *J Physiol* 567:35–44.
- Nilius, B., Owsianik, G. (2011). The transient receptor potential family of ion channels. *Genome Biol* 12:218.
- Noirot, E., Goyens, J., Buhot, M. (1975). Aggressive behavior of pregnant mice towards males. *Hormones and Behavior* 6:9-17.
- Norwitz, E.R., Schust, D.J., Fisher, S.J. (2001). Implantation and the survival of early pregnancy. *N Engl J Med* 345:1400-1408.
- Novotny, M.V., Ma W., Wiesler D., Zidek L. (1999). Positive identification of the puberty-accelerating pheromone of the house mouse: the volatile ligands associating with the major urinary protein. *Proc. Biol. Sci.* 266:2017-2022.
- Ogura, T., Szebenyi, S.A., Krosnowski, K., Sathyanesan, A., Jackson, J., Lin, W. (2011). Cholinergic microvillous cells in the mouse main olfactory epithelium and effect of acetylcholine on olfactory sensory neurons and supporting cells. *J. Neurophysiol.* 106:1274-1287.
- Omura, M., Mombaerts, P. (2014). *Trpc2*-expressing sensory neurons in the main olfactory epithelium of the mouse. *Cell Rep* 8:583-595.
- Omura, M., Mombaerts, P. (2015). *Trpc2*-expressing sensory neurons in the mouse main olfactory epithelium of type B express the soluble guanylate cyclase *Gucy1b2*. *Mol Cell Neurosci* 65:114-124.

- Oshimoto, A., Wakabayashi, Y., Garske, A., Lopez, R., Rolen, S., Flowers, M., Arevalo, N., Restrepo, D. (2013). Potential role of transient receptor potential channel M5 in sensing putative pheromones in mouse olfactory sensory neurons. *PLoS One* 8:e61990.
- Owsianik, G., D'hoedt, D., Voets, T., Nilius, B. (2006a). Structure-function relationship of the TRP channel superfamily. *Rev Physiol Biochem Pharmacol* 156:61–90.
- Pacifico, R., Dewan, A., Cawley, D., Guo, C., Bozza, T. (2012). An olfactory subsystem that mediates high-sensitivity detection of volatile amines. *Cell Reports* 2:76-88.
- Papes, F., Logan, D.W., Stowers, L. (2010). The vomeronasal organ mediates interspecies defensive behaviors through detection of protein pheromone homologs. *Cell* 141:692-703.
- Pedersen, P.E., Stewart, W.B., Greer, C.A., Shepherd, G.M. (1983). Evidence for olfactory function in utero. *Science* 221:478-480.
- Pérez, C.A., Huang, L., Rong, M., Kozak, J.A., Preuss, A.K., Zhang, H., Max, M., Margolskee, R.F. (2002). A transient receptor potential channel expressed in taste receptor cells. *Nat. Neurosci.* 5:1169-1176.
- Pérez-Gómez, A., Stein, B., Leinders-Zufall, T., Chamero, P. (2014). Signaling mechanisms and behavioral function of the mouse basal vomeronasal neuroepithelium. *Front Neuroanat.* 8:135.
- Pérez-Gómez, A., Bleymehl, K., Stein, B., Pyrski, M., Birnbaumer, L., Munger, S.D., Leinders-Zufall, T., Zufall, F., Chamero, P. (2015). Innate predator odor aversion driven by parallel olfactory subsystems that converge in the ventromedial hypothalamus. *Current Biology* 25:1340-1346.
- Persoons, E., Hennes, A., De Clercq, K., Van Bree, R., Vriens, G., O, D.F., Peterse, D., Vanhie, A., Meuleman, C., Voets, T., Tomassetti, C., Vriens, J. (2018). Functional Expression of TRP Ion Channels in Endometrial Stromal Cells of Endometriosis Patients. *Int J Mol Sci* 19:2467.
- Pfaus, J.G., Flanagan-Cato, L.M., Blaustein, J.D. (2015). Female sexual behavior. in Plant T., Zeleznik A. (Eds). *Knobil and Neill's Physiology of Reproduction*. Academic Press, 4th edition.

- Pifferi, S., Boccaccio, A., Menini, A., (2006). Cyclic nucleotide-gated ion channels in sensory transduction. *FEBS Lett* 580:2853-2859.
- Potter, S.M., Zheng, C., Koos, D.S., Feinstein, P., Fraser, S.E., Mombaerts, P. (2001). Structure and emergence of specific olfactory glomeruli in the mouse. *J. Neurosci.* 21:9713-9723.
- Prawitt, D., Monteilh-Zoller, M.K., Brixel, L., Spangenberg, C., Zabel, B., Fleig, A., Penner, R. (2003). TRPM5 is a transient Ca<sup>2+</sup>-activated cation channel responding to rapid changes in [Ca<sup>2+</sup>]<sub>i</sub>. *Proc. Natl. Acad. Sci. USA* 100:15166-15171.
- Pyrski, M., Eckstein, E., Schmid, A., Bufe, B., Weiss, J., Chubanov, V., Boehm, U., Zufall, F. (2017). Trpm5 expression in the olfactory epithelium. *Mol. Cell. Neurosci.* 80:75-88.
- Qiao, S., Nordström, K., Muijs, L., Gasparoni, G., Tierling, S., Krause, E., Walter, J., Boehm, U. (2016). Molecular Plasticity of Male and Female Murine Gonadotropes Revealed by mRNA Sequencing, *Endocrinology* 157:1082-1093.
- Ramsey, S., Delling M., Clapham D. E. (2006). An introduction to TRP channels. *Annual review of physiology* 68:619-47.
- Restrepo, D., Arellano, J., Oliva, A.M., Schaefer, M.L., Lin, W. (2004). Emerging views on the distinct but related roles of the main and accessory olfactory systems in responsiveness to chemosensory signals in mice. *Horm Behav.* 46:247-256.
- Riviere, S., Challet, L., Fluegge, D., Spehr, M., Rodriguez I. (2009). Formyl peptide receptor-like proteins are a novel family of vomeronasal chemosensors. *Nature* 459:574–577.
- Rodriguez, I., Del Punta, K., Rothman, A., Ishii, T., Mombaerts, P. (2002). Multiple new and isolated families within the mouse superfamily of V1r vomeronasal receptors. *Nat Neurosci* 5:134-140.
- Rodriguez, I. (2013). Singular expression of olfactory receptor genes. *Cell* 155:274-277.
- Santen, R.J., Brodie, H., Simpson, E.R., Siiteri, P.K., Brodie, A. (2009). History of aromatase: saga of an important biological mediator and therapeutic target. *Endocr. Rev.* 30:343-375.

- Sakuraba, M., Murata, J., Teruyama, R., Kamiya, K., Yamaguchi, J., Okano, H., Uchiyama, Y., Ikeda, K. (2014). Spatiotemporal expression of Trpm4 in the mouse cochlea. *J Neurosci Res* 92:1409-1418.
- Saraiva, L.R., Ibarra-Soria, X., Khan, M., Omura, M., Scialdone, A., Mombaerts, P., Marioni, J.C., Logan, D.W. (2015). Hierarchical deconstruction of mouse olfactory sensory neurons: from whole mucosa to single-cell RNA-seq. *Sci. Rep.* 5:18178.
- Sasaki, K., Okamoto, K., Inamura, K., Tokumitsu, Y., Kashiwayanagi, M. (1999). Inositol-1,4,5-trisphosphate accumulation induced by urinary pheromones in female rat vomeronasal epithelium. *Brain Res.* 823:161-168.
- Schaal, B., Orgeur, P. (1992). Olfaction in utero: can the rodent model be generalized? *Q. J. Exp. Psychol. B* 44:245-278.
- Schaefer, M., Plant, T.D., Stresow, N., Albrecht, N., Schultz, G. (2002). Functional differences between TRPC4 splice variants. *J Biol Chem* 277:3752–3759.
- Schmid, A., Pyrski, M., Biel, M., Leinders-Zufall, T., Zufall, F. (2010). Grueneberg ganglion neurons are finely tuned cold sensors. *Journal of Neuroscience* 30:7563-7568.
- Schwarting, G.A., Henion, T.R. (2012). Regulation and function of axon guidance and adhesion molecules during olfactory map formation. *J Cell Biochem* 112:2663-2671.
- Sisk, C.L., Richardson, H.N., Chappell, P.E., Levine, J.E. (2001). In vivo gonadotropin-releasing hormone secretion in female rats during peripubertal development and on proestrus. *Endocrinology* 142:2929-2936.
- Soucy, E.R., Albeanu, D.F., Fantana, A.L., Murthy, V.N., Meister, M. (2009). Precision and diversity in an odor map on the olfactory bulb. *Nat Neurosci* 12:210–220.
- Shpak G., Zylbertal A., Yarom Y., Wagner S. (2012). Calcium-activated sustained firing responses distinguish accessory from main olfactory bulb mitral cells. *J. Neurosci.* 32:6251-6262.
- Spehr, J., Hagedorf, S., Weiss, J., Spehr, M., Leinders-Zufall, T., Zufall, F. (2009). Ca<sup>2+</sup>-calmodulin feedback mediates sensory adaptation and inhibits pheromone-sensitive ion channels in the vomeronasal organ. *J. Neurosci.* 29:2125-2135.

- Staaf, S., Franck, M.C., Marmigere, F., Mattsson, J.P., Ernfors, P. (2010). Dynamic expression of the TRPM subgroup of ion channels in developing mouse sensory neurons. *Gene Expr. Patterns* 10:65-74.
- Stowers, L., Holy, T.E., Meister, M., Dulac, C., Koentges, G. (2002). Loss of sex discrimination and male-male aggression in mice deficient for TRP2. *Science* 295:1493-1500.
- Talavera, K., Yasumatsu, K., Voets, T., Droogmans, G., Shigemura, N., Ninomiya, Y., Margolskee, R.F., Nilius, B. (2005). Heat activation of TRPM5 underlies thermal sensitivity of sweet taste. *Nature* 438:1022-1025.
- Thompson, R.N., Robertson, B.K., Napier, A., Wekesa, K.S. (2004). Sex-specific Responses to Urinary Chemicals by the Mouse Vomeronasal Organ. *Chemical senses*. 29:749-54.
- Thoß, M., Luzynski, K.C., Enk, V.M., Razzazi-Fazeli, E., Kwak, J., Ortner, I., Penn, D. (2019). Regulation of volatile and non-volatile pheromone attractants depends upon male social status. *Sci Rep* 9:489.
- Tian, H., Ma, M. (2004). Molecular Organization of the Olfactory Septal Organ. *J Neurosci* 24:8383-8390.
- Tirindelli, R., Dibattista, M., Pifferi, S., Menini, A. (2009). From pheromones to behavior. *Physiol Rev* 89:921-956.
- Trouillet, A.C., Keller, M., Weiss, J., Leinders-Zufall, T., Birnbaumer, L., Zufall, F., Chamero, P. (2019). Central role of G protein Gai2 and Gai2+ vomeronasal neurons in balancing territorial and infant-directed aggression of male mice. *PNAS* 116:5135-5143.
- Ullrich, N.D., Voets, T., Prenen, J., Vennekens, R., Talavera, K., Droogmans, G., Nilius, B., (2005). Comparison of functional properties of the Ca<sup>2+</sup>-activated cation channels TRPM4 and TRPM5 from mice. *Cell Calcium* 37:267-278.
- Underwood, M.A., Gilbert, W.M., Sherman, M.P. (2005). Amniotic fluid: not just fetal urine anymore. *J. Perinatol.* 25:341-348.
- Vandenbergh, J.G. (1969). Male odor accelerates female sexual maturation in mice. *Endocrinology* 84:658-660.
- Vennekens, R., Olausson, J., Meissner, M., Bloch, W., Mathar, I., Philipp, S.E., Schmitz, F., Weissgerber, P., Nilius, B., Flockerzi, V., et al. (2007). Increased IgE

- dependent mast cell activation and anaphylactic responses in mice lacking the calcium activated nonselective cation channel TRPM4. *Nat. Immunol.* 8:312-320.
- Venkatachalam, K., Montell C. (2007). "TRP channels." *Annual review of biochemistry* 76:387-417.
- Verhaagen J., Oestreicher A.B., Grillo M., Khew-Goodall Y.S., Gispen W.H., Margolis F.L. (1990). Neuroplasticity in the olfactory system: differential effects of central and peripheral lesions of the primary olfactory pathway on the expression of B-50/GAP43 and the olfactory marker protein. *J. Neurosci. Res.* 26:31-44.
- Voet, D., Voet, J.G., Pratt, C.W. (2006). *Fundamentals of biochemistry: life at the molecular level* (2. ed.). Hoboken, NJ: Wiley.
- Voolstra, O., Huber, A. (2014). Post-Translational Modifications of TRP Channels. *Cells.* 3:258-287.
- Voyron, S., Giacobini, P., Tarozzo, G., Cappello, P., Perroteau, I., Fasolo, A. (1999). Apoptosis in the development of the mouse olfactory epithelium. *Brain Res. Dev. Brain Res.* 115:49-55.
- Wang, F., Nemes, A., Mendelsohn, M., Axel, R. (1998). ORs govern the formation of a precise topographic map. *Cell.* 93:47-60.
- Wang, C., Hu, H.Z., Colton, C.K., Wood, J.D., Zhu, M.X. (2004). An alternative splicing product of the murine *trpv1* gene dominant negatively modulates the activity of TRPV1 channels. *J Biol Chem* 279:37423–37430.
- Wen, S., Götze, I.N., Mai, O., Schauer, C., Leinders-Zufall, T., Boehm, U. (2011). Genetic identification of GnRH receptor neurons: a new model for studying neural circuits underlying reproductive physiology in the mouse brain. *Endocrinology* 152:1515-1526.
- Whitten, W.K., Bronson, F.H., Greenstein, J.A. (1968). Estrus-inducing pheromone of male mice: transport by movement of air. *Science* 161:584-585.
- Wilson, K.C., Raisman, G. (1980). Age-related changes in the neurosensory epithelium of the mouse vomeronasal organ: extended period of postnatal growth in size and evidence for rapid cell turnover in the adult. *Brain Res* 185:103–113.

- Woo, S.K., Kwon, M.S., Ivanov, A., Geng, Z., Gerzanich, V., Simard, J.M. (2013). Complex N-Glycosylation Stabilizes Surface Expression of Transient Receptor Potential Melastatin 4b Protein. *J. Biol. Chem.* 288:36409.
- Wood, G.A., Fata, J.E., Watson, K.L., Khokha, R. (2007). Circulating hormones and estrous stage predict cellular and stromal remodeling in murine uterus. *Reproduction* 133:1035-1044.
- Wu, L.J., Sweet, T.B., Clapham, D.E. (2010). International Union of Basic and Clinical Pharmacology. LXXVI. Current progress in the mammalian TRP ion channel family. *Pharmacological reviews* 62:381-404.
- Wyatt, T.D. (2014). *Pheromones and animal behavior*, Second Edition. Cambridge University Press.
- Xiao, K., Kondo, Y., Sakuma, Y. (2004). Sex-specific effects of gonadal steroids on conspecific odor preference in the rat. *Horm Behav.* 46:356-361.
- Xu, X.Z., Moebius, F., Gill, D.L., Montell, C. (2001). Regulation of melastatin, a TRP-related protein, through interaction with a cytoplasmic isoform. *Proc Natl Acad Sci USA* 98:10692–10697.
- Yamaguchi, T., Yamashita, J., Ohmoto, M., Aoude, I., Ogura, T., Luo, W., Bachmanov, A.A., Lin, W., Matsumoto, I., Hirota, J. (2014). Skn-1a/Pou2f3 is required for the generation of Trpm5-expressing microvillous cells in the mouse main olfactory epithelium. *BMC Neurosci.* 15:13.
- Yamashita, J., Ohmoto, M., Yamaguchi, T., Matsumoto, I., Hirota, J. (2017). Skn-1a/Pou2f3 functions as a master regulator to generate Trpm5-expressing chemosensory cells in mice. *PLoS one* 12:e0189340.
- Yang, C., Delay, R.J. (2010). Calcium-activated chloride current amplifies the response to urine in mouse vomeronasal sensory neurons. *J Gen Physiol.* 135:3-13.
- Yu, C.R. (2015). TRICK or TRP? What Trpc2(-/-) mice tell us about vomeronasal organ mediated innate behaviors. *Front Neurosci* 9:221.
- Zhang, Y., Hoon, M.A., Chandrashekar, J., Mueller, K.L., Cook, B., Wu, D., Zuker, C.S., Ryba, N.J. (2003). Coding of sweet, bitter, and umami tastes: different receptor cells sharing similar signaling pathways. *Cell* 112:293-301.

- 
- Zhang, J., Pacifico, R., Cawley, D., Feinstein, P., Bozza, T. (2013). Ultrasensitive detection of amines by a trace amine-associated receptor. *J Neurosci* 33:3228-3239.
- Zheng, J., Zagotta, W.N. (2004). Stoichiometry and assembly of olfactory cyclic nucleotide-gated channels. *Neuron* 42:411-421.
- Zou, D.J., Feinstein, P., Rivers, A.L., Mathews, G.A., Kim, A., Greer, C.A., Mombaerts, P., Firestein, S. (2004). Postnatal refinement of peripheral olfactory projections. *Science* 304:1976-1979.
- Zufall, F., Munger, S.D. (2010). Receptor guanylyl cyclases in mammalian olfactory function. *Mol Cell Biochem* 334:191-197.
- Zufall, F., Leinders-Zufall, T. (2007). Mammalian pheromone sensing. *Curr. Opin. Neurobiol.* 17:483-489.
- Zufall, F., Leinders-Zufall, T., Greer, C.A. (2000). Amplification of odor-induced  $Ca^{2+}$  transients by store-operated  $Ca^{2+}$  release and its role in olfactory signal transduction. *83:501-512.*
- Zufall, F. (2014). TRPs in olfaction. *Handbook of experimental pharmacology* 223:917-933.

## 7 Appendix

### 7.1 Publications

1. Moritz, C.P., Eckstein, E., Tenzer, S., Friauf, E. (2015). Neuroproteomics in the auditory brainstem: Candidate proteins for ultrafast and precise information processing. *Mol Cell Neurosci.* 64, 9-23.
2. Pyrski, M., Eckstein, E., Schmid, A., Bufe, B., Weiss, J., Chubanov, V., Boehm, U., and Zufall, F. (2017). Trpm5 expression in the olfactory epithelium. *Mol Cell Neurosci.* 80, 75–88.
3. Pyrski, M., Tusty, M., Eckstein, E., Oboti, L., Rodriguez-Gil, D., Greer, C., Zufall, F. (2018). P/Q type calcium channel Cav2.1 defines a unique subset of glomeruli in the mouse olfactory bulb. *Front Cell Neurosci.* 12, 295.
4. Eckstein, E., Pyrski, M., Freichel, M., Vennekens, R., Zufall, F. (in preparation). Sex hormone-regulated Trpm4 channel in the vomeronasal organ is a candidate for gender-specific responses.

Bachelor Thesis:

Eckstein E (2011). Phylogenie und Struktur der ITS2 bei *Monomorpha* sp. (Euglenophyceae).

Master Thesis:

Eckstein E (2013). The inwardly rectifying potassium channel Kir4.1 in the rat auditory brainstem; Immunohistochemical and Western Blot analyses.

## 7.2 Acknowledgements

First and foremost, I would like to thank my supervisor **Professor Dr. Dr. Frank Zufall** for this interesting project. I appreciate the support, the immense knowledge, and ideas that made my doctoral thesis so exciting and productive.

Besides my supervisor, I would also like to thank **Dr. Martina Pyrski** for the valuable guidance. The joy and enthusiasm she had for her research was contagious and inspiring, and motivated me even in difficult periods.

Many thanks go to **Prof. Dr. Trese Leinders-Zufall** for her insightful comments and the encouragement to look at my research from various perspectives. This enabled me to think outside the box and to find new solutions especially in difficult tasks.

I want to thank **Prof. Dr. Marc Freichel**, **Prof. Dr. Ulrich Boehm**, and **Prof. Dr. Rudi Vennekens** for their scientific input and kind provision of mouse models.

The **members of the Zufall and Leinders-Zufall Group** have contributed tremendously to my personal and academic life in Homburg. The group was a source of friendships, good advice, and cooperation. I would like to thank all the lab mates for the stimulating discussions, for the long evenings we were working together before deadlines, and for all the fun we have had. The warm atmosphere and the individual support have been the basis for a very pleasant and productive time.

I want to thank **Thomas Blum** for the friendship, for the fun and the interesting conversations. Without him the time would have been only half as exciting.

I would also like to thank **Dr. Jan Weiss** and **Prof. Dr. Bernd Bufe** for the instruction in behavioral and molecular techniques, as well as for the stimulating discussions and fresh inspirations.

Additional thanks go to **Ana Moreno-Pérez**, **Yannick Teuchert**, **Kohei Koike**, **Hui Fan**, **Dennis Bakker**, **Katherin Bleymehl**, **Florian Bolz**, **Hendrik Stempel**, **Anabel Pérez-Gómez**, and **Michael Konzmann** for all the nice discussions and the fun times.

Many thanks go to **Petra Hammes** for the technical support, all organizational matters in the lab, for the help with cryostat sections and immunohistochemical methods, and **Monika Vorndran** for the genotyping. I want to thank both for all the kind words and good laughs.

Also, thanks go to **Gabriele Mörschbacher**, who facilitated my work immensely through her organizational skills in many situations.

In addition, I would like to thank the animal facility staff, especially **Lisa Knieriemen**, **Kerstin Becker**, and **Angelika Ströer**.

Special thanks go to my parents, **Tatjana Eckstein** and **Harri Eckstein**, my sister **Ina Blehm**, my brother-in-law **Viktor Blehm**, my nephew **Michael**, and my niece **Melissa**. Thank you very much for the loving support during my entire life.

I also want to thank **Dr. Christian Backes**, my best friend, soul mate and partner. He unconditionally supported and motivated me during all my good and bad times. Additional thanks go to **Elfriede Backes** and **Franz-Josef Backes** for everyday support and valuable advice in any situation.

Last, but not least I would like to thank all my friends, in particular **Henrike Reder**, **Jens Scherer**, and **Melanie Schmitt** for their never-ending patience and understanding when I have canceled yet another get-together during the last years.